TÉCNICO LISBOA

Bactericidal effect of silver in cellulose acetate mixed matrix membranes

Silver nanoparticles vs silver loaded zeolite

Ana Rita Batista Vilas Boas

Thesis to obtain the Master of Science Degree in

Integrated Master in Chemical Engineering

Supervisors:
Prof. Maria Amélia Nortadas Duarte de Almeida Lemos
Prof. Maria Norberta Neves Correia de Pinho

Examination Committee

Chairperson: Prof. José Manuel Félix Madeira Lopes
Supervisor: Prof. Maria Amélia Nortadas Duarte de Almeida Lemos
Members of the Committee: Prof. Eduardo Jorge Morilla Filipe

December 2016

Bactericidal effect of silver in cellulose acetate mixed matrix membranes

Silver nanoparticles vs silver loaded zeolite

Ana Rita Batista Vilas Boas

Thesis to obtain the Master of Science Degree in

Integrated Master in Chemical Engineering

Supervisors:
Prof. Maria Amélia Nortadas Duarte de Almeida Lemos
Prof. Maria Norberta Neves Correia de Pinho
Dr. Ricardo Jaime Pereira Rosário dos Santos
Sílvia Patrícia Nunes Monteiro

Examination Committee

Chairperson: Prof. José Manuel Félix Madeira Lopes
Supervisor: Prof. Maria Amélia Nortadas Duarte de Almeida Lemos
Members of the Committee: Prof. Eduardo Jorge Morilla Filipe

December 2016

ACKNOWLEDGEMENTS

Gostaria de agradecer aos meus orientadores, Professora Amélia Lemos, Professora Norberta de Pinho, Ricardo Santos e Sílvia Monteiro, e ao Professor Francisco Lemos, pela orientação, apoio e transferência de conhecimento que me possibilitaram a realização desta tese.

A todos os que me ajudaram nos diferentes laboratórios que frequentei pela simpatia e por me fazerem sentir à-vontade para fazer todas as perguntas.

Gostaria de agradecer o apoio da minha família e dos meus amigos, pelo ânimo que me deram ao longo destes meses e por ouvirem os meus constantes desabafos.

Um agradecimento especial à minha mãe, ao meu pai e ao meu avô pelo incentivo e apoio constantes, por me ouvirem sempre e pelos bons conselhos.

Ao Gonçalo pelo apoio incondicional, pela paciência, pela óptima companhia, por sempre acreditar nas minhas capacidades e me ajudar a chegar a este momento.

RESUMO

A nanofiltração é afectada pelo *biofouling*, que pode ser minimizado utilizando membranas de matriz mista com propriedades antibacterianas. Assim, foram preparadas sete membranas de matriz mista assimétricas de acetato de celulose através do método de inversão de fases incorporando, nas soluções poliméricas de preparação das membranas, nanopartículas de prata, zeólito ZSM-5 e diferentes teores de zeólitos permutados com prata (0,005%, 0,03%, 0,07% e 0,14% de prata na membrana), composições estas confirmadas por termogravimetria.

A formação de nanopartículas de prata, utilizando nitrato de prata, borohidreto de sódio (agente redutor) e PVP (agente estabilizante), pode ser descrita por uma cinética de segunda ordem. A adição de formamida a nitrato de prata forma partículas de prata com diferentes distribuições de tamanho. Pode-se afirmar que as nanopartículas de prata, assim como o aumento da concentração de zeólito permutado com prata e ao contrário do zeólito ZSM-5, aumentam a permeabilidade hidráulica das membranas de acetato de celulose. A incorporação destes materiais diminui os coeficientes de rejeição para glucose, NaCl, Na_2SO_4, $MgCl_2$ e $MgSO_4$, assim como o potencial zeta das membranas. A prata presente no zeólito, tanto em pó como na membrana, está na forma catiónica, como observado por voltametria cíclica. A membrana de zeólito com prata (0,14% de prata) apresentou o menor crescimento bacteriano de *Escherichia coli* e *Pseudomonas aeruginosa* após 300 minutos. O zeólito ZSM-5 não teve efeito bactericida contra as culturas, ao contrário do zeólito permutado com prata que apresentou maior efeito contra *E. coli*.

Palavras-Chave: Membranas de acetato de celulose; Membranas nanocompósitas; Nanopartículas de prata; Zeólito ZSM-5; Propriedades bactericidas

ABSTRACT

Nanofiltration is still affected by biofouling, which can be minimized using mixed matrix membranes with antibacterial properties. Thus, seven cellulose acetate asymmetric composite membranes were prepared via the wet-phase inversion method incorporating, in the membrane casting solutions, silver nanoparticles, ZSM-5 zeolite and different contents of silver exchanged zeolite (0,005%, 0,03%, 0,07% and 0,14% of silver in the membrane), which compositions were confirmed by thermogravimetric analysis.

The silver nanoparticles formation, using silver nitrate, sodium borohydride (reducing agent) and PVP (stabilising agent), can be described by a second order kinetics. The addition of formamide to silver nitrate forms silver particles with different size distributions. It can be stated that silver nanoparticles increase the hydraulic permeability of cellulose acetate membranes, contrary to ZSM-5 zeolite, and the increasing concentration of silver exchanged zeolite increases this parameter. The incorporation of these materials decreases the rejection coefficients to glucose, NaCl, Na_2SO_4, $MgCl_2$ and $MgSO_4$, as the zeta potential of the membranes. The silver present in the zeolite, both in powder and in the membrane, is in the cationic form, as seen in the cyclic voltammetry curves. The silver zeolite membrane (0,14% silver) showed the lowest bacterial growth of *Escherichia coli* and *Pseudomonas aeruginosa* after 300 minutes. The ZSM-5 zeolite had no bactericidal effect against the cultures, contrary to the silver exchanged zeolite that showed higher effect against *E. coli*.

Keywords: Cellulose acetate membranes; Nanocomposite membranes; Silver nanoparticles; ZSM-5 zeolite; Antibacterial properties

CONTENTS

LIST OF FIGURES

LIST OF TABLES

SYMBOLS

Abbreviation	Explanation
A	absorbance
AgNP	silver nanoparticles
BOD_5	biochemical oxygen demand
CA	cellulose acetate
CEC	cation-exchange capacities
CFU	colony forming units
COD	chemical oxygen demand
CV	cyclic voltammetry
Da	Dalton
DBP	disinfection by-product
EDL	electrochemical double layer
E. coli	*Escherichia coli*
FAU	faujasite
HS	Helmholtz-Smoluchowski
HWW	hospital wastewater
IC	inorganic carbon
IHP	inner Helmholtz plane
L-Asp	L-aspartic acid
L-Phe	L-phenylalanine
LTA	Linde Type A
LTL	Linde Type L
MF	microfiltration
MIC	minimum inhibitory concentration
MWCO	molecular weight cut-offs
NF	nanofiltration
NOM	natural organic matter
NP	nanoparticle
OD	optical density
OHP	outer Helmholtz plane
P. aeruginosa	*Pseudomonas aeruginosa*
PAN	polyacrylonitrile
PES	polyethersulfone
PP	polypropylene
PSf	polysulfone
PTFE	polytetrafluoroethylene
PVDF	polyvinylidine fluoride
PVP	polyvinylpyrrolidone

R	correlation coefficient
RO	reverse osmosis
rpm	rotations per minute
SOD	sodalite
SS	suspended solids
S. aureus	*Staphylococcus aureus*
Susp	silver nanoparticle suspension
SWRO	seawater reverse osmosis
TC	total carbon
TGA	thermogravimetric analysis
TOC	total organic carbon
TSA	tryptic soy agar
TSB	tryptic soy broth
UF	ultrafiltration
UV	ultraviolet
UV-Vis	ultraviolet-visible spectroscopy
UWW	urban wastewater
ZAg	silver containing zeolite
ZSM-5	Zeolite Socony Mobil–5

Symbol	**Explanation**	**Unit**
C	concentration	g/L
C_b	solute concentration in the bulk feed solution	g/L
C_p	solute concentration in the permeate	g/L
E_s	streaming potential	V
f	rejection coefficient	-
J_{pw}	pure water permeate flux	kg/(h·m^2)
L_p	hydraulic permeability	kg/(h·m^2·bar)
MW	molecular weight	g/mol
P	pressure	Pa
R	resistance of the channel in the measurement solution	Ω
R^H	resistance of the channel in a concentrated ionic solution	Ω
t	time	s
γ	wavelength	nm
ΔP	transmembrane pressure	bar
ε	dielectric constant of the electrolyte	-
ε_0	vacuum permittivity	F·m^{-1}
ζ	zeta potential	V

η	electrolyte viscosity	(Pa·s)
λ_0	electrical conductivity of the electrolyte solution	$S \cdot m^{-1}$
λ^H	conductivity of the solution of high salt concentration	$S \cdot m^{-1}$
ρ	specific weight	kg/m^3
σ	conductivity	μS/cm

1 INTRODUCTION

All life on Earth depends upon one essential good: water. So much so that nations' development is directly linked to the freshwater availability and quality, since it is used for agricultural (75%), industrial (20%) and domestic purposes (5%) (UNEP 2008).

In the mid of 2015, the world population reached 7,3 thousand millions and, according to the medium hypothesis proposed by the United Nations, is expected to increase to 9,7 thousand millions by 2050 (Melorose, Perroy, and Careas 2015). Not only the increasing population, but also the climate changes that disturbed the water cycle and the contamination of water reservoirs contributed to water scarcity (UNEP 2008). Even more when only around 1% of the total water is accessible for consumption, since 97,5% of total water in the planet is saline and the majority of freshwater is unavailable in glaciers (USGS 2015).

In a planet were the volume of water is approximately constant, it will be difficult to provide enough quality water to an increasing population, under the present circumstances, mainly when the freshwater resources are unevenly distributed (Figure 1-1). It is necessary to find solutions that avoid threatening water reserves and harming the environmental balance (UNEP 2008).

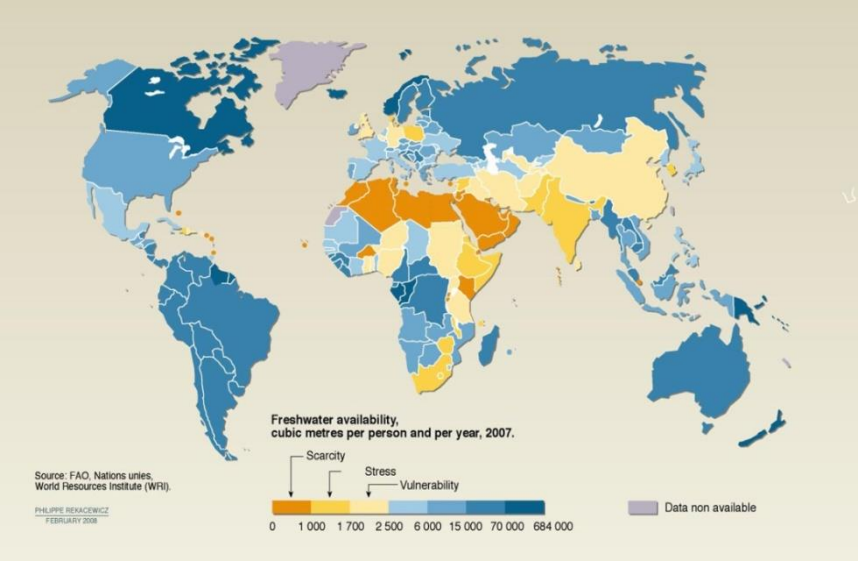

Figure 1-1 – Freshwater availability in 2007 (UNEP 2008)**.**

Nanofiltration is increasingly used in wastewater treatment and drinking/process water production and is the best available technique for removal of natural organic matter (NOM) and to avoid formation of disinfection by-products (DBP), surpassing the traditional methods as a result of the development of the membranes and the better prices due to enhanced use coupled with a more demanding water quality. Although being an efficient and effective technology to use in wastewater treatment and water reuse, nanofiltration is still hindered by membrane fouling, as it reduces membrane permeability (Van der Bruggen, Mänttäri, and Nyström 2008; J. Wang et al. 2014; Wiesner and Chellam 1999). The fouling, caused by membrane surface deposition, is hard to remove even with periodic cleaning, which largely increases maintenance and operating costs. For this reason, the best option is to prevent fouling at its earliest stages (Xie, Saito, and Hickner 2011).

Since membranes can have a wide range of characteristics by changing the material or fabrication process, it is possible to create membranes with fouling resistance, by incorporating materials such as zeolites, and antimicrobial properties, such as silver nanoparticles (Pendergast and Hoek 2011; J. Wang et al. 2014).

1.1 OBJECTIVES OF THE THESIS

In order to investigate the bactericidal properties of silver nanoparticles, ZSM-5 zeolite and silver exchanged zeolite incorporated in nanofiltration cellulose acetate (CA) membranes, the following partial objectives were set:

1. Synthesis of asymmetric cellulose acetate and mixed matrix CA membranes with 0,14% of silver nanoparticles, with ZSM-5 zeolite and with different contents of silver exchanged ZSM-5 zeolite (0,005%, 0,03%, 0,07% and 0,14% of silver in the membrane);
2. Characterization of the silver nanoparticles formation and the role of formamide as a reducing agent using UV-Vis spectroscopy;
3. Characterization of the membranes in case of pure water hydraulic permeability and rejection coefficients for glucose, NaCl, Na_2SO_4, $MgCl_2$ and $MgSO_4$;
4. Characterization of the membranes by electrochemical studies (state of the silver), thermogravimetric analysis and zeta potential;
5. Investigation of the bactericidal effect of the CA mixed matrix membranes, zeolite and silver exchanged zeolite on *Escherichia coli* and *Pseudomonas aeruginosa*.

1.2 THESIS STRUCTURE

The thesis is divided in five chapters with the following content:

- Chapter 1 Scope, objective and structure of the present thesis.
- Chapter 2 Literature review on pressure-driven membranes processes and its applications, membranes structure and separation process, nanocomposite membranes, type of incorporated particles, method of nanoparticles incorporation in membrane structure and effects of silver nanoparticles/zeolites in the biofouling control of nanocomposite membranes.
- Chapter 3 Description of the experimental methods used in the preparation, characterization, permeation and antibacterial experiments of the membranes.
- Chapter 4 Presentation and discussion of experimental results obtained in membrane permeation experiments with pure water, glucose and salts (NaCl, Na_2SO_4, $MgCl_2$ and $MgSO_4$), with UV-Vis spectroscopy, with characterization through cyclic voltammetry, thermogravimetric analysis and streaming potential and antibacterial activity against *Escherichia coli* and *Pseudomonas aeruginosa*.
- Chapter 5 Conclusions and recommendations to future work.

2 LITERATURE REVIEW

The literature review of this thesis will focus in the applications of pressure-driven processes, in particular biofouling control of nanofiltration membranes.

2.1 NANOFILTRATION AND ITS APPLICATIONS

Nowadays, the membrane separation technologies have an important role on wastewater reclamation and particularly on desalination. These processes are favoured over others for not requiring chemical additives, thermal inputs or regeneration of spent media. The pressure-driven membranes are classified according to separation mechanism or intended application and include microfiltration (suspended solids, protozoa and bacteria removal), ultrafiltration (virus and colloid removal), nanofiltration (hardness, heavy metals and dissolved organic matter removal) and reverse osmosis (desalination, water reuse and ultrapure water production), as presented in Figure 2-1 (Pendergast and Hoek 2011; J. Wang et al. 2014).

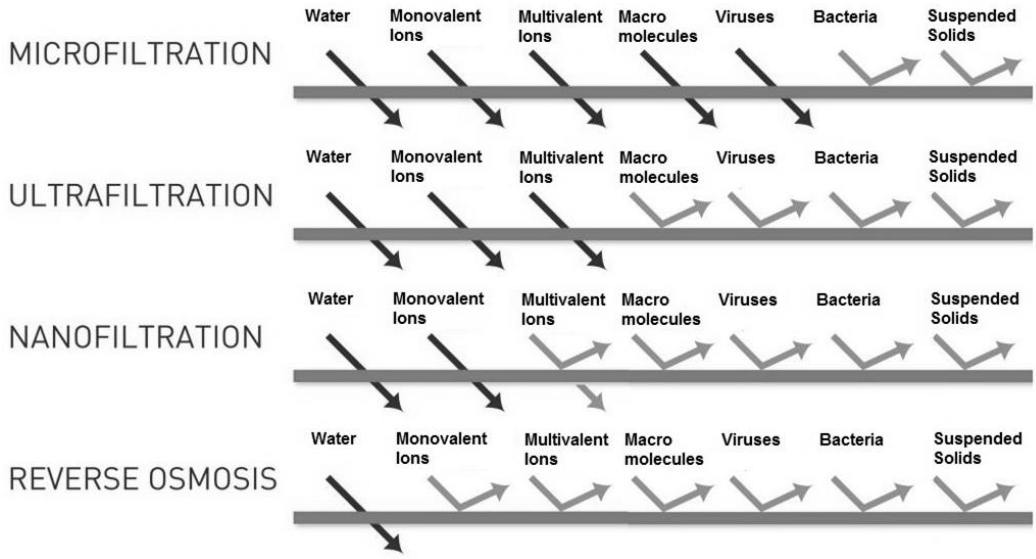

Figure 2-1 – Types of membranes and characteristics (adapted from (X-Flow n.d.)**).**

The nanofiltration (NF) membrane is characterized by the molecular weight cut-offs (MWCO) between reverse osmosis (RO) and ultrafiltration (UF) membranes (200 to 2000 Da) and the separation of electrolytes in aqueous solutions due to the membrane materials containing charged groups (molecular exclusion and solution diffusion mechanisms, respectively). It has been largely developed and commercialized in the past decade as a promising technology for its low operation pressure, high flux, high retention of multivalent anion salts, relatively low investment, long lifetimes and low operation and maintenance costs. The applications of NF membranes include desalination and concentration, separation and purification, drinking water production and wastewater treatment. This process enables highly energy-efficient removal of turbidity, microorganisms and hardness, from both natural and industrial waters (Hilal et al. 2004; J. Wang et al. 2014; X.-L. Wang et al. 2009).

2.1.1 WATER TREATMENT

Due to an intensive use of pesticides in agriculture, groundwater and surface water are increasingly contaminated. These organic pollutants were usually removed using activated carbon and through oxidation by ozone, techniques that have disadvantages. The activated carbon process uses carbon filters that saturate rapidly, which efficiency to eliminate pesticides decreases with a high presence of natural organic matter (NOM) due to a competitive adsorption, and has an enhanced cost by the frequent regeneration of the carbon. The oxidation by ozone leads to the formation of small molecules after the cut of pesticide molecules that can cause bacterial regrowth in water distribution systems and also the formation of by-products (peroxides, ozonides, organobromine and bromate). Nanofiltration can be used to treat all kinds of water (ground, surface and wastewater) or as a pre-treatment for desalination in a more efficiently way (Boussahel et al. 2000; Hilal et al. 2004).

GROUNDWATER

Groundwater is an essential source of fresh water which quality has deteriorated due to the increased human population and its activities. Nanofiltration is used to remove hardness, NOM, disinfection by-product (DBP) precursors and multivalent ions from the groundwater (Hilal et al. 2004; Yang et al. 2016), as shown in the following examples: the NF membranes used by Schaep et al. (Schaep et al. 1998) had retentions higher than 90% for multivalent ions (e.g. sulphate and magnesium) and, for monovalent ions, such as chloride and sodium, had retentions around 60-70%; Van der Bruggen et al. (Van Der Bruggen et al. 2001) showed that the UTC-20 and NF70 membranes can remove the major fraction of the hardness to less than the desired concentration in the drinking water and NF70 membrane had a rejection of pesticides (atrazine, simazine, diuron and isoproturon) of around 95%; the NF membrane tested by E. Gwon et al. (Gwon et al. 2003) had a removal efficiency of dissolved inorganic and organic matter of, respectively, 76,3% and 80%.

SURFACE WATER

Surface water is the most accessible fresh water reservoir and its composition often varies with seasonal changes or rain. Nanofiltration is a reliable option to remove organics from the groundwater (Hilal et al. 2004). K. Moons and Van der Bruggen (Moons and Van der Bruggen 2006) used self-made membranes, produced with phase-inversion technique, to evaluate the organic micro pollutants most commonly found in the Flemish surface water: estradiol, estrone and salicine. The retention coefficients of these compounds for the UTC-20 membrane were, respectively, 75%, 83% and higher than 97%. S. Köhler et al. (Köhler et al. 2016) studied a chemically resistant hollow-fibre NF membrane in pilot scale at a drinking water treatment plant in Stockholm, Sweden, fed with full scale process water from a rapid sand filter after aluminum sulphate coagulation. This combination removed more than 90% of dissolved organic carbon and 96% of the absorbance at 254 nm. According to W. Huang et al. (Huang et al. 2016), the all-cellulose nanocomposite membrane, with an electronegative nature, were fabricated to remove nanoparticles and virus from aqueous medium. Rejections of 100% for positively charged latex beads and 98,7% for *Hepatitis C* virus were obtained.

WASTEWATER

Nanofiltration is an efficient process for decontamination and recycling of all types of wastewater; the only drawback is that in this type of water the water recovery rate should be approximately 100% (Hilal et al. 2004). The textile industry is a water intensive industry which wastewater is loaded with pollutants (textile dyes, suspended solids, mineral oils, electrolytes, surfactants). Y. Ong et al. (Ong et al. 2014) used polyamide-imide hollow fibre nanofiltration membrane in various operating conditions (temperature range: 25-70℃; solute concentration range: 100-1000ppm; pH range: 3-10) with rejections of various dyes higher than 90%. The membrane permeates NaCl and Na_2SO_4 (over 80% and 90%, respectively) that can be reused in the dyeing process. Liang et al. (Liang et al. 2014) used a positively charged NF hollow fibre membrane that was also used in the treatment of dyes and was able to remove almost 100% dyes at low flow and pressure. A coagulation-flocculation step before nanofiltration can reduce membrane fouling and increase permeate flux. Pulido and Férez (Ochando Pulido and Martínez Férez 2015) examined the performance of a thin-film composite polymeric NF membrane as the tertiary treatment of secondary-treated two-phase olive mill wastewater and the results were high feed recovery (90%) and significant rejection efficiencies for the electro conductivity (58,1%) and organic matter (76,1%). S. Zulaikha et al. (Zulaikha et al. 2014) used NF membranes to treat restaurant wastewater; the NF-90 membrane obtained COD, turbidity, BOD_5 and conductivity removal of, respectively, 97,8%, 99,9%, 86,8% and 82,3%. After the wastewater treatment, the original water flux of the membrane was retrieved by over 50% after a simple rinsing process.

SALINE WATER

The success of a desalination process depends on the feed pre-treatment. Using NF as a pre-treatment prevented seawater reverse osmosis (SWRO) membrane fouling by the removal of turbidity and bacteria and scaling by removal of scale forming hardness ions and lowered required operating pressure by reducing seawater TDS (Hilal et al. 2004). In a process of NF integrated with RO desalination, the NF pre-treatment effectively removed divalent ions (rejections for Ca^{2+}, Mg^{2+}, SO_4^{2-}, HCO_3^- and total hardness of 89,4%, 94,0%, 97,8%, 96,6% and 93,3%, respectively) and monovalent ions (rejection of 40,3% for Cl^- and Na^+) at low pressure (22 bar) (Zhou et al. 2015).

OTHERS

Nanofiltration can also be used to treat hospital wastewater (HWW) effluent, which is toxic for the receptor ecosystems. The common pollutants in HWW can be divided in two categories, macro and micropollutants. The macropollutants correspond to BOD_5, COD, SS (usually 2-3 times higher than in urban wastewater (UWW)), nitrogen and phosphorus compounds and *Escherichia coli*. The micropollutants are mainly pharmaceuticals, detergents and disinfectants. Heavy metals are also found in HWW (Beier et al. 2010; Verlicchi et al. 2010). P. Palma et al. (Palma et al. 2016) characterized and evaluated the efficiency of NF membranes (NF90 and NF270) in this type of wastewater. The membranes had high rejection coefficients for the majority of the studied parameters (>90%) and the permeate concentrations were below limit values. The membranes removed the toxicity detected in the initial samples (NF90 membrane promoted a greater decrease in the toxicity). It

was possible to obtain water with high quality and low ecotoxicological potential, without risks for human populations and endangering the environmental balance.

2.1.2 FOOD AND PHARMACEUTICAL INDUSTRY

Membrane processes are an economically viable way to obtain water which meets the stringent water quality regulation. In the food industry, one of the first industries to use membrane filtration, NF membranes are required to avoid contamination of products and needed to meet the essential quality and safety standards. Its main application is for concentration and demineralization of salty whey, since the presence of monovalent salt ions in whey powders results in a negative sensorial perception of consumers. In contrast, divalent ions contribute to the healthy image of the product. The value of the products increases when monovalent cations are removed (Van der Bruggen, Mänttäri, and Nyström 2008; X.-L. Wang et al. 2009). Separations of mixture solutions of neutral organic solute and electrolyte are important in the food industry. Wang et al. (X.-L. Wang, Zhang, and Ouyang 2002) investigated the possibility of separating saccharides from a NaCl solution by using a NF45 membrane and expected a possible separation of the mixture solutions of bivalent anion electrolytes or neutral organic solutes with few hundreds of MW and univalent anion electrolytes or neutral organic solutes with few 10-folds of MW.

In the pharmaceutical industry, NF technology can be applied to separate amphoteric materials, such as amino acids and proteins, due to the diverse rejection performance for solutes at different pH values showed by commercial membranes. In these separations the most important factors are the isoelectric points and the molecular weight of solutes. Wang et al. (X.-L. Wang, Ying, and Wang 2002) performed permeation experiments of L-phenylalanine (L-Phe) and L-aspartic acid (L-Asp) aqueous solutions with two commercial NF membranes, ESNA2 and ES20. The rejections to l-Phe and l-Asp by ESNA2 membrane are about 0 and 90%, respectively, at a pH range of 4 - 9, while the rejections to l-Phe and l-Asp by ES20 membrane are almost 100%, irrespective of pH value, which indicates that the membranes can concentrate and separate l-Phe and l-Asp effectively by choosing proper conditions, such as the pH value of the solution.

Nanofiltration plays an important role in water treatment, dairy industry and biomedical processes due to the ability to separate monovalent and multivalent ions. Commercially available membranes have good performance in many applications; however, the drive to protect existing water resources and to produce new water resources demands membranes with improved productivity, selectivity, fouling resistance and stability available at lower cost and with fewer manufacturing defects. Better membranes require better materials (Pendergast and Hoek 2011).

2.2 MEMBRANES

The process industries produce a wide variety of chemicals and components which presents the manufacturer with a need for separation, concentration and purification of a range of materials. In the last decades this type of separations are based on one simple concept: a membrane. A membrane is

a thin barrier that permits selective mass transport. It is essentially a barrier that controls the relative rates of transport of various species through itself and, by the feed stream separation, gives one product depleted in certain components and a second product concentrated in these components. The performance of a membrane is defined by two factors: flux (flowrate of fluid passing through the membrane per unit area of membrane per unit time) and selectivity (fraction of solutes and particulates in the feed retained by the membrane). An ideal membrane would have high selectivity and permeability; however the attempt to maximise one factor implies a reduction in the other. It would have also chemical resistance (to both feed and cleaning fluids), mechanical and thermal stability, fouling resistance, manufacturing reproducibility, low manufacturing cost and ability to be packaged into high surface area modules. The main uses of membranes in industry are the filtration of suspended solids from liquid and gases containing dissolved solids, the removal of macromolecules and colloids from liquids containing ionic species, the separation of mixtures of miscible liquids, the selective separation of gases and vapours from gas and vapour streams, the selective transport of ionic species and the virtually complete removal of all material, suspended and dissolved, from water (Pinnau and Freeman 1999; Scott and Hughes 1997).

2.2.1 MEMBRANES STRUCTURE

The functioning of a membrane depends on its structure, as it determines the mechanism of separation and, therefore, its application. The solid membranes have two types of structures, symmetric (uniform structure throughout the entire membrane thickness) and asymmetric (gradient in structure). The separation properties of symmetric membranes are determined by the entire structure, while in asymmetric membrane are determined primarily by the densest region in the membrane (Pinnau and Freeman 1999; Scott and Hughes 1997).

SYMMETRIC MEMBRANES

Symmetric membranes, which by definition are of a uniform structure, are of three general types (with approximate cylindrical pores, porous and non-porous, as shown in Figure 2-2) and can be produced by sintering or stretching (microporous membranes), casting (ion-exchange membranes), phase inversion (pore membranes used in MF and UF) and extrusion (diffusion membranes for gas permeation and pervaporation) (Pinnau and Freeman 1999; Scott and Hughes 1997).

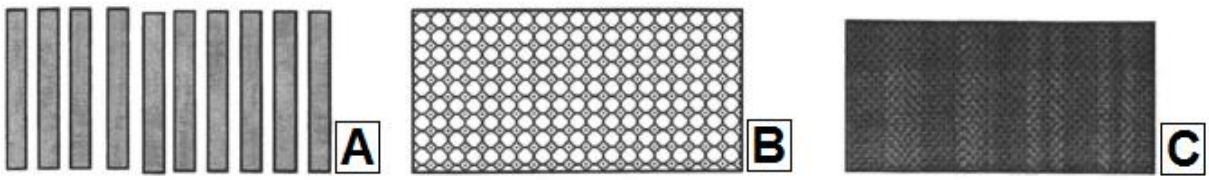

Figure 2-2 – Schematic representation of symmetric membrane structures: A) porous cylindrical; B) porous web or sponge; C) dense polymer film (Pinnau and Freeman 1999)**.**

Inorganic materials such as microporous glass and ceramics are used to manufacture symmetric membranes and can be coated to form composites to introduce specific improved properties (Pinnau and Freeman 1999; Scott and Hughes 1997).

ASYMMETRIC MEMBRANES

Asymmetric membranes, currently the most employed membranes in industry, have variable structure and transport properties across the membrane thickness. Its structure normally consists of a thin dense layer (active layer, 0,1 – 1 μm) supported by a highly porous thick support layer (100 – 200 μm), as presented in Figure 2-3. The dense layer provides the majority of selectivity for the membrane, due to its chemical nature, size of pores and thickness, and the support layer is assumed to provide mechanical support for the thin and fragile selective layer and a resistance-free path for water and permeated solutes (Pendergast and Hoek 2011; J. Wang et al. 2014). Asymmetric membranes can be categorized into three basic structures: A) integrally-skinned with a porous skin layer, B) integrally-skinned with a dense skin layer and C) thin-film composite membranes (Figure 2-4).

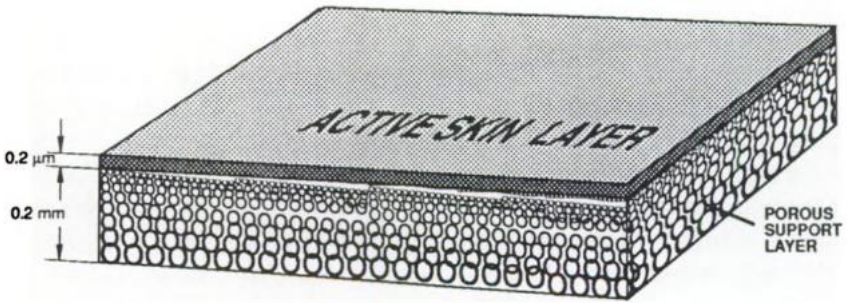

Figure 2-3 – Asymmetric membrane structure (Scott and Hughes 1997)**.**

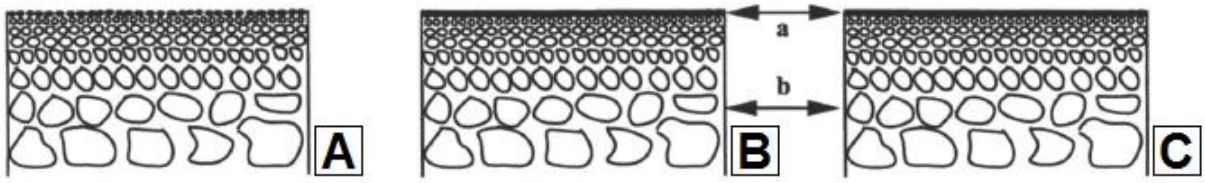

Figure 2-4 – Schematic representation of asymmetric membrane structures: A) integrally-skinned (porous skin layer); B) integrally-skinned (non-porous skin layer) – a) selective skin layer (material A) – b) microporous support (material A); C) thin-film composite – a) selective coating layer (material A) – b) microporous support (material B) (Pinnau and Freeman 1999)**.**

Thin-film composite membranes consist of at least two structural elements made from different materials: a porous support that provides mechanical strength and a thin selective top-layer responsible for the separation. This characteristic enables the tailoring of membrane function for specific applications and, for that, gives potential improvements to the membrane. They are usually applied in processes in which permeation is controlled by the solution-diffusion mechanism (nanofiltration, reverse osmosis, gas separation and pervaporation). The selective layer can be applied by lamination, solution coating, interfacial polymerization or plasma polymerization methods (Pinnau and Freeman 1999; Scott and Hughes 1997).

The integrally-skinned asymmetric membranes are prepared by the phase inversion method developed by Loeb and Sourirajan, which confers the ability to vary the surface morphology (pore size) of the active layer. In the phase inversion process induced by immersion precipitation, it is necessary to prepare a ternary casting solution (polymer-solvent-nonsolvent), spread the solution as a

thin film, partially evaporate the solvent and immerse it into a nonsolvent bath (gelation of the polymer film). Upon immersion of the cast solution into a liquid, which is a non-solvent for the polymer but miscible with the solvent, an asymmetric structure with either a porous or non-porous skin layer is formed. The structural gradient in integrally-skinned asymmetric membranes results from a very steep polymer concentration gradient in the nascent membrane at the onset of phase separation. Phase separation occurs by exchange of solvent and nonsolvent and an asymmetric membrane with a denser top layer is formed. The final porous structure of the entire membrane, including the active layer, and hence the subsequent performance (permeability and selectivity) depends on the method steps. The phase inversion technique relies upon the controlled interaction of solvent and nonsolvent solutions to induce a phase separation transitioning a polymer from a liquid dispersion into a solid state (Murphy and de Pinho 1995; Pendergast and Hoek 2011; Pinnau and Freeman 1999; Sadrzadeh and Bhattacharjee 2013; Scott and Hughes 1997).

The morphology and separation performance of the synthesized membranes can be controlled by numerous parameters, such as solvent type, polymer type and concentration, nonsolvent system type and composition, additives to the polymer solution and film casting conditions. Introducing additives into the casting solution is the most important technique for improving performance of the resultant membrane. The role of organic and inorganic additives, such as polymeric additives, alcohols, surfactants and salts, was mainly reported as pore forming agents enhancing permeation properties (Sadrzadeh and Bhattacharjee 2013).

Cellulose acetate (CA) is one of the first polymer membranes employed in aqueous based separations, with properties ranging from MF to RO. The CA membranes are hydrophilic, offer a good fouling resistance due to their smooth surfaces, as reported by M. Elimelech et al. (Elimelech et al. 1997), are relatively inexpensive and easy to manufacture. However, cellulose acetate presents low oxidation (pH between 4 and 6), chemical (chlorine intolerance), thermal (temperatures lower than 30°C), and mechanical resistance, since it causes degradation of the polymer. Besides, CA membranes are biodegradable and can be consumed by organisms growing in biofilms. Therefore, the modification of cellulose acetate gains importance (Guillen et al. 2011; Pendergast and Hoek 2011; Sivakumar, Mohan, and Rangarajan 2006).

Other types of polymers used to fabricate membranes are polysulfone (PSf), polyethersulfone (PES), sulfonated PSf or PES, polyacrylonitrile (PAN), polypropylene (PP), poly-tetrafluoroethylene (PTFE or Teflon) and polyvinylidine fluoride (PVDF). These materials exhibit excellent permeability, selectivity, and stability in water treatment applications (Guillen et al. 2011; Pendergast and Hoek 2011).

2.2.2 MEMBRANE SEPARATION PROCESSES

In membrane processes, it is possible to operate in two modes: dead-end mode filtration (conventional filtration) and cross-flow filtration (tangential filtration). In dead-end mode, the feed flow is perpendicular to the membrane surface and the retained particles accumulate on the surface, forming a filter cake that increases with time and decreases the permeation rate. To avoid the cake build-up, an alternative cross-flow operation can be used (Figure 2-5), in which a feed stream flows tangentially

to the membrane surface and, as a result of the application of an appropriate driving force, a permeate passes through the membrane (Scott and Hughes 1997).

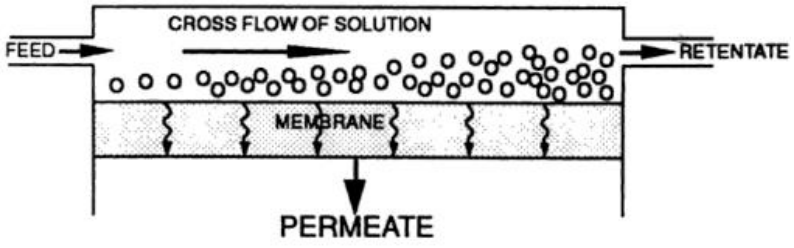

Figure 2-5 – Cross-flow membrane separation (Scott and Hughes 1997)**.**

When the permeate is collected, the feed is gradually reduced in concentration of the permeating species along the membrane until it exits as retentate. Cross-flow velocities should be high to minimise the impact of the accumulation of particulate material, although during a continued operation a decline in flux rate occurs due to the fouling formation at the surface of the membrane (Scott and Hughes 1997).

2.3 FOULING

Membrane fouling is the major drawback for pressure-driven processes, as it causes severe flux decline, reducing the production efficiency and increasing energy consumption. Membrane fouling can be of different types depending on the solutes (biofouling, organic and inorganic fouling) and of different degrees (reversible and irreversible). The fouling formation largely varies with hydrodynamic conditions and foulant−membrane or foulant−foulant interactions, which, in turn, depends on membrane characteristics, feed composition and operating parameters. The different fouling types and formation mechanisms are summarized in Table 2-1 (Zhang et al. 2015).

Organic fouling is generally produced by NOM, proteins and polysaccharides and has four mechanisms of formation: complete pore blocking, intermediate blocking, standard blocking and cake-layer formation (Figure 2-6). Inorganic fouling appears due to the deposition of inorganic matter on the membrane surface and, subsequently, the formation of a cake layer by crystallization ($CaSO_4$ and $CaCO_3$ as the main components) (Zhang et al. 2015). Biofouling occurs due to the deposition, accumulation, growth and metabolism of microorganisms on a membrane surface. The membranes adsorption of large molecular weight metabolic products, such as humus, polysaccharides fats and microorganisms, promotes the growth of a biofilm and provides ideal living conditions for microorganisms, resulting in irreversible fouling and flux decline (Zhang et al. 2015).

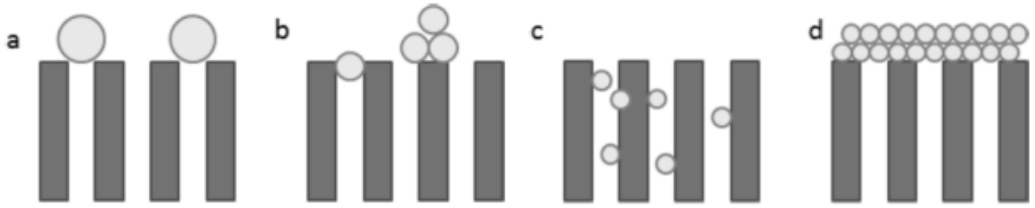

Figure 2-6 – Mechanisms of organic fouling formation: a) complete pore blocking; b) intermediate blocking; c) standard blocking; d) cake-layer formation (Zhang et al. 2015)**.**

Table 2-1 – Summarization of fouling types (Zhang et al. 2015)**.**

Classification Standard	Fouling type	Description
Fouling Mechanism	concentration polarization	particle accumulation and deposition on the membrane with good solubility and mobility
	adsorption fouling	particle adsorption on the membrane surface or pore wall with accumulation by hydrophobic and electrostatic adsorption
	cake, gel or scaling layer	particle precipitation, aggregation, or gelation on the membrane or on the adsorption fouling layer
	pore blocking	particle entrapment in the pores with no aggregation
	biofouling	microorganism adherence or growth on the membrane
Fouling Location	external fouling	fouling on the membrane
	internal fouling	fouling in the membrane
Fouling Reversibility	reversible fouling	fouling layer can be removed when pressure is released or by specific physical cleaning
	irreversible fouling	fouling layer cannot be removed when pressure is released or by specific physical cleaning
Fouling Composition	inorganic fouling	fouling by inorganic scaling or adsorption of multivalent ions
	organic fouling	fouling by organic matters
	combined fouling	fouling by organic−inorganic interactions

The formation of a biofilm in an aqueous environment is represented in Figure 2-7: in the presence of organic matter, a conditioning film of adsorbed components is formed on the surface prior to the arrival of the first organisms (1); the microorganisms are transported to the surface through diffusion, convection, sedimentation or active movement (2); initial microbial adhesion occurs (3); attachment of adhering microorganisms is strengthened through exopolymer production and unfolding of cell surface structures (4); surface growth of attached microorganisms and continued secretion of exopolymers (5); localized detachment of biofilm organisms caused by occasionally high fluid shear or other detachment operative forces (6). Localized detachment of biofilm organisms starts after initial adhesion. As the number of biofilm organisms increases, growth rates will decrease due to nutrient and oxygen limitations and accumulation of organic acids, eventually leading to a stationary biofilm thickness, where adhesion and growth counterbalance detachment (Gottenbos, Van Der Mei, and Busscher 1999).

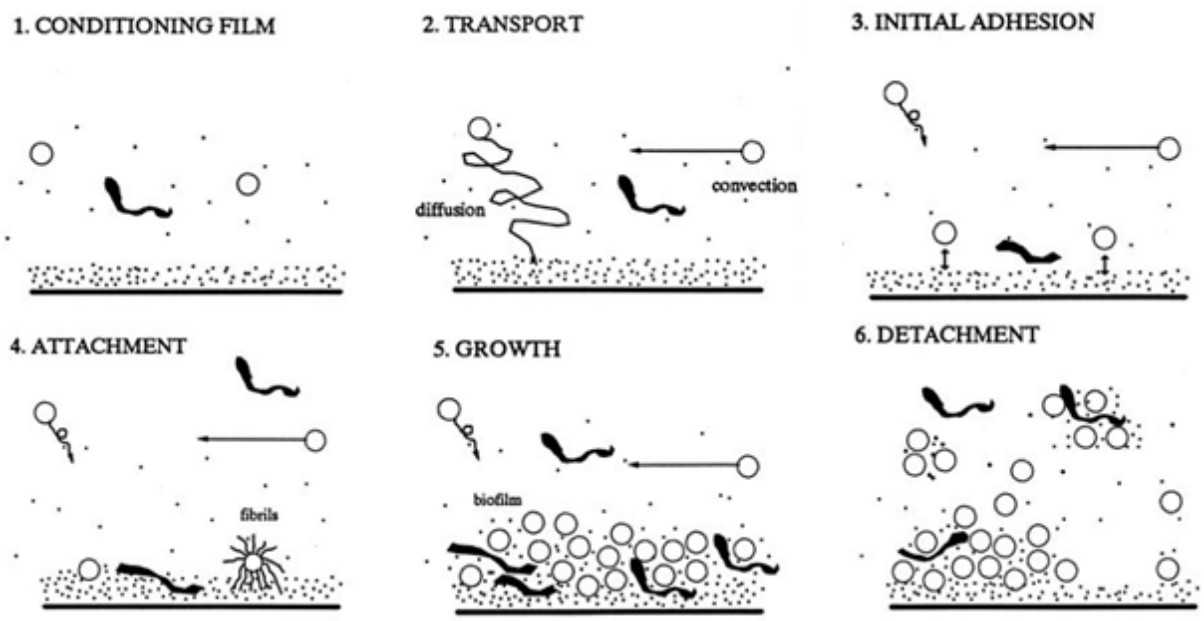

Figure 2-7 – Schematic, sequential presentation of the steps in biofilm formation (adapted from (Gottenbos, Van Der Mei, and Busscher 1999)**).**

To study the population growth the microorganisms need to be in a phase where the chemical and physiological properties are most uniform. This phase, the exponential phase, is characterized for a constant rate of growth, without limitations of nutrients and other components (Figure 2-8) (Prescott, Klein, and Harley 2002). The phase identification can be made spectrophotometrically, since there is a relation between optical density (OD) and cell number: 10^9 cells/OD (Myers, Curtis, and Curtis 2013).

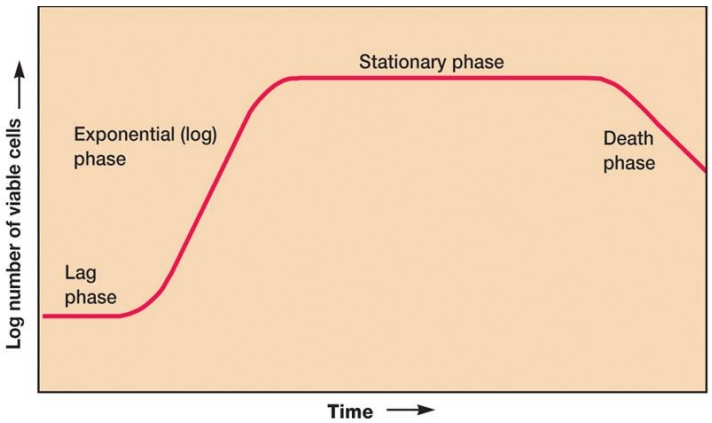

Figure 2-8 – Microbial Growth Curve in a Closed System (Prescott, Klein, and Harley 2002)**.**

2.3.1 CONVENTIONAL DISINFECTION METHODS

To comply with the regulations, disease-causing organisms present in water supply have to be destroyed or inactivated by means of disinfection. Primary disinfection provides the necessary inactivation of bacteria and viruses in source water, while secondary disinfection maintains a residual disinfectant that prevents the regrowth of microorganisms in the water distribution system. Disinfection treatment methods include chlorination, chloramines, ozone and ultraviolet light; the advantages/disadvantages of each technique are presented in Table 2-2. Disinfection effectiveness is

evaluated by analysing an indicator organism (total coliform bacteria); however harmless, its presence indicates the possible survival of pathogens (Center for Environmental Research Information 1990; National Environmental Services Center 1966).

Table 2-2 – Advantages and disadvantages of conventional disinfection methods (Center for Environmental Research Information 1990; National Environmental Services Center 1966; US Environmental Protection Agency 1995)**.**

Disinfection Method	Advantage	Disadvantage
Chlorination	- Economical - Easy to operate - Very effective - Appropriate as both a primary and secondary disinfectant.	- Potential for harmful by-products under certain conditions - Safety problems with gaseous units - Corrosive effect of sodium hypochlorite
Chloramine	- Appropriate to use as a secondary disinfectant - Produces few disinfection by-products	- Week disinfectant - Imparts a disagreeable taste and odour to the water
Ozone	- Very effective - Minimal harmful by-products - Requiring shorter contact time and dosage than chlorine	- Relatively high cost - Ozone gas is unstable and must be generated onsite - Requires a secondary disinfectant
Ultraviolet Light (UV)	- Very effective for viruses and bacteria - Easy to operate and maintain - Produces no known toxic by-products - Safer than chlorine for operations	- Inappropriate for surface water - Requires a secondary disinfectant

According to M. Khan et al. (M. T. Khan et al. 2015), chlorine is used to control/prevent biofouling in cellulose triacetate (CTA) RO membranes used for desalting seawater in the Middle East region. It was identified biofilm development in the membranes, which indicates an incapability of chlorination on preventing its formation. Biofilm forming bacteria can sustain chlorine disinfection and acidic cleaning either because of their developed resistance against acidic solution or because of the protection given by the fouling matrix accumulated around them. N. Weerasekara et al. (Weerasekara, Choo, and Lee 2016) also stated that chlorine, even using an high dosage, is insufficient for preventing biofouling. Thus, chlorination is not recommended as a pre-treatment due to its ineffectiveness in deterring biofouling and the high risk of generating toxic disinfectant by-products.

L. Applegate et al. (Applegate, Erkenbrecher, and Winters 1989) used chloramine to control biofouling in a surface seawater RO plant in Middle East using Permasep^{R} B-10 permeators. The chloramine (disinfectant generated *in situ*) was used as an alternative to chlorine and showed to be a better disinfectant and to reduce bacterial after-growth and biofouling.

The use of NF membrane with pre-ozonation for highly-concentrated surface water brine treatment was studied by M. Park et al. (Park et al. 2016). The organic fouling potential was significantly reduced using relatively low ozone doses (cake filtration as the dominant fouling mechanism) and is considered a viable option to achieve higher recovery of NF membrane systems.

The effect of UV irradiation on NF membrane biofouling has been studied in pilot scale installations by C. Marconnet et al. (Marconnet et al. 2011) using two identical parallel membrane pilots and a low pressure UV reactor. UV irradiation was an efficient NF pre-treatment to reduce membrane biofouling as it reduced the extent of biofouling (the global quantity of deposit, the sessile bacteria concentration and the amount of extracellular polymeric substances present on the surface of the membrane) and had a favourable effect on the water permeability of the membranes.

2.3.2 USE OF SILVER NANOPARTICLES

In nanotechnology, a nanoparticle is a material with dimensions of 0,1 – 100 nm that behaves as a whole unit in terms of its transport, properties and unique characteristics. Nanoparticles, in particular metallic nanoparticles (copper, zinc, titanium, magnesium, gold and silver), have unique optical, electrical and thermal properties and are being incorporated into products for their remarkable antibacterial effect, due to their extremely large surface area, which provides better contact with microorganisms. However, greater attention has been given to silver nanoparticles (AgNP) since they exhibit strong antimicrobial effectiveness against bacteria, viruses and eukaryotic microorganisms due to the continuous release of a low level of silver ions. This release is a function of the nanoparticle size (smaller particles have a faster release rate), the temperature (higher temperatures accelerate dissolution) and exposure to oxygen, sulphur and light. It is important to understand the relationship between the physical and chemical properties of AgNP and their potential risk to the environment and human health. Understanding how their size, shape, surface and aggregation state change after integration into a target application is critical for optimizing performance (C. Caro et al. 2010; Rauwel et al. 2015).

PREPARATION METHODS

The properties of nanoparticles depend on synthesis techniques (radiation, chemical, photochemical and electrochemical) and the kind of stabilising and reducing agent used (nature, concentration, addition rate and mixing order). Chemical reduction of silver salts, such as silver nitrate, by inorganic compounds, as sodium borohydride, is the most frequently applied method for the preparation of stable silver nanoparticles and its colloidal dispersions in water or organic solvents, once it is the most versatile, economical and easy method to control the shape and size of metal nanoparticles and allows monitoring the growth process by spectroscopic methods, using a UV-Vis spectrophotometer.

The addition of a stabilising agent (polymers as polyvinylpyrrolidone (PVP)) is essential to prevent the agglomeration of colloidal particles in the dispersion, as it coats the particle surface and causes a steric stabilisation (Z. Khan et al. 2011; Widoniak, Eiden-Assmann, and Maret 2005; Zielińska et al. 2009). J. Widoniak et al. (Widoniak, Eiden-Assmann, and Maret 2005) found that the average particle sizes decreases with an increase of silver precursor (silver nitrate), reducing and stabilising agents concentration. Furthermore, the protecting agents also act reductively and support the activity of reducing agents. M. Maillard et al. (Maillard, Giorgio, and Pileni 2003) found that the initial synthesis conditions influence the solution colour, from red for the lowest reducing agent ratio to green and grey for the highest. A. Zielińska et al. (Zielińska et al. 2009) used silver nitrate as precursor of silver nanoparticles and PVP as stabilizer and a greenish colloid was obtained. The silver colloids spectra contained a strong band close to 410 nm, confirming the reduction of silver ions to Ag^0.

BIOFOULING CONTROL

Since the middle of the last century that silver is known for its antibacterial properties against *Staphylococcus aureus*, *Pseudomonas aeruginosa* and *Escherichia coli* (C. Caro et al. 2010). Although the exact mechanism of action of silver nanoparticles on the microbes is not yet understood, some suggestions have been made according to the morphological and structural changes found in the bacterial cells. The silver nanoparticles get attached to the cell membrane, penetrating inside the bacteria and attacking the respiratory chain and cell division, which leads to cell death. This effect is enhanced with the release of silver ions in the cells (Rai, Yadav, and Gade 2009). According to Ouay and Stellacci (Le Ouay and Stellacci 2015), Ag^+ is the actual antibacterial agent of silver nanoparticles, which act as a silver ions reservoir from where the trapped silver ions are released, although the role of metallic silver nanoparticles cannot be excluded. This oxidation can be due to the presence of dissolved atmospheric oxygen in the colloidal solution.

R. Das et al. (Das, Gang, and Nath 2011) investigated the antimicrobial activity of linoleic acid capped silver nanoparticles against *Staphylococcus bacillus*, *Staphylococcus aureus* and *Pseudomonas aeruginosa*, which revealed an effective growth inhibition by more than 97%. The diameter of inhibition zones around the disk containing silver nanoparticles was 9 mm, 11 mm and 10 mm, respectively. This high activity is attributed to the dissolution of the released Ag^0 and Ag^+ clusters.

W. Chou et al. (Chou, Yu, and Yang 2005) investigated the antibacterial activity of silver-loading asymmetric cellulose acetate hollow fibre membrane against *E. coli* and *S. aureus*. After immersing in water bath for 180 days, the silver content decreased to 60% in the bulk of the hollow fibres and to 10% on the surface comparing with the content after the manufacturing process. Despite the leaching of the silver particles, the membranes still showed antibacterial activity. However, after permeating with water for 5 days, the silver content in the hollow fibres decreased and did not show antibacterial activity. To have a long-term antibacterial effect, the concentration of silver precursor should be 0,01% – 0,1 wt.%.

D. Koseoglu-Imer et al. (Koseoglu-Imer et al. 2013) prepared polysulfone membranes with different concentrations of silver nanoparticles (0% – 1 wt.%) and observed the following: after the addition of AgNP there was a change in the surface structure of bare PS membrane; the increasing concentration

of AgNP leads to aggregation; hydraulic permeability increases and adsorptive fouling decreases with low concentrations of silver nanoparticles (up to 0,25wt.%), comparing with the bare membrane; the growth of bacterial colonies decreased with increasing silver nanoparticles concentration; the ionic silver loss from the composite membranes during pure water filtration was minimal.

In the study of J. Li et al. (J. H. Li et al. 2013), silver nanoparticles improved poly(vinylidine fluoride) membrane surface hydrophilicity and antifouling performance. The enhancement of membrane surface hydrophilicity with the addition of silver nanoparticles was verified by the decrease of the water contact angle. Relatively to the antifouling performance the incorporation of silver nanoparticles decreases organic and biofouling activity. The most concentrated membrane reduced irreversible resistance ratio in almost 80% compared with the virgin PVDF membrane. Using the inhibition zone method to conclude about biofouling activity against *S. aureus* and *E. coli*, it was evident that the membranes with AgNP incorporated had an antibacterial zone, contrary to the result obtained for the simple membranes.

There are several types of nanoparticles that can be incorporated into polymer membranes capable of control biofouling (Arthanareeswaran and Thanikaivelan 2010; Asapu et al. 2014; Jhaveri and Murthy 2016). Silver nanoparticles are suitable for the improvement of membrane surface hydrophilicity and antifouling performance under the proper conditions.

2.3.3 USE OF ZEOLITES

A zeolite is a crystalline, hydrated aluminosilicate of alkali and alkaline earth cations having a nanometre, open, three-dimensional structure. Zeolite crystals consist of a three-dimensional cross-linked $(Si/Al)O_4$ tetrahedral framework, in which each Al or Si atom occupies the vertex of a network connecting four oxygen atoms. Zeolites are able to lose and gain water reversibly, present in the large structural cavities and the entry channels leading into them, and to exchange extra framework cations, without changing the crystal structure. The “molecular sieve” property of crystalline zeolites, due to a very regular pore structure of molecular dimensions, selectively sorts molecules based primarily on a size exclusion process. The weakly bonded extra framework cations can be exchanged by washing with a strong solution of another cation. The zeolite cation-exchange capacities (CEC) depend on temperature, water content, ion type and the ratio of Si to Al atoms in the matrix. The unique adsorption, cation-exchange, dehydration–rehydration and catalytic properties of the zeolites allow their use in industrial, agricultural, environmental and biological technology. The most common zeolite employed in membranes are MFI-type, sodalite (SOD) and Linde Type A (LTA) (Mumpton 1999; Pendergast and Hoek 2011).

ZSM-5 ZEOLITE

Zeolite ZSM-5 (MFI), the most commonly applied zeolite in membranes, is composed of a unit cell with the chemical formula $Na_nAl_nSi_{96-n}O_{192}\cdot 16H_2O$ (n<27), with a structure composed by straight channels in one direction and perpendicular sinusoidal channels that are not interconnected (Figure 2-9). Zeolites

have a high thermal stability (up to 1100℃) (Ali, Brisdon, and Thomas 2003; Pendergast and Hoek 2011; Structure Commission of the International Zeolite Association (IZA) 2007).

When incorporating MFI-type zeolite in porous membranes for water separations, crystals should be oriented to the permeation direction, as pore size determines ion selectivity and framework density determines water permeability. The ability to replace atoms *via* ion exchange may imbue the zeolite with alternate charge and structural properties (sieve property, for example). Additionally, both the ion and water molecule mobility through a zeolite depend upon the relative density of the framework structure; open porous structures will facilitate less hindered transport (Pendergast and Hoek 2011).

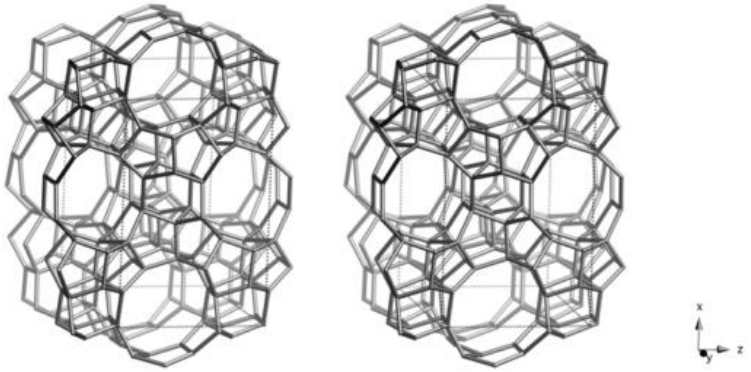

Figure 2-9 – ZSM-5 framework viewed along [010] (Structure Commission of the International Zeolite Association (IZA) 2007)**.**

According to P. Lalueza et al. (Lalueza et al. 2011), silver exchanged ZSM-5 zeolite has higher bactericidal effect comparing with silver nanoparticles, result related with the total amount of ionic silver bioavailable, the oxidation state of the silver species and the particle size of the material.

BIOFOULING CONTROL

Zeolites can be used in biofouling control, with and without ion exchange. However, antibacterial activity is achieved with cation-exchanged zeolites. Zeolites are considered an inorganic reservoir for hosting ions that regulate their release, providing a rigid and stable structure. The silver ions embedded in zeolites are responsible for the antimicrobial activity, most likely due to their intake by bacterial cells when in contact with silver zeolite, which inhibits cellular functions and damages the cell, or due to the generation of reactive oxygen molecules, which inhibit the respiration (Ferreira et al. 2012; Rai, Yadav, and Gade 2009).

L. Dong et al. (Dong et al. 2015) evaluated the bacteria adhesion, bacteria inactivation and biofilm formation in Linde Type L (LTL) zeolite nanoparticles embedded polysulfone ultrafiltration membrane. The anti-adhesion efficiency to *Escherichia coli* and *Pseudomonas aeruginosa* was high (reduction of 61% and 97%, respectively), which resulted in an enhanced anti-biofouling ability, demonstrated by the reduced biofilm thickness of *P. aeruginosa* compared with the PSf membrane. The embedded LTL nanoparticles showed no bactericidal effect on *E. coli*.

The antimicrobial activity of faujasite (FAU) zeolites doped with silver was reported by L. Ferreira (Ferreira et al. 2012) using bacteria (*Escherichia coli* and *Bacillus subtilis*) and yeast (*Saccharomyces cerevisiae* and *Candida albicans*). Contrary to the silver exchanged samples, the virgin zeolites did not

show microbial inhibitory effects, indicating that this behaviour is due to the presence of silver. The Y FAU zeolite displayed lower minimum inhibitory concentration (MIC) for the bacteria (0,2 mg/mL) compared with X FAU (0,3 mg/mL), which could be explained by the presence of metallic silver in the last zeolite verified by XPS analysis. The effect of the silver zeolites on the yeast cultures were less sensitive than bacteria (1,0 mg/mL), which can be explained by the complex cellular organization of eukaryotic cells and the structure of the cellular wall.

D. Boschetto et al. (Boschetto et al. 2012) prepared polyethylene composite films with silver exchanged zeolite-Y (5% silver) with application in food industry, such as the inclusion of antimicrobial substances in plastic films with a controlled release on the surface of the food, inhibiting the growth of microorganisms, increasing the shelf life and safety of the product. The zeolite Y without exchanged silver showed no antimicrobial growth, while silver zeolite inhibited the growth of *E. coli* for concentrations higher than 0,5 $mg_{zeolite}$/mL within 24 hours, which reveals an effective antimicrobial activity. When incorporated in the polymer, by pressing and wet casting, the zeolite impregnated with silver showed inhibitory effects against bacteria, evidenced by the inhibition halos obtained (3 mm and 7 mm, respectively), which did not occurred with the free-zeolite polymer. This antimicrobial activity difference may be due to the high temperatures used in the pressing process (80 – 130℃), which may affect the silver stability, causing its reduction. Approximately 56% of silver was leached from the zeolite to the medium, which contrasts with the 5% obtained when the zeolite is trapped into a polymeric matrix. A Luria Bertani medium was used for leaching tests instead of water, since ionic silver release can be increased by ion exchange due to the presence of other cations in water. This situation leads to a lower release rate due to increased resistance for diffusion of the ions from the zeolite to the bulk medium.

Higher bioavailability of cationic silver results in a higher bactericidal action of the silver-carrier material. Silver ions bind particularly to zeolites, resulting in a gradual, stable and long-lasting release of silver ions from zeolite, resulting in an increased antimicrobial potential, compared with silver nanoparticles. However, further studies are required to clarify the possible long-term toxic effects of silver (Boschetto et al. 2012; Lalueza et al. 2011; Matsuura et al. 1997).

The increasing public awareness and concern over the safety of products, processes and conditions inspire and demand the development of new safe and cost-effective antimicrobial solutions, encouraging the emergence and growth of new materials with antimicrobial properties. Mixed matrix membranes seek to take advantage of both the low cost and ease of fabrication of organic polymeric membranes and the mechanical strength and functional properties of inorganic materials (Ferreira et al. 2012; Pendergast and Hoek 2011).

3 EXPERIMENTAL

3.1 EXPERIMENTAL PLANNING

Asymmetric cellulose acetate (CA) and mixed matrix membranes – CA/silver nanoparticles, CA/ZSM-5 zeolite and CA/silver loaded zeolite – were prepared by the wet phase inversion method. In the case of mixed matrix membranes, besides the conventional polymeric casting solutions (polymer, solvent system and additives), special attention is required for the incorporation of silver nanoparticles, zeolite and silver loaded zeolite. To manufacture the different membranes, it was necessary to undertake previous steps: preparation of silver nanoparticles, zeolite and casting solutions (characterized via UV-Vis spectroscopy) and the casting of the membranes. An annealing treatment had to be performed to obtain nanofiltration membranes. In order to characterize the prepared membranes, different experiments were performed: evaluation of the permeation performance, electrochemical studies, thermogravimetric analysis, determination of the zeta potentials and evaluation of the bactericidal properties (Figure 3-1). All the reagents were used as-received, without further purification.

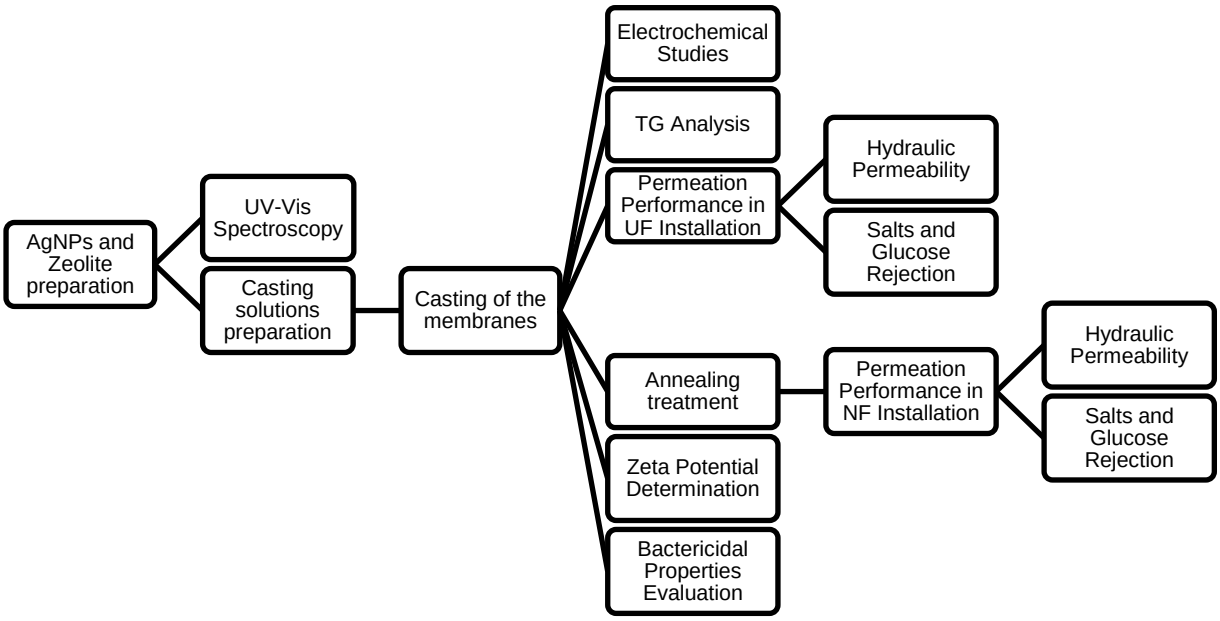

Figure 3-1 – Flowchart of the experiments performed.

3.2 MANUFACTURING OF THE MEMBRANES

3.2.1 PREPARATION OF SILVER NANOPARTICLES

To manufacture the silver containing membranes, the silver nanoparticles were prepared *ex-situ* according to the synthesis protocol of Figueiredo et al. 2015 and using the concentrations presented in Beisl, 2015. The concentrated nanoparticle aqueous solution was obtained by the reduction of silver nitrate with sodium borohydride (Equation 3.1), both dissolved in an aqueous solution of polyvinylpyrrolidone (PVP), which is used to protect the silver nanoparticles from growing and agglomerating (H. Wang et al. 2005).

The nanoparticle synthesis protocol to prepare 8 mL of the silver nanoparticle suspension started with the preparation of an aqueous solution of PVP (0,08 g of PVP in a total volume of 8 mL), followed by the dissolving of 0,4988 g of $AgNO_3$ and 0,03026 g of $NaBH_4$, separately, in a total volume of 4 mL of the PVP solution previously prepared. An Erlenmeyer flask filled with the $AgNO_3$ solution was submerged in an ultrasonic bath and the $NaBH_4$ was dropwise added to the $AgNO_3$ solution while the Erlenmeyer flask was being shaken. The suspension had to be stored in a fridge without exposure to light. The chemicals used are stated in Table 3-1. To obtain a complete dissolution of the chemicals, mechanical agitation and ultrasonic bath were used. The concentrations used to prepare the nanoparticle suspension are presented in appendix 1A.1, Table A-1.

The estimated weight of the silver nanoparticles was obtained based on the volume of the solution that was added and its concentration in silver nitrate.

$$AgNO_3 + NaBH_4 \rightarrow Ag^0 + 0{,}5H_2 + 0{,}5B_2H_6 + NaNO_3 \quad (3.1)$$

Table 3-1 – Chemicals used in the preparation of silver nanoparticles suspension.

Chemical	Manufacturer	LOT	Purity	MW (g/mol)
PVP	BDH Chemicals	4722900G	>88,18%	~44.000
$AgNO_3$	Panreac	0000172531	>99,8%	169,87
$NaBH_4$	Panreac	0000182216	>96%	37,83

Figure 3-2 – Silver nanoparticles suspension.

It is visible in Figure 3-2 that the obtained suspension had a homogeneous greenish brown tone. The silver concentration of the prepared silver nanoparticles suspension was 0,040 g_{Ag}/mL and the weight percentage of silver in the suspension 3,75 wt.%.

3.2.2 PREPARATION OF THE ZEOLITE

Of the seven membranes prepared, five have embedded zeolite: one with only zeolite and the other four with silver in its structure. The zeolite used was ZSM-5, with a molar ratio of Si/Al of 15 and in the ammonium form ($Si_{15}Al(O_2)_{16}NH_4$). To introduce the silver ions in the zeolite, a 0,1 M $AgNO_3$ aqueous solution was prepared and mixed with the zeolite (20 g of zeolite in 400 mL of the $AgNO_3$ solution) during three days with a magnetic stirrer at 600 rpm and without exposure to light to avoid the reduction of the silver. After the complete exchange, the suspension was filtrated and purged with deionized water. The quantity of silver present in all the solutions was measured by titration after Mohr's method (Canterbury 2015) in order to determine the silver content of the zeolite after the exchange. This is obtained by the difference between the content in the mother solution (400 mL) and in both filtrate (395 mL) and purging water (787 mL), which were, respectively, 10,5 mmol/L, 76,0

mmol/L and 0,7 mmol/L, assuming that all silver ions are either in the zeolite or in the filtrate and purging water. Therefore, the ZSM-5 zeolite used has a silver content in weight of 4,85 wt.% ($Si_{15}Al(O_2)_{16}Ag$). After the titration, the silver containing zeolite was dried under vacuum and then in a drying oven at 140℃ for 24 hours. Both zeolites, with and without silver, were at last calcined at 500℃ for 24 hours in a muffle furnace. The chemicals used in the preparation and titration of the zeolite are stated in Table 3-2.

Table 3-2 – Chemicals used in the preparation and titration of the zeolite.

Chemical	Manufacturer	LOT	Purity	MW (g/mol)
ZSM-5	Zeolyst International	2493-60	-	-
$AgNO_3$	Panreac	0000172531	>99,8%	169,87
NaCl	VWR	11D120005	>99,9%	58,44

Figure 3-3 – ZSM-5 zeolite after calcination: A) zeolite without silver; B) zeolite with embedded silver.

The calcined zeolites presented in Figure 3-3 have no visible difference, except the agglomeration in the silver containing zeolite due to the previous ion exchange procedure. A grey colour appeared in some parts of the zeolite with embedded silver, result of silver oxidation by exposure to light.

3.2.3 PREPARATION OF THE CASTING SOLUTIONS

To manufacture the membranes used, it was necessary to prepare a casting solution, which consisted of a polymer, cellulose acetate (CA), and a solvent system, acetone and formamide (strong and weak solvent, respectively). In order to improve the bactericidal effect, the silver nanoparticles suspension and the zeolite with and without embedded silver can be added to the casting solution. The solutions prepared were mixed in a bottle and agitated until CA was completely dissolved in a P Selecta Vibromatic mechanical agitator (Figure 3-4) at 550 rpm.

Figure 3-4 – P Selecta Vibromatic mechanical agitator.

The different membranes prepared were of cellulose acetate without incorporated materials, with silver nanoparticles, with zeolite and with different percentage of silver containing zeolite and the according designation and abbreviation were, respectively, CA400-30 (CA), CA400-30Ag0,14 (CA/Ag0,14),

CA400-30ZSM5 (CA/ZSM-5) and CA400-30ZAg0,005 (CA/ZAg0,005), CA400-30ZAg0,03 (CA/ZAg0,03), CA400-30ZAg0,07 (CA/ZAg0,07), CA400-30ZAg0,14 (CA/ZAg0,14). The percentage shown corresponds to the silver content in the membrane.

The preparation mode of the casting solutions was different accordingly to what was added. In all the membranes, the addition sequence was cellulose acetate, formamide and acetone (added at last for being the most volatile). In the silver nanoparticles membrane, the respective suspension was added to the acetone in a flask, homogenised and then poured into the bottle with the cellulose acetate and formamide. In the membranes with zeolite, this one was added after the polymer.

The chemicals used are presented in Table 3-3 and the quantities in Table 3-4 and Table 3-5. The ones that contain silver were protected from light with aluminium foil and all the flasks were covered with duct tape to avoid acetone evaporation. The added zeolite was in the powder form to avoid grains in the casting solution.

Table 3-3 – Chemicals used in the preparation of the casting solutions.

Chemical	Manufacturer	LOT	Purity	MW (g/mol)
Cellulose acetate	Sigma-Aldrich	MKBM8033V	≥97%	~30.000
Acetone	LabChem	AC-49-2013	≥99,7%	58,08
Formamide	Sigma-Aldrich	BCBH9281V	≥99,5%	45,04

Table 3-4 – Composition of the CA400-30, CA400-30Ag0,14 and CA400-30ZSM5 membranes.

	CA400-30		CA400-30Ag0,14		CA400-30ZSM5	
	m (g)	%wt	m (g)	%wt	m (g)	%wt
Cellulose Acetate	8,51	17,02	8,54	16,35	8,50	16,22
Formamide	15,01	30,01	15,16	29,02	15,12	28,84
Acetone	26,49	52,97	26,60	50,92	26,75	51,03
AgNP's suspension	-	-	1,94	3,71	-	-
Zeolite	-	-	-	-	2,05	3,91
Total	50,01	100	52,24	100	52,42	100
Silver percentage	-		0,14		-	

Table 3-5 – Composition of the CA400-30ZAg0,005, CA400-30ZAg0,03, CA400-30ZAg0,07 and CA400-30ZAg0,14 membranes.

	CA400-30ZAg0,005		CA400-30ZAg0,03		CA400-30ZAg0,07		CA400-30ZAg0,14	
	m (g)	%wt	m (g)	%wt	m (g)	%wt	m (g)	%wt
Cellulose Acetate	8,51	16,83	8,52	16,83	8,58	16,67	8,51	16,50
Formamide	15,37	30,40	15,23	30,09	15,50	30,11	15,06	29,19
Acetone	26,63	52,67	26,60	52,55	26,65	51,77	26,55	51,46
Zeolite with silver	0,05	0,10	0,27	0,53	0,75	1,46	1,47	2,85
Total	50,56	100	50,26	100	51,48	100	51,59	100
Silver percentage	0,005		0,03		0,07		0,14	

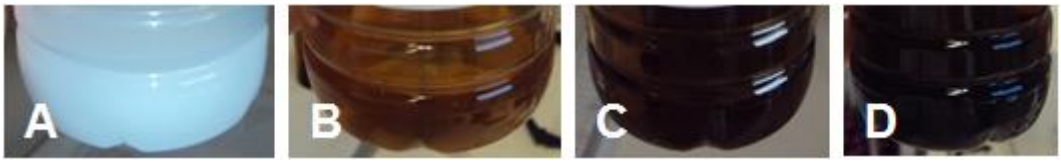

Figure 3-5 – Comparison of the casting solutions with zeolite and silver loaded zeolite with A: 0%; B: 0,005%; C: 0,03% and D: 0,07% of silver in the casting solution.

When prepared, the casting solutions have a white colour characteristic of the cellulose acetate. After the agitation time, the solutions with silver incorporated gain a brown tone which is darker with the increasing content of silver. Figure 3-5 shows four of the casting solutions with zeolite and silver containing zeolite. To note that the CA400-30 casting solution has a similar colour to the CA400-30ZSM5 (0% silver), the CA400-30Ag0,14 to the CA400-30ZAg0,005 and the CA400-30ZAg0,14 to the CA400-30ZAg0,07.

3.2.4 CASTING OF THE MEMBRANES

To cast the membranes it was necessary to have a glass plate with a smooth surface without imperfections, a casting knife and a coagulation bath, composed of deionized water and ice (Figure 3-6). This knife has a groove of 0,25 mm on one side which is responsible for casting a membrane with the required thickness.

The casting solution was poured equally into the slot of the casting knife and the 30 seconds of evaporation time began. The knife, placed with the groove faced down and to the upper part of the glass, was moved through it up to the end, spreading out the casting solution evenly, as shown in Figure 3-7. To assure a uniform membrane, both the glass and the casting knife had to be clean and dry.

After the evaporation time, with all the glass covered with the casting solution, the plate was immersed in the coagulation bath at 0℃. When the membrane started to detach from the plate, it was identified and stored in the fridge immersed in deionized water in a hermetic box specific to the type of membrane (simple, with silver nanoparticles, zeolite or silver containing zeolite).

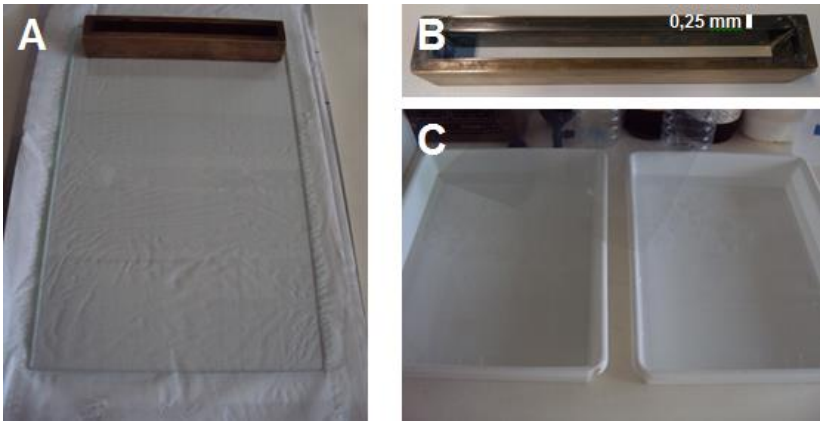

Figure 3-6 – Casting set-up: A) Casting support; B) Casting knife; C) Coagulation bath.

Figure 3-7 – Casting process (Beisl 2015)**.**

It was difficult to cast the membranes with higher concentrations of silver containing zeolite (CA400-30ZAg0,14) since the zeolite agglomerates ripped the membrane during the casting.

3.2.5 ANNEALING TREATMENT

The casted membranes have a pore diameter characteristic of ultrafiltration. As the experiments were made in ultra and nanofiltration conditions, to obtain nanofiltration characteristics the membranes had to be annealed in order to contract the pores (Figure 3-8). The annealing treatment consists in a heat treatment, in which the membranes, inside two petri dishes filled with deionized water, were placed in a thermic bath at 95℃ ± 1℃ for 11 minutes (De Pinho 1988).

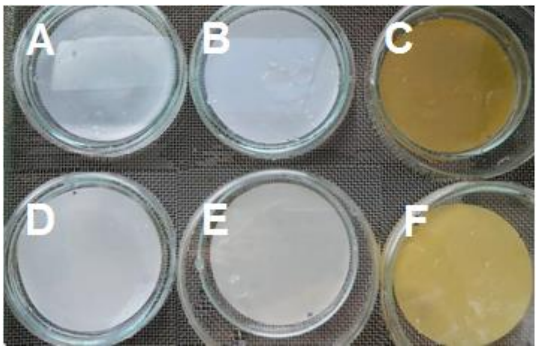

Figure 3-8 – Annealed membranes: A) CA400-30; B) CA400-30ZSM5; C) CA400-30Ag0,14; D) CA400-30ZAg0,005; E) CA400-30ZAg0,03; F) CA400-30ZAg0,07.

After this time, the annealed membranes were cooled with deionized water at room temperature and stored.

The membranes used in the bactericidal studies and a membrane with silver containing zeolite with 0,14% of silver content (CA400-30ZAg0,14$_P$) were annealed in a heating plate, inside a measurement beaker, at 95℃ ± 2℃ for 11 minutes.

3.3 EVALUATION OF THE PERMEATION PERFORMANCE

3.3.1 SET-UP

The characterization of the membranes was made in two crossflow filtration installations. These units of ultrafiltration/nanofiltration (Figure 3-9/Figure 3-10, respectively) are similar and are composed of a feed tank, a pump, a flowmeter, two manometers, five/six permeation cells in row and a pressure valve.

Figure 3-9 – Ultrafiltration installation.

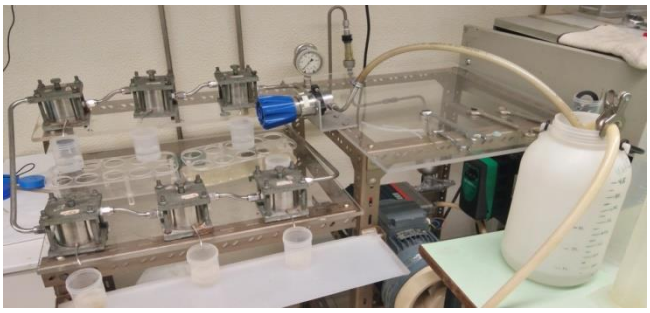

Figure 3-10 – Nanofiltration installation.

The flat plate cells have two detachable parts separated by a porous plate (membrane support) with a permeation area of 13,2 cm^2 (Figure 3-11 and Figure 3-12). To avoid damaging the membrane during the experiments, a circular filter paper was placed between the porous plate and the membrane. In the pressurized upper part of the cell, the feed inlet enters and, due to its conical geometry specially designed to achieve a high degree of turbulence, passes tangentially through the membrane, exiting as concentrate (Rosa and De Pinho 1994). The experiments were carried in concentration mode where only the concentrate was recirculated to the feed tank and the permeate was collected in a different vessel. As the circulating solution in the installations is considerably higher than the collected permeates, the steady state is maintained and different membranes can be tested at once with the same feed solution.

Figure 3-11 – Permeation cell used in ultra and nanofiltration installations.

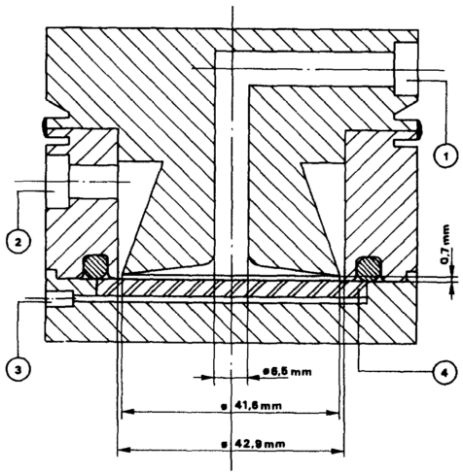

Figure 3-12 – Cell cross-section. 1. Feed inlet; 2. Feed outlet; 3. Permeate outlet; 4. Porous stainless steel plate (membrane support) (Afonso and De Pinho 1990)**.**

In the ultrafiltration installation, the pump (ISGEV AS 71 B 4 three-phase induction pump) is used to collect the solution from the variable capacity feed tank to the five permeation cells, where the circulation flow rate, measured in a flowmeter, is controlled simultaneously by the pump frequency and the backpressure valve. Two manometers are placed before and after the cells to detect the feed pressure and the pressure drop, respectively (Afonso and De Pinho 1990).
In the nanofiltration installation, similar to the ultrafiltration unit, a Hydra Cell G-03 diaphragm pump, coupled with a damper to reduce pressure fluctuations, feeds the six permeation cells with a pressure controlled by the backpressure valve and a circulating flow rate controlled by the hydraulic positive displacement pumping action.

3.3.2 COMPACTION OF THE MEMBRANES

To avoid fluctuations in the permeation experiments, the membranes had to be compacted for two hours at a pressure approximately 20% higher than the maximum operating pressure (40 bar and 6 bar at the nanofiltration and ultrafiltration installations, respectively) (Afonso and De Pinho 2000).

3.3.3 HYDRAULIC PERMEABILITY

The hydraulic permeability coefficient (L_p), the simplest characterization parameter, reveals the pure water permeation capacity of a membrane. It is the slope of the Equation 3.2 and describes the linear variation of the pure water permeation fluxes (J_{pw}) as a function of applied transmembrane pressure (ΔP). This value is the variation of permeate mass per unit of time, membrane area and applied pressure.

$$J_{pw} = L_p \cdot \Delta P \Leftrightarrow L_p = \frac{J_{pw}}{\Delta P} \tag{3.2}$$

The hydraulic permeability was measured with nanofiltration and ultrafiltration membranes. In nanofiltration conditions, the fluxes were obtained at 5, 10, 15, 20, 25, 30, 35 and 40 bar, with a 0,6 L/min feed flow rate (Afonso and De Pinho 2000). At the ultrafiltration installation, the fluxes were measured at a feed flow rate of 180 L/h at 1, 2, 3, 4 and 5 bar.

3.3.4 REJECTION COEFFICIENTS TO SOLUTES

In order to characterize the membranes in terms of the rejection coefficient (f), five solutions were prepared using glucose, NaCl, Na_2SO_4, $MgCl_2$ and $MgSO_4$ (Table 3-6). This important parameter is obtained by the Equation 3.3, which reveals the solute fraction that was retained by the membrane by the difference of the solute concentration in the bulk feed solution, C_b, and the concentration of the solute in the permeate, C_p.

$$f = \frac{C_b - C_p}{C_b} \tag{3.3}$$

The solutions had an initial feed concentration of 2 g/L and samples were taken from permeates and before and after the experiment from the feed. The average of the feed values was assumed as the bulk feed concentration. The experiment in nanofiltration conditions was conducted at 30 bar and a

flow rate of 0,6 L/min, while in ultrafiltration was at 3 bar and 180L/min. The feed tank had a volume of 5 L and the total collected volume less than 100 mL to maintain the steady state. The collected samples were analysed by conductivity measurement for the salts (NaCl, Na_2SO_4, $MgCl_2$ and $MgSO_4$) and by total organic carbon (TOC) measurement for glucose.

Table 3-6 – Chemicals used in the determination of the rejection coefficient.

Chemical	Manufacturer	LOT	Purity	MW (g/mol)
Glucose ($C_6H_{12}O_6 \cdot H_2O$)	Scharlau	86294	≥99,6%	198,17
NaCl	VWR	11D120005	99,9%	58,44
Na_2SO_4	Scharlau	83068	≥99,9%	142,04
$MgCl_2 \cdot 6H_2O$	Riedel-de Haën	32940	≥99%	203,30
$MgSO_4 \cdot 7H_2O$	Merck	A217086 026	≥99,5%	246,48

At the end of each experiment, the installations were purged with deionized water for 10 minutes at high flows and low pressures (Afonso and De Pinho 2000).

3.3.5 CONDUCTIVITY MEASUREMENT

In order to estimate the salts rejection coefficient, the concentration of permeates and feed solutions was determined by conductivity measurement. The conductivity values were obtained in a Crison Conductimeter GLP 32 at room temperature and converted to a reference temperature of 25℃ by the equipment, with a reproducibility of ±0,1% and a measurement error ≤0,5% (Crison 2001). To obtain the concentration values of the samples, a calibration curve for each salt (NaCl, Na_2SO_4, $MgCl_2$ and $MgSO_4$) in the applied range was prepared (Figure 3-13, Figure 3-14, Figure 3-15 and Figure 3-16).
The conductivity of the water used to prepare both standard solutions and the ones used in the experiments was lower than 10 μS/cm and was measured with the same conductivity meter.

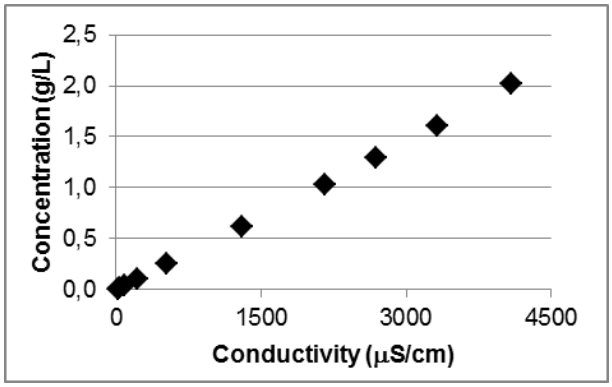

Figure 3-13 – Conductivity calibration curve for NaCl at 25℃

$\left(C\ (g/L) = 4,856 \times 10^{-4} \cdot \sigma\ (\mu S/cm),\ R^2 = 0,9996\right)$.

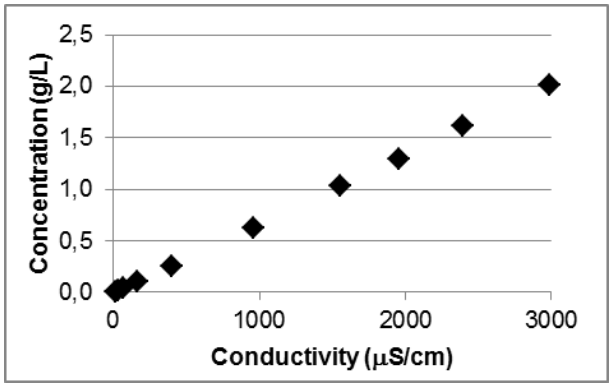

Figure 3-14 – Conductivity calibration curve for Na_2SO_4 at 25℃

$\left(C\ (g/L) = 6,675 \times 10^{-4} \cdot \sigma\ (\mu S/cm),\ R^2 = 0,9996\right)$.

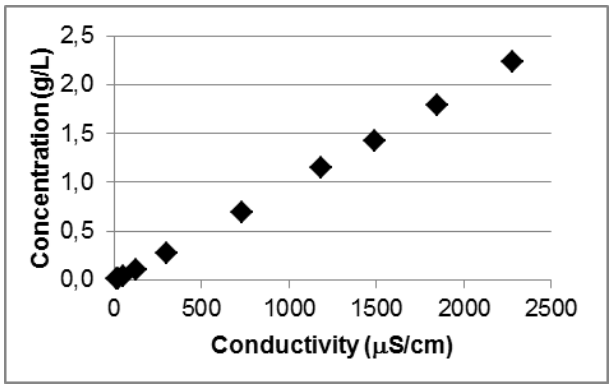

Figure 3-15 – Conductivity calibration curve for $MgCl_2$ at 25℃ $\left(C\ (g/L) = 9,689 \times 10^{-4} \cdot \sigma\ (\mu S/cm\ ), R^2 = 0,9997\right)$.

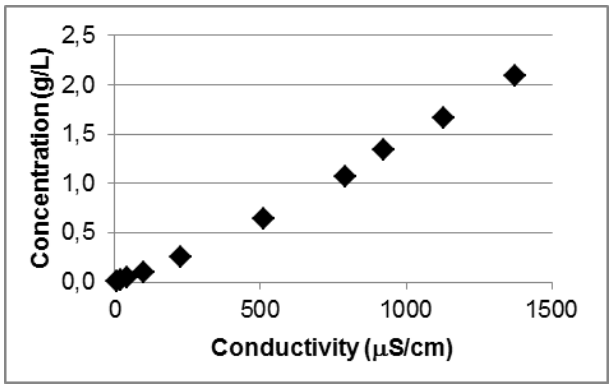

Figure 3-16 – Conductivity calibration curve for $MgSO_4$ at 25℃ $\left(C\ (g/L) = 2,870 \times 10^{-7} \cdot \sigma^2 + 1,139 \times 10^{-3} \cdot \sigma(\mu S/cm\ ), R^2 = 0,9994\right)$.

3.3.6 TOTAL ORGANIC CARBON MEASUREMENT

To obtain the membranes rejection coefficient for glucose, the total organic carbon content was measured in a Shimadzu Total Organic Carbon Analyser TOC-V_{CSH} (Figure 3-17). To analyse the collected samples, a calibration curve with a wide range of glucose concentrations was acquired (Figure 3-18). The TOC values were measured as total carbon (TC) since inorganic carbon (IC) was previously eliminated (Equation 3.4). Both permeates, feed and calibration curve solutions were acidified with 10 µL of concentrated sulfuric acid to a pH lower than 2 and then agitated to purge the volatile organic carbon (American Public Health Association, American Water Works Association 1999). A dilution was then made (usually 1:10) to avoid high carbon concentrations and corrosive effect from a low pH solution.

The temperature of the equipment furnace was at 680℃ and the reconstituted air pressure at 200 kPa (Corporation 2009).

$$TOC = TC - IC \tag{3.4}$$

Figure 3-17 – Shimadzu Total Organic Carbon Analyser TOC-V_{CSH}.

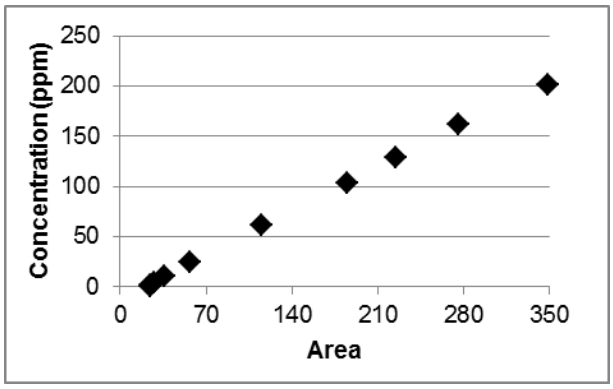

Figure 3-18 – TOC calibration curve for glucose $(\boldsymbol{C\ (ppm) = 0,6227 \cdot Area - 12,39, R^2 = 0,9993})$**.**

3.4 CHARACTERIZATION TECHNIQUES

3.4.1 UV-VIS SPECTROSCOPY

In order to characterize the formation of silver nanoparticles and to conclude about formamide use as a reducing agent, UV-Vis spectra were obtained in a UV-Vis spectrophotometer with diode array detector coupled to a DH-2000-BAL UV-VIS-NIR light source from Micropack and Spectra Suite software (Figure 3-19). Deionized water was used as the reference sample to take the blank spectrum for all measurements.

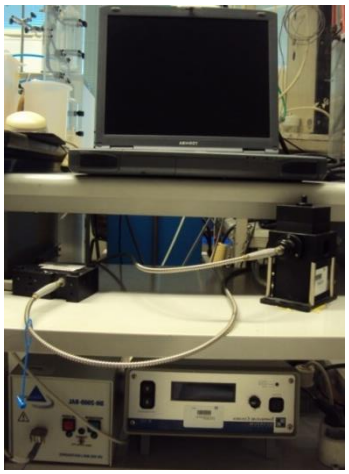

Figure 3-19 – UV-Vis spectrophotometer.

To conclude about the type of silver particles, three spectra were acquired 30 minutes, three days and four months after the silver nanoparticles preparation. The first two spectra were diluted several times and had an unknown concentration. The spectrum acquired after 120 days had a suspension concentration of 0,016 g_{Ag}/L. Normalizations by peak and by area were made to easily compare the three obtained spectra.

The formation of the silver nanoparticles suspension was captured in the UV-Vis spectrophotometer. In the 1 mL spectrophotometer cell, 10 μL of the $NaBH_4$ solution (0,02 mol/L) were added to 700 μL of the $AgNO_3$ solution (0,06 mol/L) (both compounds were dissolved in an aqueous solution of PVP), homogenized with a magnetic stirrer. From the variation of maximum absorbance with time it was possible to obtain the kinetics of the formation of silver nanoparticles.

The effect of the addition of 10 μL of formamide to 500 μL of the $AgNO_3$ solution (solution used in the formation of the silver nanoparticles, 0,06 mol/L) was also monitored in the UV-Vis spectrophotometer. The shape of the curves is sensitive to particle size, shape and polydispersity (Widoniak, Eiden-Assmann, and Maret 2005).

3.4.2 ELECTROCHEMICAL STUDIES

Cyclic voltammetry (CV) consists in the measurement of the current intensity at the working electrode during the potential scan, being considered the response signal to the potential excitation signal, resulting in a current-potential curve (Kissinger and Heineman 1983). This method was used to investigate the electrochemical behaviour of the silver inside the porous structure of the used zeolite.

The electrode consisted in a mixture of zeolite with graphite powder, in a 2:1 (w/w) proportion, a membrane or a membrane placed between two layers of conductive powder (Figure 3-20). The membranes were cut in the pellet press assembly layout (Figure 3-21) by inserting the membrane in the chamber and pressing it with the piston.

The homogenised pellets, which weighted around 5,5 mg, were prepared by simple mixture and subjected to a total applied pressure of 0,5 tonnes during 10 minutes in a PIKE CrushIR hydraulic press (Figure 3-22). As in Figure 3-23, the pellets were then placed in a three-electrode cell, in contact with a platinum auxiliary electrode disc, filled with 5 mL of 0,2 M electrolyte solution of optical grade NaCl (99,99%, Aldrich), and the potentials measured using a silver reference electrode in a Luggin tube (Lemos et al. 1999).

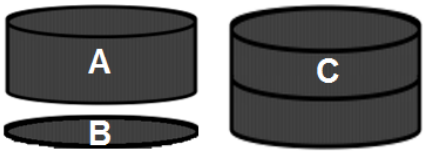

Figure 3-20 – Schematic representation of the electrodes used: A) zeolite/graphite pellet; B) membrane; C) membrane/graphite pellet.

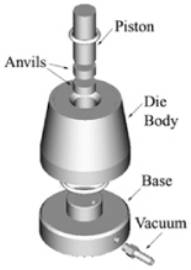

Figure 3-21 – Pellet press assembly layout.

Figure 3-22 – PIKE CrushIR hydraulic press.

Figure 3-23 – Electrochemical cell used to study the electrochemical behaviour of silver entrapped inside zeolites.

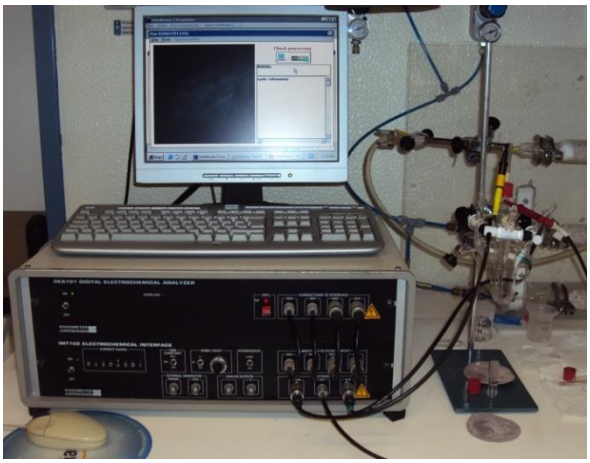

Figure 3-24 – Potentiostat/Potential programmer and data acquisition unit for cyclic voltammetry.

A pellet of silver nanoparticles was made evaporating the suspension in a watch glass during 72 hours. The cyclic voltammetry of this pellet was not possible to perform since it dissolved in the aqueous solution of NaCl. The experiment should be made using a different electrolyte.

The electrochemical studies were carried out in a Radiometer/Copenhagen DEA101 digital electrochemical analyser, coupled to an IMT102 electrochemical interface, controlled by a computer, which also acquired the data (

Figure 3-24).

The results obtained using the membrane/graphite pellets were not reproducible and conclusive.

3.4.3 THERMOGRAVIMETRIC ANALYSIS

The thermogravimetric analysis (TGA) measures the amount of change in the weight of a material as a function of temperature or time when the sample is subjected to a controlled temperature programme in a controlled atmosphere (Dean 2014). This technique was used to indirectly characterize the membranes in terms of their composition.

This analysis was performed in a PerkinElmer STA 6000 (Figure 3-25) coupled to a Pyris Software and a F12-ED Refrigerated/Heating Circulator from Julabo (Figure 3-26). The membranes were cut in small pieces with a total approximate weight of 20 mg, accommodated in a ceramic pan and then placed over the precision balance. For the sample atmosphere, air was used as the oxidative gas, with a purge rate of 20 mL/minute. The defined temperature scanning programme was the following: hold for 10 min at 30℃, heat from 30℃ to 110℃ at 10℃/min, hold for 15 min at 110℃, heat from 110℃ to 800℃ at 10℃/min, hold for 10 min at 800℃ and cool from 800℃ to 30℃ at 50℃/min (Figure 3-27) (Inc. 2004).

In the acquired TGA thermal curves, the absorbed water was lost up to the first isothermal step and it was possible to calculate the evaporated water percentage. The volatile organic matter and other components were lost in the next step of the programme (Bower and Yu 2011) and the remaining, zeolite and silver, compared with the initial percentage weighted for the casting solution. The CA400-30 membrane was considered as the reference value for weight loss.

Figure 3-25 – STA 6000 from PerkinElmer.

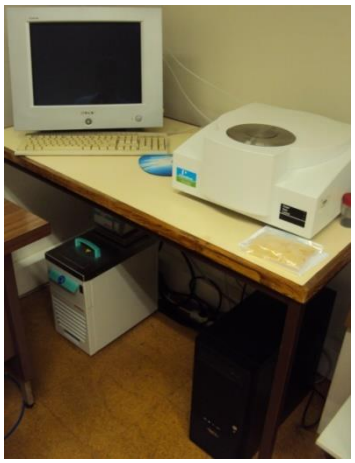

Figure 3-26 – TGA data acquisition unit.

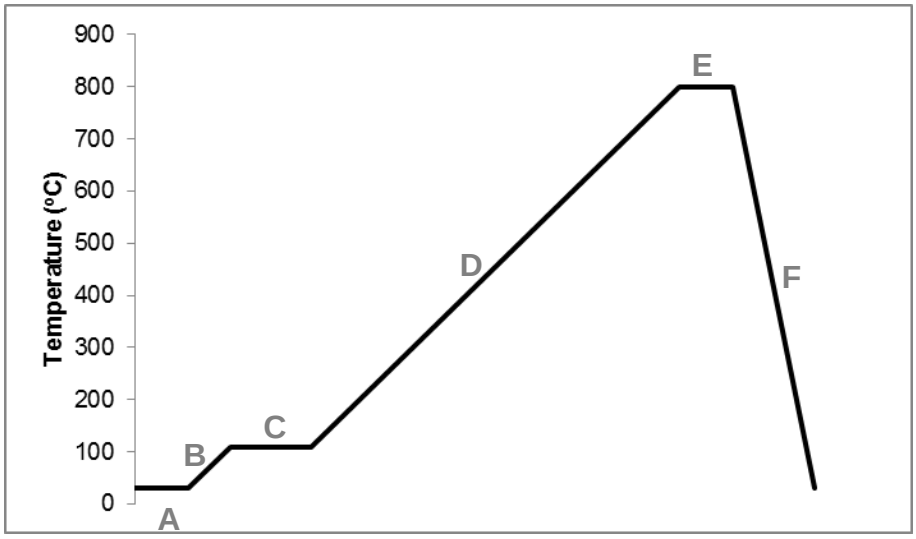

Figure 3-27 – Temperature scanning programme: A) 30℃ for 10 min; B) 30℃ to 110℃, 10℃/min; C) 110℃ for 15 min; D) 110℃ to 800℃, 10℃/min; E) 800℃ for 10 min; F) 800℃ to 30℃, 50℃/min.

3.4.4 DETERMINATION OF THE ZETA POTENTIAL

The surface charge properties of a membrane used in aqueous applications strongly influences fouling processes and retention capacity and can be described measuring zeta potential (Xie, Saito, and Hickner 2011). This technique is influenced by surface composition, pH, nature of ions and ionic strength (Bhattacharjee 2016). This method can also be used to determine the extent and efficiency of chemical modification, such as silver exchanged zeolite (Thielbeer, Donaldson, and Bradley 2011).

In the presence of a liquid-solid interface, the solid component acquires a surface charge that attracts counter ions from the liquid (Lauffer and Gortner 1939). These immobilized opposite charges are located in the outer Helmholtz plane (OHP) compensating the charges of the specifically adsorbed ions present in the inner Helmholtz plane (IHP). At the end of OHP, a more diffuse layer appears, formed by mobile ions attracted by the surface charge. The two adjacent layers (Stern layer and diffuse layer), separated by a plane of shear, form the electrochemical double layer (EDL). The potential between the slip plane and the medium is the zeta potential (Figure 3-28) (Delgado et al.

2005; Schweiss et al. 2001; Thielbeer, Donaldson, and Bradley 2011). Since direct measurements of the electrical potential at the solid surface are not possible, zeta potential is used to characterize double-layer properties (Xie, Saito, and Hickner 2011).

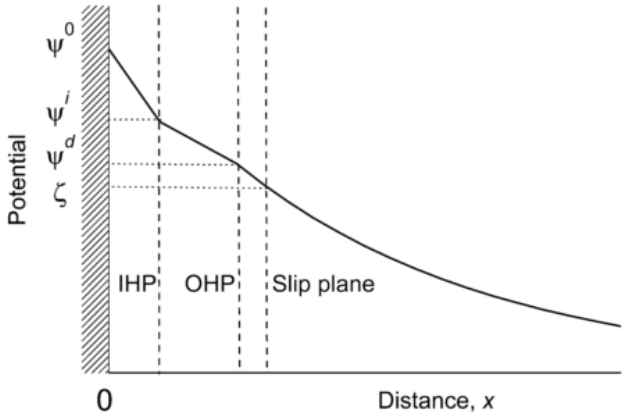

Figure 3-28 – Schematic representation of the electrochemical double layer (adapted from (Delgado et al. 2005)**).**

The tangential movement of a liquid through a static solid surface tends to carry the diffuse layer charges, creating a streaming potential (Lauffer and Gortner 1939). When surface conduction can be neglected, this relation is expressed by the Helmholtz-Smoluchowski (HS) equation (Equation 3.5), where ζ is the zeta potential, dE_s/dP is the change in streaming potential with pressure, η is the electrolyte viscosity, λ_0 is the electrical conductivity of the electrolyte solution, ε is the dielectric constant of the electrolyte and ε_0 is the vacuum permittivity (Delgado et al. 2005; Lauffer and Gortner 1939; Xie, Saito, and Hickner 2011). The streaming potential technique is the most suitable technique to determine the zeta potential of flat membrane surfaces (Xie, Saito, and Hickner 2011).

$$\zeta = \frac{dE_s}{dP} \cdot \frac{\eta}{\varepsilon \cdot \varepsilon_0} \lambda_0 \tag{3.5}$$

As CA membranes have a significant surface conductivity (GmbH 2003), the Fairbrother-Mastin procedure was used to eliminate its contribution. It assumes that surface conductance is supressed at high electrolyte concentration and is given by Equation 3.6, where R^H is the resistance of the channel when the cell is filled with a solution of high salt concentration, λ^H is the conductivity of this solution and R is the resistance of the channel when filled with the measurement solution (Delgado et al. 2005; Fairbrother and Mastin 1924; Xie, Saito, and Hickner 2011).

$$\zeta = \frac{dE_s}{dP} \cdot \frac{\eta}{\varepsilon \cdot \varepsilon_0} \cdot \frac{\lambda^H R^H}{R} \tag{3.6}$$

To characterize the zeta potential, an EKA electro kinetic analyser from Anton Paar (Figure 3-29), coupled with a rectangular cell, Ag/AgCl electrodes and a control and evaluation software (VisioLab for EKA) was used. Two membranes were put into the cell together, with the active layer facing each other, sealed and separated by polytetrafluoroethylene (PTFE) foils.

The measurements were carried out with an electrolyte solution of KCl 0,001M and the pH, varied between 4 and 9, was adjusted with NaOH and HCl 0,1M. The cell and the bypass were at first rinsed for 60 and 30 seconds, respectively, at 300 mbar. To induce flow two cycles of pressure ramping in

each direction were conducted, raising the pressure from 0 to 500 mbar in 120 seconds. The surface conductivity correction was made filling the system with 0,1M KCl (GmbH 2003).

Figure 3-29 – EKA Electro Kinetic Analyser from Anton Paar (GmbH 2003)**.**

3.5 EVALUATION OF THE BACTERICIDAL PROPERTIES

To assess the bactericidal effect of the seven prepared membranes, the behaviour of two different bacteria cultures (*Escherichia coli* (*E. coli*) and *Pseudomonas aeruginosa* (*P. aeruginosa*)) in the presence of each membrane was evaluated. The cultures were grown in Bacto™ Tryptic Soy Broth (TSB) liquid medium. An optical density around 0,12 at 600 nm read in the spectrophotometer (TSB as the blank) was recommended.

Each side of the annealed membranes, placed in a sterilized petri dish with sterilized water, was sterilized with UV radiation in a laminar flow biological safety cabinet for 30 minutes in order to inactivate microorganisms.

After reading the optical density, 1 mL of the inoculum and 9 mL of sterilized water were placed in a 100 mL sterile cup. After taking a blank sample, each membrane was added to *E. coli* and *P. aeruginosa* cultures and shacked in an incubator at 37℃ and 180 rpm. After 18 hours the last sample was collected. To determine bactericidal effect, 100 μL of each culture was taken, approximately every 15 minutes, dilutions were made (Figure 3-30) and spread on Difco™ Tryptic Soy Agar (TSA) (Figure 3-31). The first experiment with *P. aeruginosa* was made during approximately three hours and the second experiment with *E. coli* and *P. aeruginosa* during approximately five hours. The plates were incubated for 24 hours at 37℃ and the number of colonies enumerated in Quebec colony counter.

The number of colonies was expressed in percentage colony forming units (%CFU), given by the equation 3.7, to easily compare the results of the different membranes in both cultures, since the initial number of bacteria cells in each experiment was different.

$$\%CFU = \frac{\#colonies_t}{\#colonies_{t=0}} \times 100\% \quad (3.7)$$

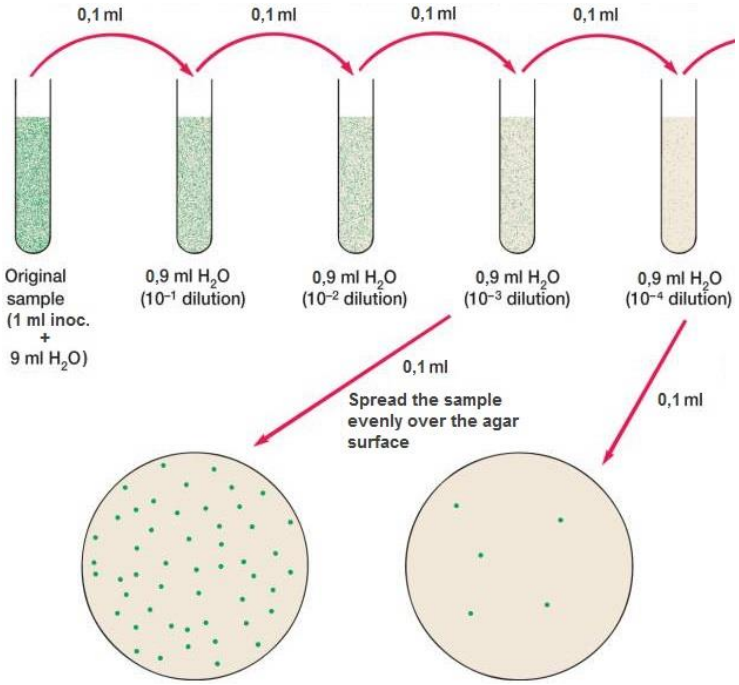

Figure 3-30 – Dilutions of the collected samples (adapted from (Prescott, Klein, and Harley 2002)**).**

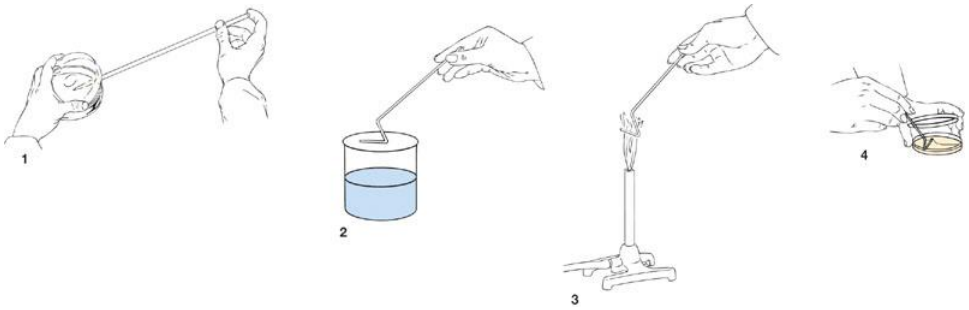

Figure 3-31 – Spread-Plate Technique (Prescott, Klein, and Harley 2002)**.**

To evaluate the growth of the cultures in the presence of ZSM-5 zeolite and silver containing zeolite, 33,3 μL of *E. coli* and *P. aeruginosa* cultures were placed in a petri dish with TSA in each part. In the experiment it was used zeolite, with and without silver, sterilized in two different ways: autoclave and by UV radiation. The zeolite was spread in two parts of the petri dish, the remaining being the blank (Figure 3-32).

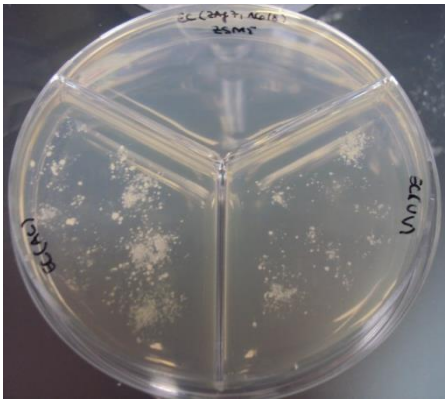

Figure 3-32 – Tripartite petri dish with spread zeolite.

The plates were incubated for 24 hours at 37℃. The results consisted in the evaluation of bacterial growth in the presence of ZSM-5 zeolite/ZAg, compared to the blank sample.

4 RESULTS AND DISCUSSION

4.1 HYDRAULIC PERMEABILITY

The hydraulic permeability coefficient (L_p), which describes the linear variation of the pure water permeation fluxes (J_{pw}) as a function of applied transmembrane pressure (ΔP), was determined for the seven prepared membranes, as described in chapter 3.3.3, for the ultrafiltration and nanofiltration membranes (Figure 4-1 - Figure 4-9 and Figure 4-10 - Figure 4-18, respectively).

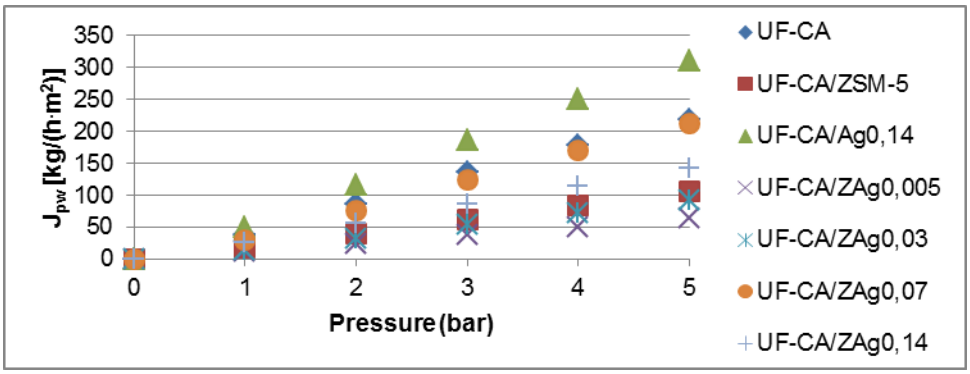

Figure 4-1 – Pure water fluxes of the ultrafiltration membranes at a pressure range of 1 - 5 bar.

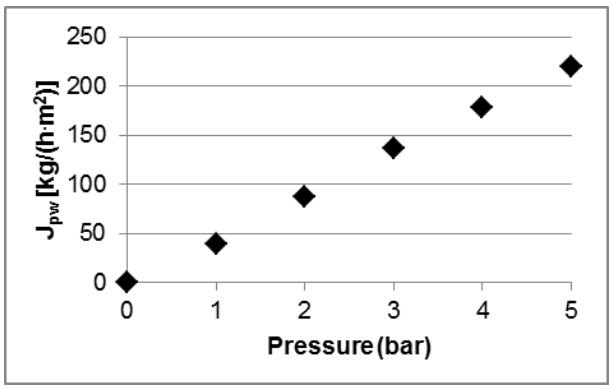

Figure 4-2 – Pure water fluxes of the UFCA400-30 membrane at a pressure range of 1 - 5 bar ($J_{pw}\ [kg/(h \cdot m^2)] = 44,2 \cdot \Delta P\ (bar), R^2 = 0,9985$).

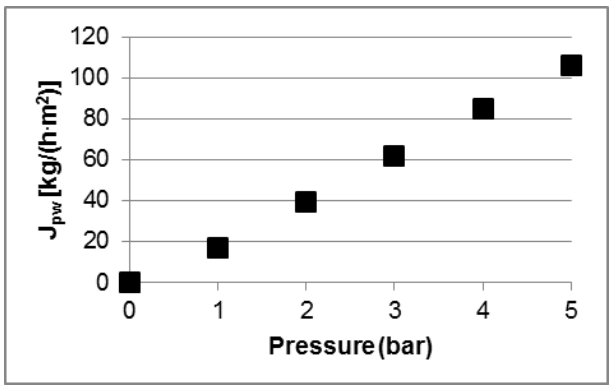

Figure 4-3 – Pure water fluxes of the UFCA400-30ZSM5 membrane at a pressure range of 1 - 5 bar ($J_{pw}\ [kg/(h \cdot m^2)] = 20,9 \cdot \Delta P\ (bar), R^2 = 0,9965$).

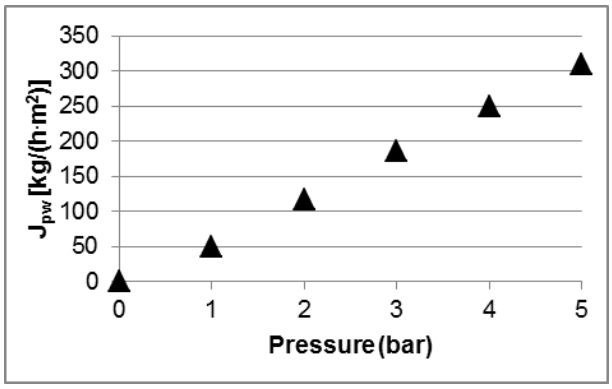

Figure 4-4 – Pure water fluxes of the UFCA400-30Ag0,14 membrane at a pressure range of 1 - 5 bar ($J_{pw}\ [kg/(h \cdot m^2)] = 61,6 \cdot \Delta P\ (bar), R^2 = 0,9971$).

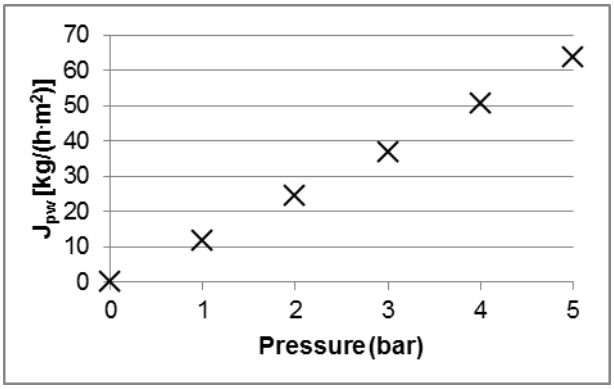

Figure 4-5 – Pure water fluxes of the UFCA400-30ZAg0,005 membrane at a pressure range of 1 - 5 bar ($J_{pw}\ [kg/(h \cdot m^2)] = 12,6 \cdot \Delta P\ (bar), R^2 = 0,9991$).

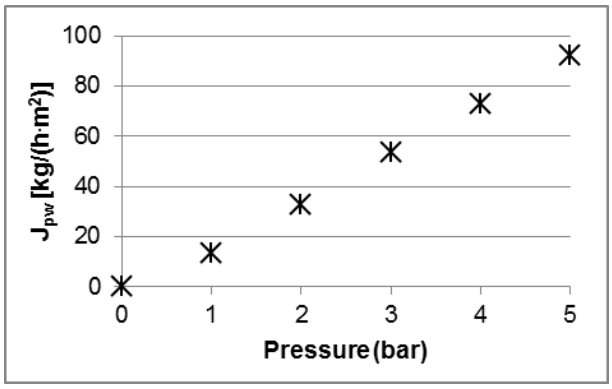

Figure 4-6 – Pure water fluxes of the UFCA400-30ZAg0,03 membrane at a pressure range of 1 - 5 bar ($J_{pw}\ [kg/(h \cdot m^2)] = 18,0 \cdot \Delta P\ (bar), R^2 = 0,9936$).

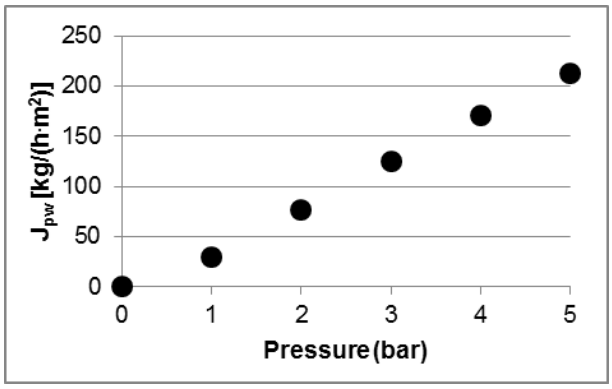

Figure 4-7 – Pure water fluxes of the UFCA400-30ZAg0,07 membrane at a pressure range of 1 - 5 bar ($J_{pw}\ [kg/(h \cdot m^2)] = 41,8 \cdot \Delta P\ (bar), R^2 = 0,9933$).

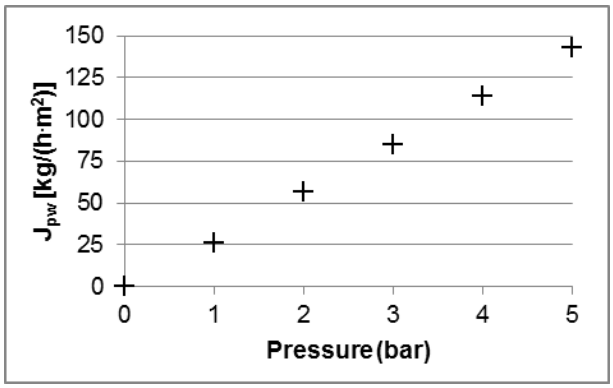

Figure 4-8 – Pure water fluxes of the UFCA400-30ZAg0,14 membrane at a pressure range of 1 - 5 bar ($J_{pw}\ [kg/(h \cdot m^2)] = 28,4 \cdot \Delta P\ (bar), R^2 = 0,9995$).

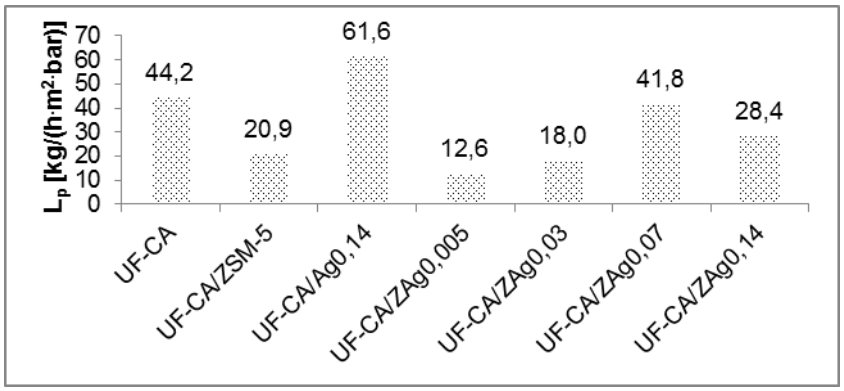

Figure 4-9 – Comparison of the hydraulic permeability of the ultrafiltration membranes.

From the comparison of the values obtained for the hydraulic permeability of the different ultrafiltration membranes (Figure 4-9), it can be stated that the incorporation of materials influences this characterization parameter. The incorporation of silver nanoparticles, as reported by Figueiredo (Figueiredo 2016), increases the hydraulic permeability of the membrane in comparison with the cellulose acetate membrane (UFCA400-30Ag0,14 has an hydraulic permeability 39,6% higher than UFCA400-30). This can be explained by the fact that silver nanoparticles prepared *ex-situ* are preferentially located in the skin layer of the membrane and are hydrophilic (Sile-Yuksel et al. 2014). In contrast, the incorporation of ZSM-5 zeolite decreases the hydraulic permeability of the membrane in 52,6% when compared with the CA membrane. This fact can be attributed to the hydrophobicity of the

ZSM-5 zeolite (J. Caro, Bülow, and Schirmer 1985) and the macrovoids reduction (Pendergast and Hoek 2011). The addition of silver containing zeolite to the membrane also decreases the hydraulic permeability, which becomes more pronounced with the increasing concentration (71,5%, 59,2% and 5,3% lower than the CA membrane). The UFCA400-30ZAg0,14 membrane does not follow the tendency (hydraulic permeability 35,6% lower than UFCA400-30), probably indicating the existence of a maximum silver zeolite concentration from which the hydraulic permeability decreases (Koseoglu-Imer et al. 2013).

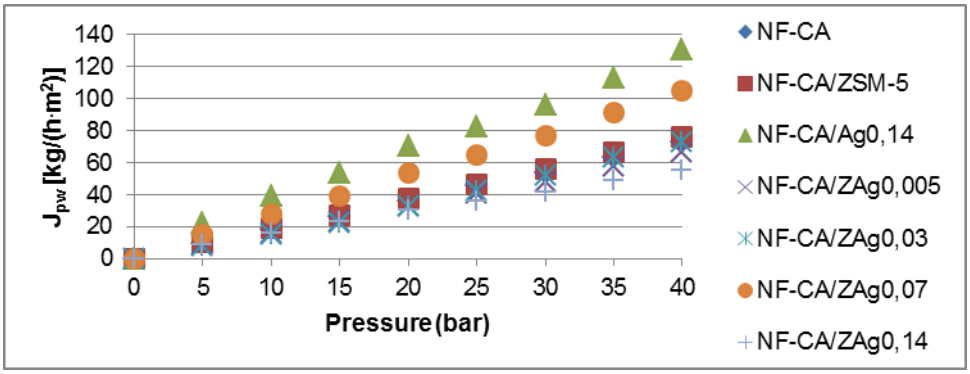

Figure 4-10 – Pure water fluxes of the nanofiltration membranes at a pressure range of 5 - 40 bar.

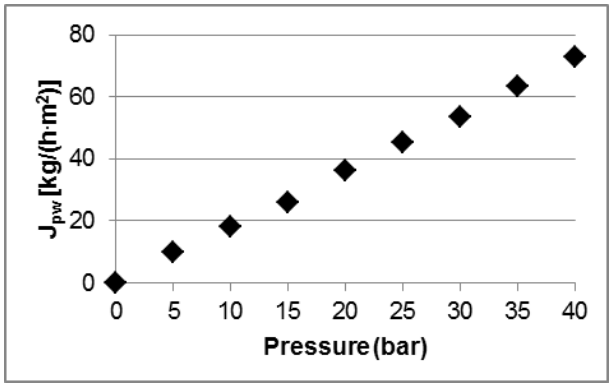

Figure 4-11 – Pure water fluxes of the NFCA400-30 membrane at a pressure range of 5 - 40 bar $(J_{pw}\ [kg/(h \cdot m^2)] = 1,8 \cdot \Delta P\ (bar), R^2 = 0,9994)$.

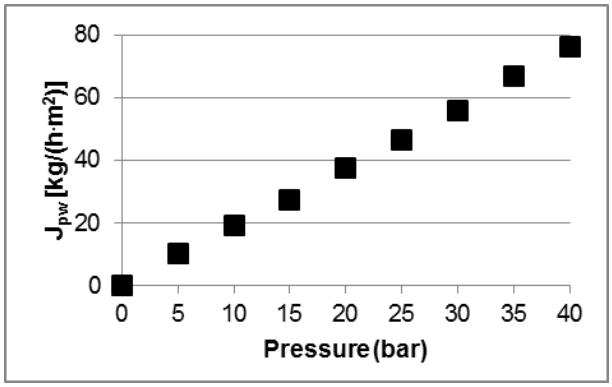

Figure 4-12 – Pure water fluxes of the NFCA400-30ZSM5 membrane at a pressure range of 5 - 40 bar $(J_{pw}\ [kg/(h \cdot m^2)] = 1,9 \cdot \Delta P\ (bar), R^2 = 0,9992)$.

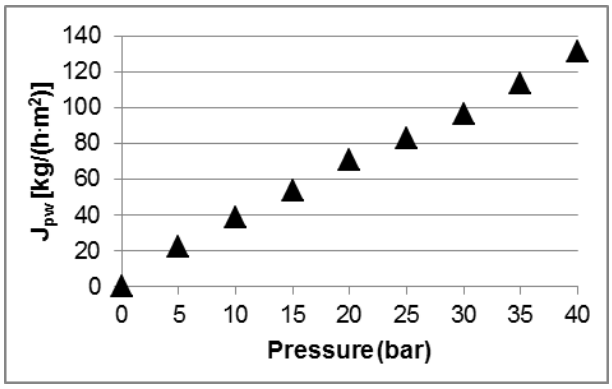

Figure 4-13 – Pure water fluxes of the NFCA400-30Ag0,14 membrane at a pressure range of 5 - 40 bar $(J_{pw}\ [kg/(h \cdot m^2)] = 3,3 \cdot \Delta P\ (bar), R^2 = 0,9918)$.

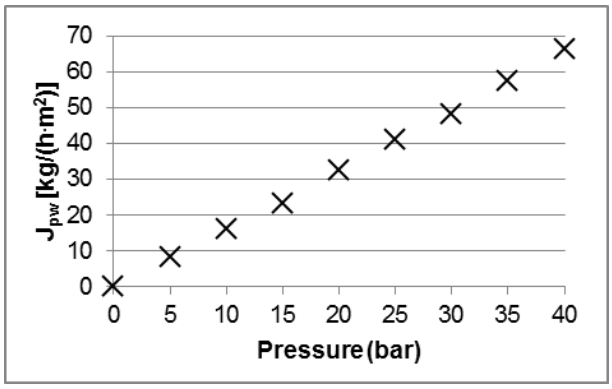

Figure 4-14 – Pure water fluxes of the NFCA400-30ZAg0,005 membrane at a pressure range of 5 - 40 bar $(J_{pw}\ [kg/(h \cdot m^2)] = 1,6 \cdot \Delta P\ (bar), R^2 = 0,9993)$.

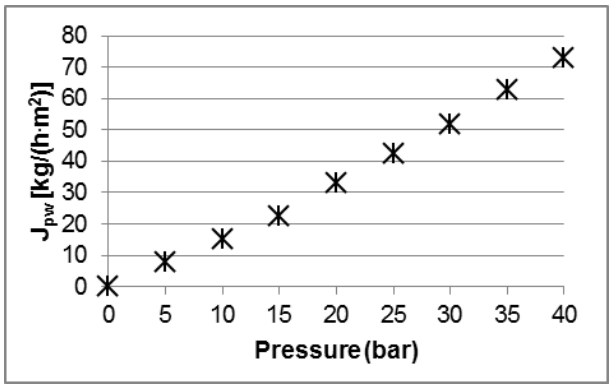

Figure 4-15 – Pure water fluxes of the NFCA400-30ZAg0,03 membrane at a pressure range of 5 - 40 bar ($J_{pw}\ [kg/(h \cdot m^2)] = 1,7 \cdot \Delta P\ (bar), R^2 = 0,9925$).

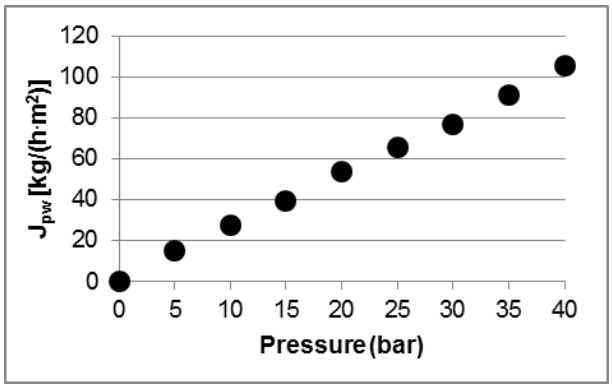

Figure 4-16 – Pure water fluxes of the NFCA400-30ZAg0,07 membrane at a pressure range of 5 - 40 bar ($J_{pw}\ [kg/(h \cdot m^2)] = 2,6 \cdot \Delta P\ (bar), R^2 = 0,9989$).

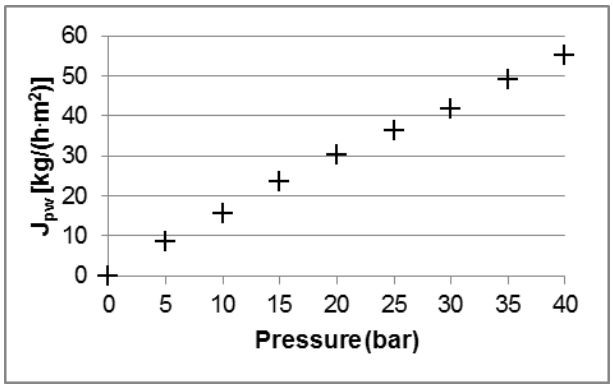

Figure 4-17 – Pure water fluxes of the NFCA400-30ZAg0,14 membrane at a pressure range of 5 - 40 bar ($J_{pw}\ [kg/(h \cdot m^2)] = 1,4 \cdot \Delta P\ (bar), R^2 = 0,9942$).

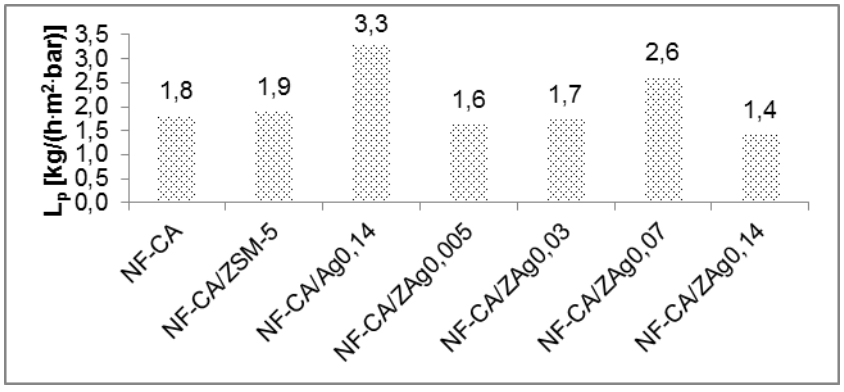

Figure 4-18 – Comparison of the hydraulic permeability of the nanofiltration membranes.

After the annealing treatment, the hydraulic permeability of the nanofiltration membranes decreased from tens to units. The incorporation of materials influences this parameter, although not as much as seen in ultrafiltration membranes. The hydraulic permeability increases with the addition of silver nanoparticles comparing with the cellulose acetate membrane, as reported by Beisl (Beisl 2015), an increase of 83,1% that is more enhanced in the nanofiltration membrane. The ZSM-5 zeolite incorporation also increases the hydraulic permeability (4,5% higher than NFCA400-30), which contrasts with the result obtained with the ultrafiltration membranes (decrease of 52,6% compared with UFCA400-30). The silver containing zeolite membranes with lower silver concentration, NFCA400-30ZAg0,005 and NFCA400-30ZAg0,03, have lower hydraulic permeability than the CA

membrane, with a decrease of 9,7% and 3,2%, respectively, and the value of the NFCA40030ZAg0,07 membrane is 44,8% higher. The NFCA400-30ZAg0,14 membrane, as mentioned for the ultrafiltration membrane, does not follow the tendency (hydraulic permeability 21,5% lower than NFCA400-30).

The hydraulic permeability obtained for the CA400-30ZAg0,14$_P$ membrane, annealed in a heating plate as explained in chapter 3.2.5, was 0,2 kg/(h·m^2·bar), 85,7% lower than the CA400-30ZAg0,14 membrane. This is due to the high dependency of hydraulic permeability of CA-400 membranes with temperature: a higher annealing temperature leads to a decrease on hydraulic permeability (De Pinho 1988).

4.2 REJECTION COEFFICIENTS TO SOLUTES

The rejection coefficient, which reveals the solute fraction that was retained by the membrane, was determined for the seven prepared membranes, as described in chapters 3.3.4, 3.3.5 and 3.3.6. This parameter was obtained for NaCl, Na_2SO_4, $MgCl_2$, $MgSO_4$ and glucose and the results are presented in Table 4-1 and Figure 4-19 for ultrafiltration membranes and in Table 4-2 and Figure 4-20 for nanofiltration membranes.

Table 4-1 – Rejection coefficients for NaCl, Na_2SO_4, $MgCl_2$, $MgSO_4$ and glucose for ultrafiltration membranes.

Rejection coefficient (%)	NaCl	Na_2SO_4	$MgCl_2 \cdot 6H_2O$	$MgSO_4 \cdot 7H_2O$	Glucose
UFCA400-30	27,4	29,1	25,0	39,0	18,8
UFCA400-30ZSM5	55,7	50,8	48,3	58,5	41,1
UFCA400-30Ag0,14	17,0	10,0	6,8	12,4	4,2
UFCA400-30ZAg0,005	78,9	50,7	35,0	77,0	74,0
UFCA400-30ZAg0,03	61,0	59,7	55,9	71,1	49,7
UFCA400-30ZAg0,07	21,6	23,1	17,0	29,0	13,6
UFCA400-30ZAg0,14	22,0	27,9	30,8	35,3	29,6

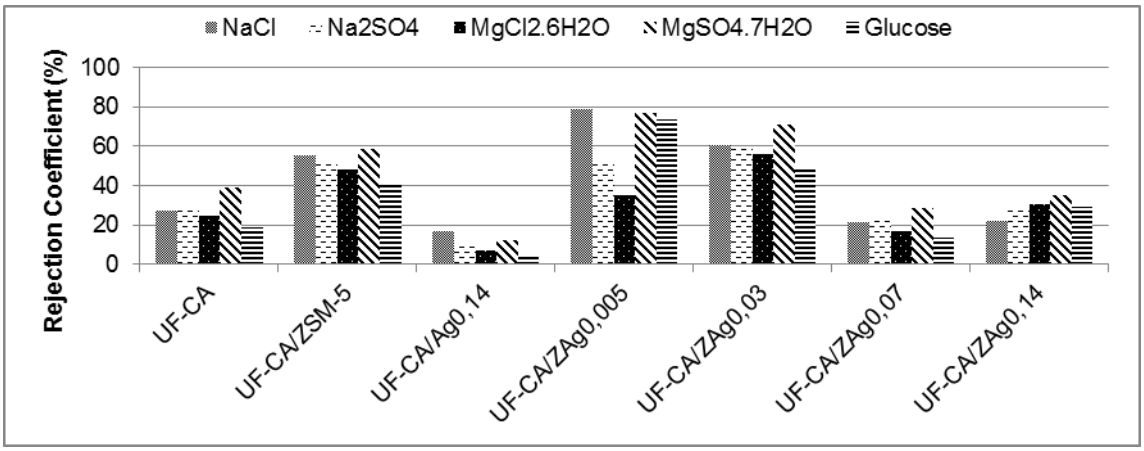

Figure 4-19 – Rejection coefficients for NaCl, Na_2SO_4, $MgCl_2$, $MgSO_4$ and glucose for ultrafiltration membranes.

The rejection coefficient of the UFCA400-30 membrane for NaCl, Na_2SO_4, $MgCl_2$, $MgSO_4$ and glucose are, respectively, 27,4%, 29,1%, 25,0%, 39,0% and 18,8%. The UFCA400-30Ag0,14 has rejection

coefficients for the salts and glucose lower than the cellulose acetate membrane, as reported by Figueiredo (Figueiredo 2016): 17,0% for NaCl, 10,0% for Na_2SO_4, 6,8% for $MgCl_2$, 12,4% for $MgSO_4$ and 4,2% for glucose. The addition of the ZSM-5 zeolite increases the rejection coefficients for NaCl, Na_2SO_4, $MgCl_2$, $MgSO_4$ and glucose when compared with the CA membrane (55,7%, 50,8%, 48,3%, 58,5% and 41,1%, respectively). The rejection coefficients of the UF membranes with silver containing zeolite for NaCl, Na_2SO_4, $MgCl_2$, $MgSO_4$ and glucose are, respectively, 78,9%, 50,7%, 35,0%, 77,0% and 74,0% for the UFCA400-30ZAg0,005 membrane, 61,0%, 59,7%, 55,9%, 71,1% and 49,7% for the UFCA400-30ZAg0,03 membrane, 21,6%, 23,1%, 17,0%, 29,0% and 13,6% for the UFCA400-30ZAg0,07 membrane and 22,0%, 27,9%, 30,8%, 35,3% and 29,6% for the UFCA400-30ZAg0,14 membrane. The membranes with lower concentration of silver containing zeolite (0,005% and 0,03% of silver) have rejection coefficients higher than the CA membrane; the UFCA400-30ZAg0,07 membrane has lower rejection coefficients compared with UFCA400-30; the rejection coefficients of the membrane with silver exchanged zeolite with 0,14% of silver vary (for NaCl, Na_2SO_4 and $MgSO_4$ are lower and for $MgCl_2$ and glucose are higher).

Table 4-2 – Rejection coefficients for NaCl, Na_2SO_4, $MgCl_2$, $MgSO_4$ and glucose for nanofiltration membranes.

Rejection coefficient (%)	NaCl	Na_2SO_4	$MgCl_2 \cdot 6H_2O$	$MgSO_4 \cdot 7H_2O$	Glucose
NFCA400-30	90,5	95,9	74,6	86,7	87,6
NFCA400-30ZSM5	78,2	93,4	61,5	77,0	83,0
NFCA400-30Ag0,14	56,1	84,4	55,6	81,1	63,7
NFCA400-30ZAg0,005	88,6	94,6	73,1	83,0	88,3
NFCA400-30ZAg0,03	91,1	95,4	73,7	85,1	87,9
NFCA400-30ZAg0,07	74,8	90,8	66,4	85,4	75,5
NFCA400-30ZAg0,14	86,3	85,7	84,8	94,0	89,6

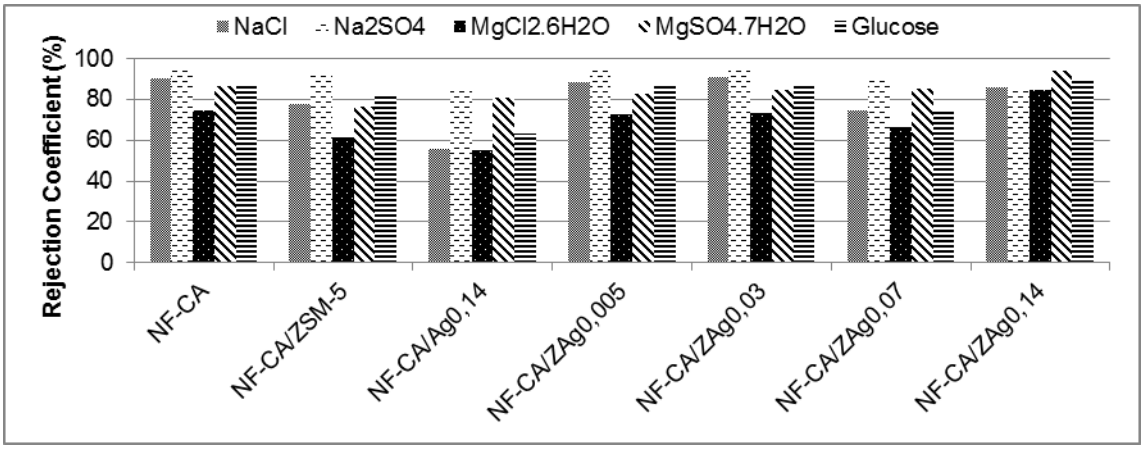

Figure 4-20 – Rejection coefficients for NaCl, Na_2SO_4, $MgCl_2$, $MgSO_4$ and glucose for nanofiltration membranes.

In order to obtain nanofiltration membranes, an annealing treatment was performed. This process reduces the pore size, improving the separation properties of the membrane, which leads to higher rejection coefficients (Murphy and de Pinho 1995). The rejection coefficients of cellulose acetate nanofiltration membrane for NaCl, Na_2SO_4, $MgCl_2$, $MgSO_4$ and glucose are, respectively, 90,5%,

95,9%, 74,6%, 86,7% and 87,6%. The NF membrane with silver nanoparticles, NFCA400-30Ag0,14, has rejection coefficients for the salts and glucose lower than the NFCA400-30 membrane, as reported by Beisl (Beisl 2015): 56,1% for NaCl, 84,4% for Na_2SO_4, 55,6% for $MgCl_2$, 81,1% for $MgSO_4$ and 63,7% for glucose. The addition of the ZSM-5 zeolite also decreases the rejection coefficients for NaCl, Na_2SO_4, $MgCl_2$, $MgSO_4$ and glucose when compared with the CA membrane (78,2%, 93,4%, 61,5%, 77,0% and 83,0%, respectively). This result is similar to the NF membrane with incorporated β-zeolite used by Beisl (Beisl 2015), although the rejection coefficient decrease is less pronounced. The rejection coefficients of the NF membranes with silver containing zeolite for NaCl, Na_2SO_4, $MgCl_2$, $MgSO_4$ and glucose are, respectively, 88,6%, 94,6%, 73,1%, 83,0% and 88,3% for the NFCA400-30ZAg0,005 membrane, 91,1%, 95,4%, 73,7%, 85,1% and 87,9% for the NFCA400-30ZAg0,03 membrane, 74,8%, 90,8%, 66,4%, 85,4% and 75,5% for the NFCA400-30ZAg0,07 membrane and 86,3%, 85,7%, 84,8%, 94,0% and 89,6% for the NFCA400-30ZAg0,14 membrane. The majority of the rejection coefficients results for these membranes are lower than the ones obtained for the NFCA400-30 membrane, except for the following: NFCA400-30ZAg0,005 with 88,3% for glucose, NFCA400-30ZAg0,03 with 91,1% for NaCl and 87,9% for glucose and NFCA400-30ZAg0,14 with 84,8% for $MgCl_2$, 94,0% for $MgSO_4$ and 89,6% for glucose.

The rejection coefficients are higher for the Na_2SO_4 salt, which is related with the negative charge of the membrane surface and the higher/lower charge density of the anion/cation, resulting in stronger electrostatic interaction forces with bivalent anions (Afonso and De Pinho 2000).

The membrane with silver containing zeolite with 0,14% of silver content annealed in a heating plate (NFCA400-30ZAg0,14$_P$) had rejection coefficients for NaCl, Na_2SO_4, $MgCl_2$, $MgSO_4$ and glucose of, respectively, 98,7%, 76,1%, 87,2%, 87,1% and 96,9%. The obtained values for NaCl, $MgCl_2$ and glucose are higher than the ones of the NF4CA400-30ZAg0,14 membrane, which annealing was performed in a thermic bath (De Pinho 1988).

4.3 UV-VIS SPECTROSCOPY

The three UV absorption spectra of the silver nanoparticles suspension, normalized by peak and by area, at different time periods, are presented in Figure 4-21 and Figure 4-22, respectively.

As the spectra exhibit a single band with peaks in the typical absorption band range (around 400 nm) and have no visible peak at 600 nm, it can be stated that the prepared suspension has well-dispersed spherical silver nanoparticles (Desai et al. 2012). However, the red shift of the maximum absorption with time from 401 nm in day 1, to 402 nm in day 4 and to 413 nm in day 120 with the bandwidth increase in the last spectrum indicates an increase in the particle size and a possible aggregation (Zielińska et al. 2009). The diameter of the silver nanoparticles, according to the obtained spectrum in day 1, is 3,2 nm $\pm$ 0,2 nm (Baia and Simon 2007; Desai et al. 2012).

The formation of the silver nanoparticles and the effect of maturing time at initial concentration of 0,01 mL of reducing agent $NaBH_4$ is presented in Figure 4-23.

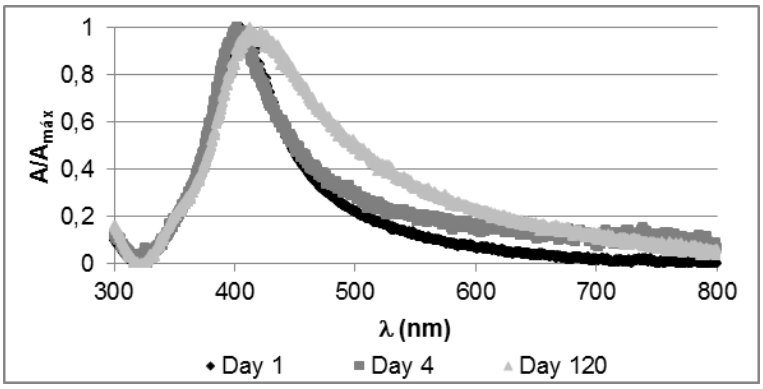

Figure 4-21 – UV absorption spectra normalized by peak of silver nanoparticles suspension at different time periods.

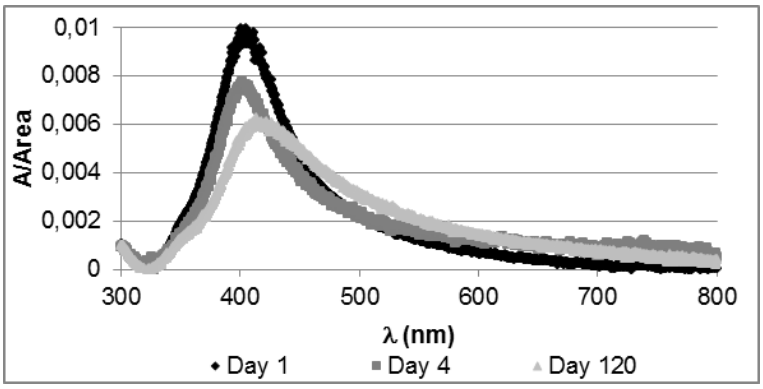

Figure 4-22 – UV absorption spectra normalized by area of silver nanoparticles suspension at different time periods.

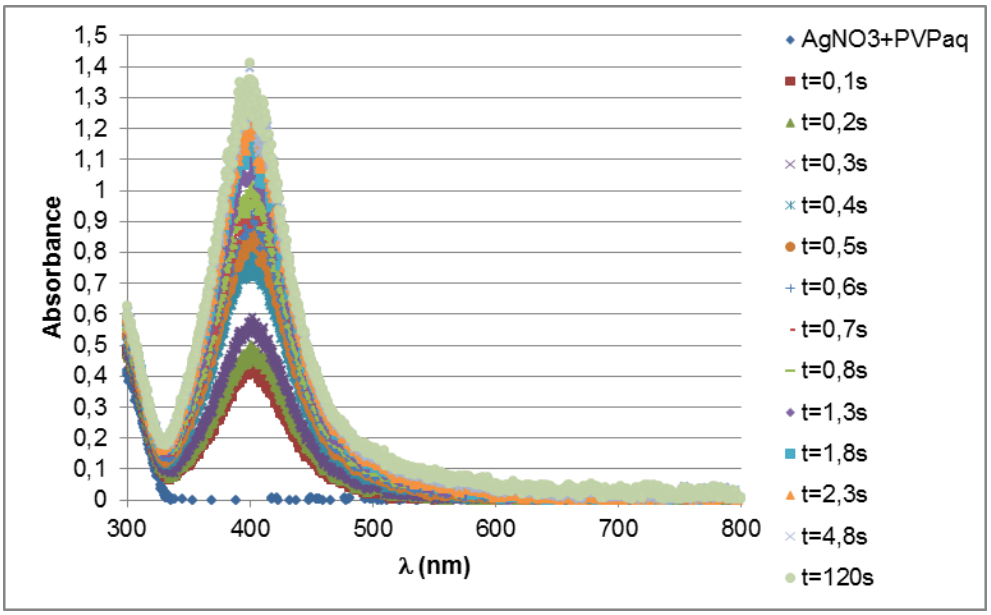

Figure 4-23 – Effect of maturing time at initial concentration of 0,01 mL of reducing agent $NaBH_4$.

It is possible to see in Figure 4-23 that the formation of silver nanoparticles prepared at fixed concentration of 0,01 mL of reducing agent $NaBH_4$ exhibits absorption peaks around 400 nm, with an increasing absorbance with time (between 0 and 1,4).

From the variation of maximum absorbance with time it was possible to obtain first and second order kinetics of the formation of silver nanoparticles, given by Equation 4.1 and Equation 4.2, respectively.

$$A(t) = 1{,}34(1 - e^{-2{,}09t}) \quad (4.1)$$

$$A(t) = 1{,}49 - \frac{1}{1{,}87t + 0{,}67} \quad (4.2)$$

As it can be seen in Figure 4-24, the second order kinetics of the silver nanoparticles formation has the best fitting to the experimental points, with 0,02 as residue sum. The first order kinetics has a residue sum of 0,07.

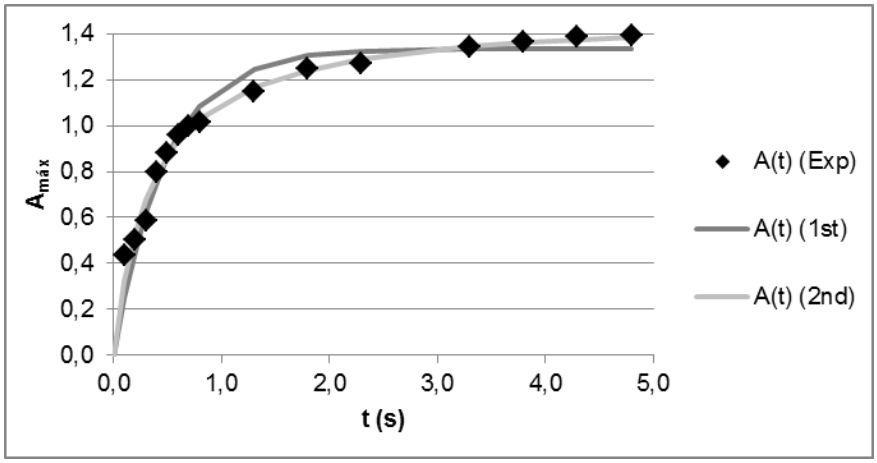

Figure 4-24 – Variation of maximum absorbance with time in the formation of silver nanoparticles.

The effect of the addition of formamide to an aqueous solution of $AgNO_3$ solution is presented in Figure 4-25. The addition of formamide leads to the appearance of a broad extinction band, which can indicate the presence of different distributions of particles sizes: at lower wavelength, well-dispersed spherical nanoparticles and, at longer wavelength, aggregates of primary particles interacting collectively with the incident light as a large silver particle (Desai et al. 2012; Widoniak, Eiden-Assmann, and Maret 2005).

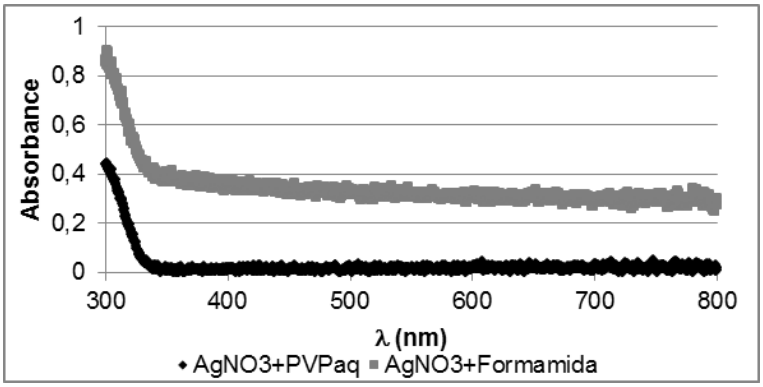

Figure 4-25 – UV absorption spectra of formamide addition to an aqueous solution of $AgNO_3$ (dissolved with PVP).

4.4 ELECTROCHEMICAL STUDIES

Cyclic voltammetry analysis, as explained in chapter 3.4.2, was used in order to determine the electrochemical state of the silver in the ion exchanged zeolite, either in powder or incorporated in a membrane.

4.4.1 ZEOLITE/GRAPHITE PELLET

The CV curves obtained for the calcined ZSM-5 zeolite and silver exchanged zeolite, starting with a reduction cycle, are presented in Figure 4-26 and Figure 4-27. The CV curves obtained for the calcined silver exchanged zeolite, starting with an oxidation cycle, are presented in Figure 4-28 and Figure 4-29.

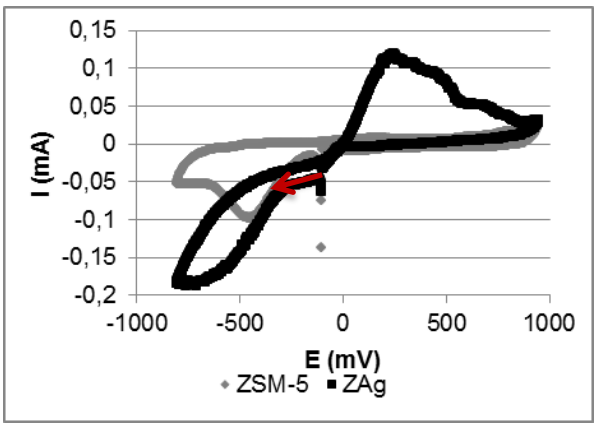

Figure 4-26 – Cyclic voltammograms of calcined ZSM-5 zeolite and silver loaded zeolite (initial scan towards negative potentials: -100mV → -800mV → 950mV → -100mV, scan rate: 10 mV/s, 1st cycle).

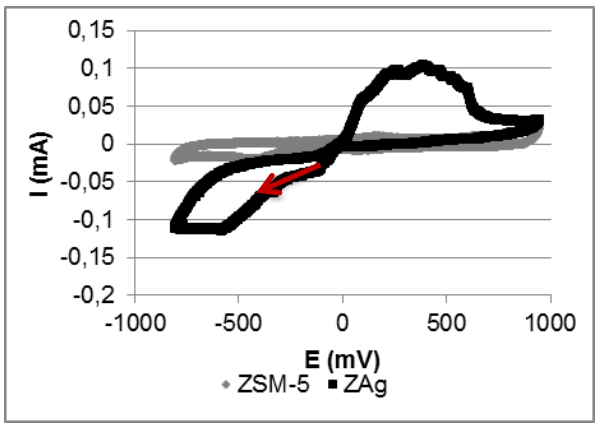

Figure 4-27 – Cyclic voltammograms of calcined ZSM-5 zeolite and silver loaded zeolite (initial scan towards negative potentials: -100mV → -800mV → 950mV → -100mV, scan rate: 10 mV/s, 2nd cycle).

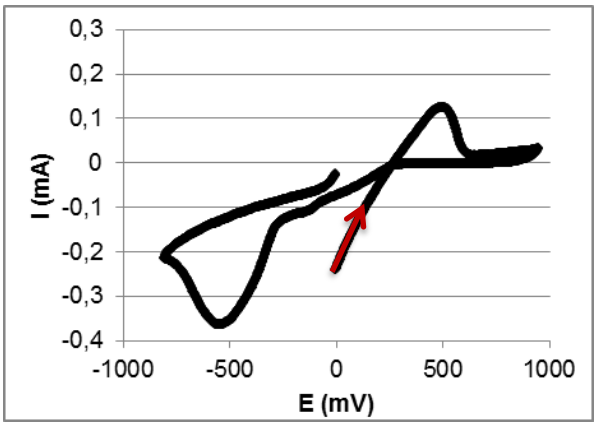

Figure 4-28 – Cyclic voltammogram of calcined silver loaded zeolite (initial scan towards positive potentials: 0mV → 950mV → -800mV → 0mV, scan rate: 10 mV/s, 1st cycle).

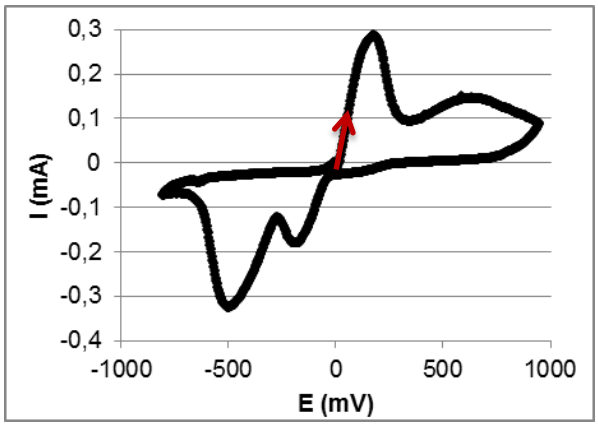

Figure 4-29 – Cyclic voltammogram of calcined silver loaded zeolite (initial scan towards positive potentials: 0mV → 950mV → -800mV → 0mV, scan rate: 10 mV/s, 2nd cycle).

The voltammogram of the ZSM-5 zeolite has an irreversible reduction peak at -450 mV in the first cycle (Figure 4-26) that does not appear in the second cycle (Figure 4-27), which may correspond to a species adsorbed. The voltammograms of the silver exchanged zeolite, starting towards negative potentials (Figure 4-26 and Figure 4-27), show a reduction peak at around -750 mV and in the reverse cycle an oxidation peak around 250 mV, with an amount of electric charge of, respectively, 13,4 mC and 6,5 mC for the first cycle and 8,4 mC and 6,4 mC for the second cycle. Comparing both CV curves for zeolite and silver loaded zeolite, it can be stated that the peaks appearing in the voltammogram of the silver exchanged zeolite are caused by the silver. The voltammograms of the silver exchanged zeolite, starting with the oxidation scan (Figure 4-28 and Figure 4-29), show a

reduction peak at 0 mV and the consequent oxidation at 450 mV (electric charge of, respectively, 3,0 mC and 2,5 mC for the first cycle), indicating the absence of metallic silver. Thus, the silver exchanged zeolite is present in the cationic form. The electric charge of the reduction peak, 9,1 mC, corresponds to the total amount of silver in the 5,5 mg prepared pellet. It was necessary to withdraw the electric charge correspondent to the ZSM-5 zeolite (4,3 mC for reduction).

The CV curves obtained for the zeolite recovered from the casting solution of the CA400-30ZAg0,03 membrane and the respective comparison with the calcined silver exchanged zeolite, starting with reduction, are presented in Figure 4-30 – Figure 4-33. The respective CV curves starting with oxidation are presented in Figure 4-34 and Figure 4-37.

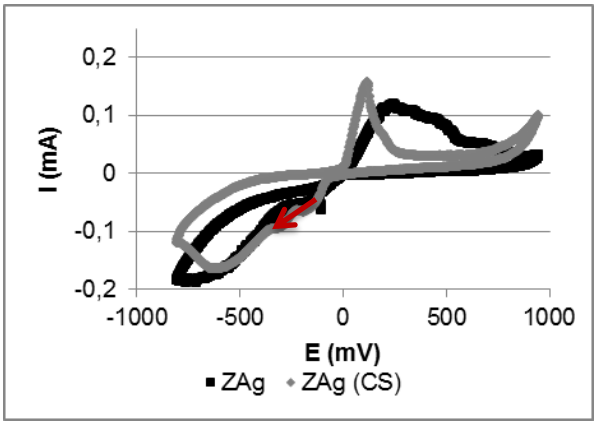

Figure 4-30 – Cyclic voltammograms of zeolite recovered from the casting solution of CA400-30ZAg0,03 membrane (initial scan towards negative potentials: -100mV → -800mV → 950mV → -100mV, scan rate: 10 mV/s, 1st cycle) and calcined silver exchanged zeolite.

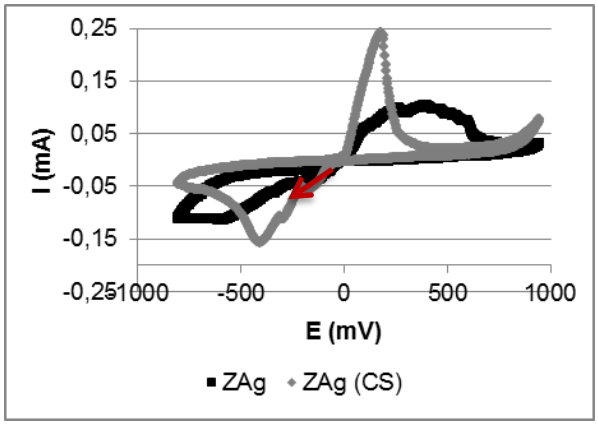

Figure 4-31 – Cyclic voltammograms of zeolite recovered from the casting solution of the CA400-30ZAg0,03 membrane (initial scan towards negative potentials: -100mV → -800mV → 950mV → -100mV, scan rate: 10 mV/s, 2nd cycle) and calcined silver exchanged zeolite.

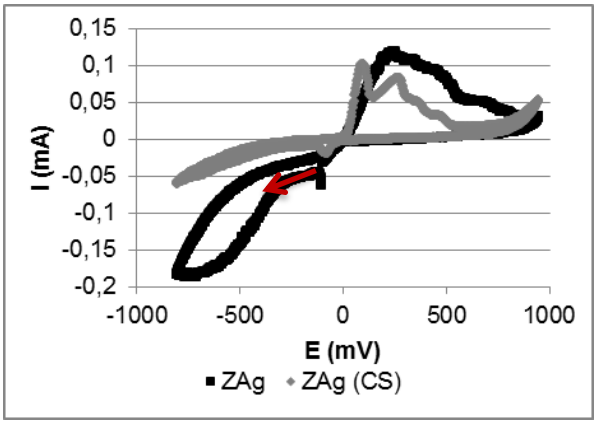

Figure 4-32 – Cyclic voltammograms of zeolite recovered from the casting solution of CA400-30ZAg0,03 membrane (initial scan towards negative potentials: -100mV → -800mV → 950mV → -100mV, scan rate: 10 mV/s, 1st cycle) and calcined silver exchanged zeolite.

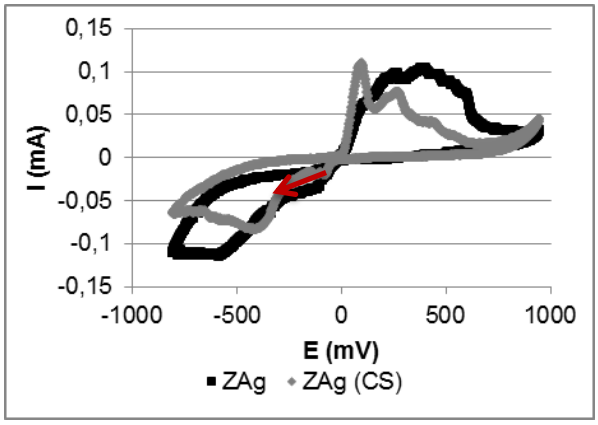

Figure 4-33 – Cyclic voltammograms of zeolite recovered from the casting solution of the CA400-30ZAg0,03 membrane (initial scan towards negative potentials: -100mV → -800mV → 950mV → -100mV, scan rate: 10 mV/s, 2nd cycle) and calcined silver exchanged zeolite.

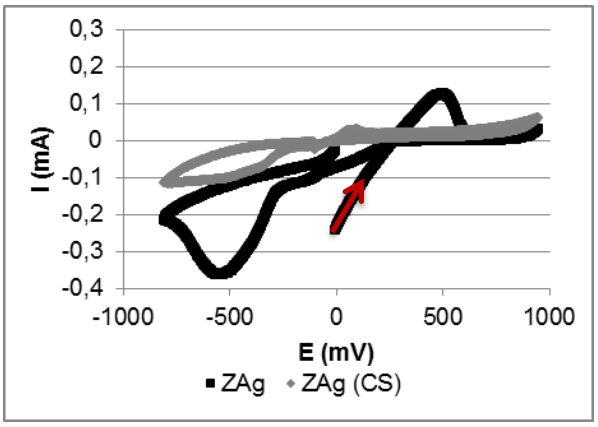

Figure 4-34 – Cyclic voltammograms of zeolite recovered from the casting solution of CA400-30ZAg0,03 membrane (initial scan towards positive potentials: -100mV → 950mV → -800mV → -100mV, scan rate: 10 mV/s, 1st cycle) and calcined silver exchanged zeolite.

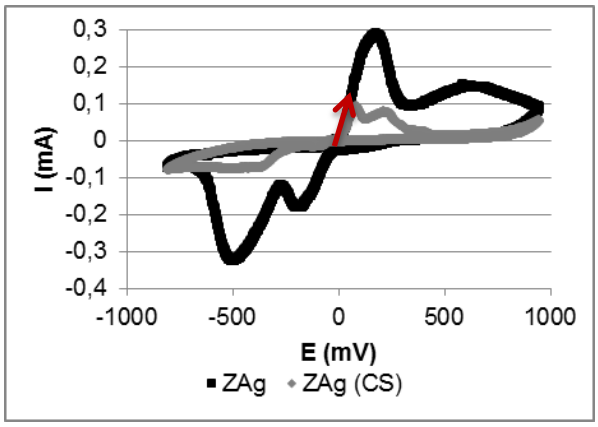

Figure 4-35 – Cyclic voltammograms of zeolite recovered from the casting solution of CA400-30ZAg0,03 membrane (initial scan towards positive potentials: -100mV → 950mV → -800mV → -100mV, scan rate: 10 mV/s, 2nd cycle) and calcined silver exchanged zeolite.

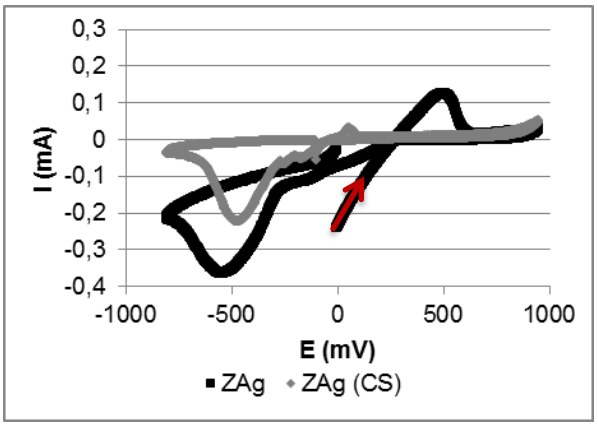

Figure 4-36 – Cyclic voltammograms of zeolite recovered from the casting solution of CA400-30ZAg0,03 membrane (initial scan towards positive potentials: -100mV → 950mV → -800mV → -100mV, scan rate: 10 mV/s, 1st cycle) and calcined silver exchanged zeolite.

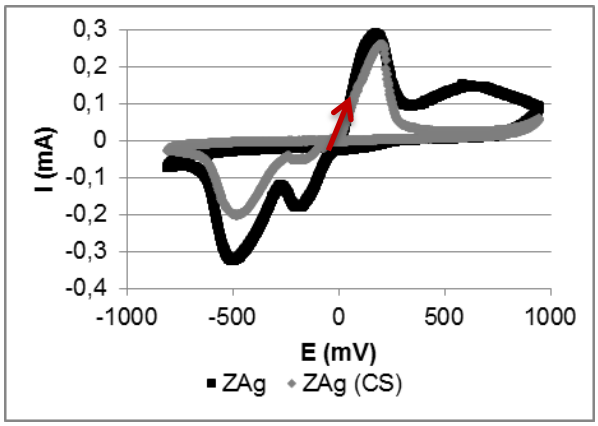

Figure 4-37 – Cyclic voltammograms of zeolite recovered from the casting solution of CA400-30ZAg0,03 membrane (initial scan towards positive potentials: -100mV → 950mV → -800mV → -100mV, scan rate: 10 mV/s, 2nd cycle) and calcined silver exchanged zeolite.

The cyclic voltammetry curves of the pellets with zeolite recovered from the casting solution of CA400-30ZAg0,03 membrane present differences in the experiments. It may be due to the lack of uniformity of the starting material since it has undergone various washes and possible reactions with the solvents used (formamide and acetone). It can be stated from the CV curves starting towards positive potentials that the silver is in the cationic form since it has no oxidation peak (Figure 4-34 and Figure 4-36), as in the calcined silver exchanged zeolite. The pellets were made from the same initial sample of graphite/zeolite.

In order to evaluate if a silver ion exchange between the pellet and the electrolyte solution occurs, a silver exchange zeolite/graphite pellet was left in the cell during 74 hours after been subjected to six cyclic voltammetry cycles, ensuring that the CV curves obtained were reproducible (Figure 4-38),

followed by an oxidation cycle, to guaranty that the silver stayed in the oxidized state. The first and last obtained voltammograms of the oxidized pellet are presented in Figure 4-39.

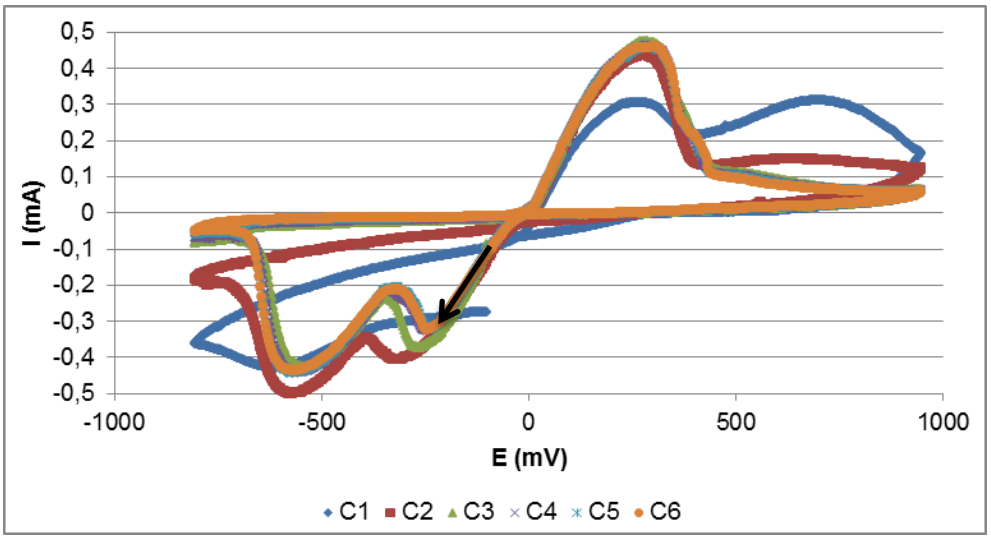

Figure 4-38 – Six sequential cyclic voltammograms of calcined silver exchanged zeolite (initial scan towards negative potentials: -100mV → -800mV → 950mV → -100mV, scan rate: 10 mV/s).

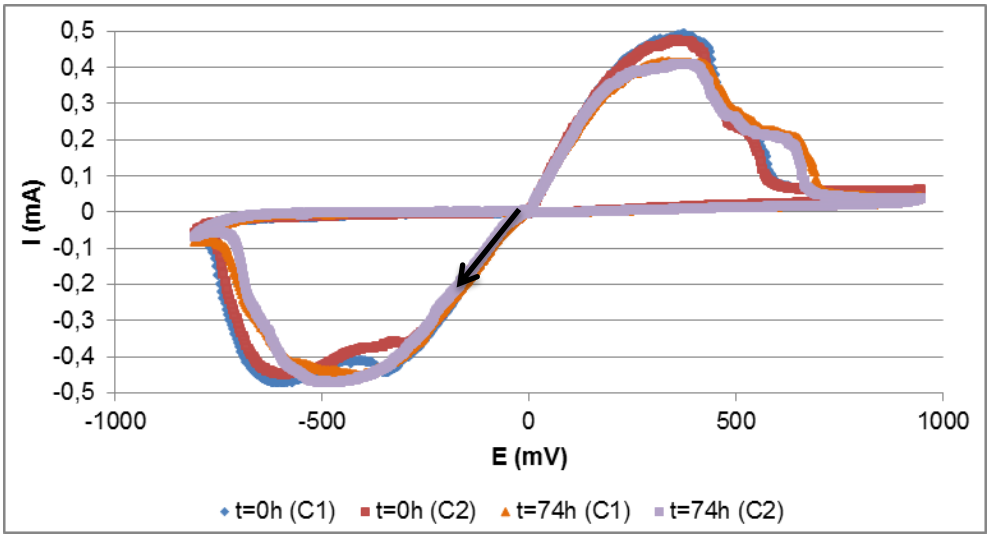

Figure 4-39 – Time evolution of the cyclic voltammograms of calcined silver exchanged zeolite to assess the silver ion leaching (initial scan towards negative potentials: 0mV → -800mV → 950mV → 0mV, scan rate: 10 mV/s).

In Figure 4-38, the reduction zone of the first cycle has a broad peak that converts into two well defined peaks in the following cycles, instead of what is observed in the oxidation zone.

To compare the cyclic voltammograms (Figure 4-39), an integration of the electric current over time was made for reduction and oxidation peaks, revealing similar values. The electric charge of the reduction peaks for the first (t=0h) and last voltammograms (t=74h) was, respectively, 19,8 mC and 23,5 mC for the first cycle (C1) and 18,1 mC and 22,8 mC for the second cycle (C2). The electric charge of the oxidation peaks of the voltammograms at zero and 74 hours was, respectively, 16,9 mC and 21,4 mC for the first cycle and 16,2 mC and 20,4 mC for the second cycle. It is visible a change of the oxidation pattern with the appearance of an oxidation peak at higher potentials, as the potential was cycled repetitively, which may be due to the diffusion of silver ions into more stable sites in the

zeolite, resulting in the slightly shift of the peak potentials towards more positive values (Y.-J. Li and Liu 2001).

4.4.2 MEMBRANES

The CV curves obtained for the UFCA400-30ZAg0,07 membrane, with the active face facing the electrolyte and the electrode, are presented in Figure 4-40 and Figure 4-41 starting with an initial cycle to negative potentials and in Figure 4-42 and Figure 4-43 starting with an oxidation cycle.

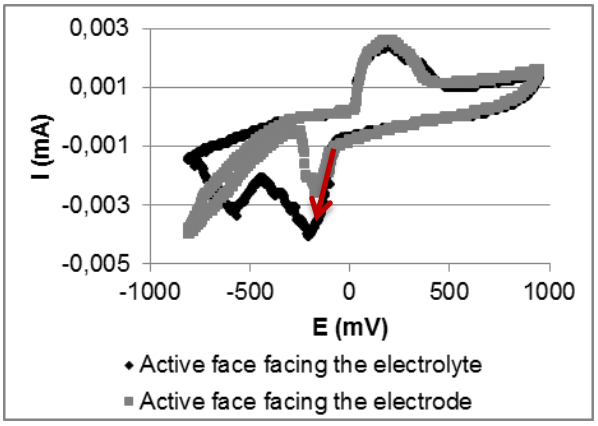

Figure 4-40 – Cyclic voltammograms of UFCA400-30ZAg0,07 membrane, active face facing the electrolyte and the electrode (initial scan towards negative potentials: -100mV → -800mV → 950mV → -100mV, scan rate: 10 mV/s, 1st cycle).

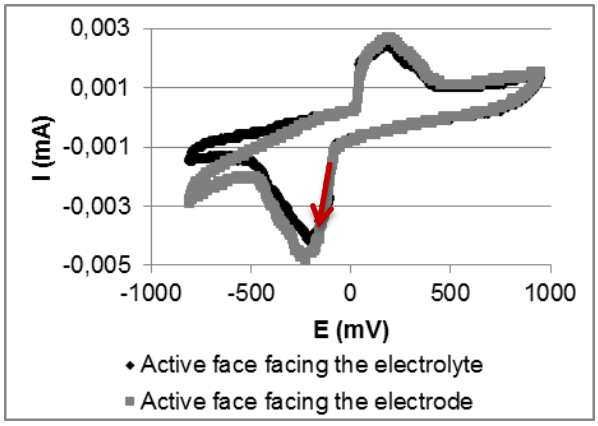

Figure 4-41 – Cyclic voltammograms of UFCA400-30ZAg0,07 membrane, active face facing the electrolyte and the electrode (initial scan towards negative potentials: -100mV → -800mV → 950mV → -100mV, scan rate: 10 mV/s, 2nd cycle).

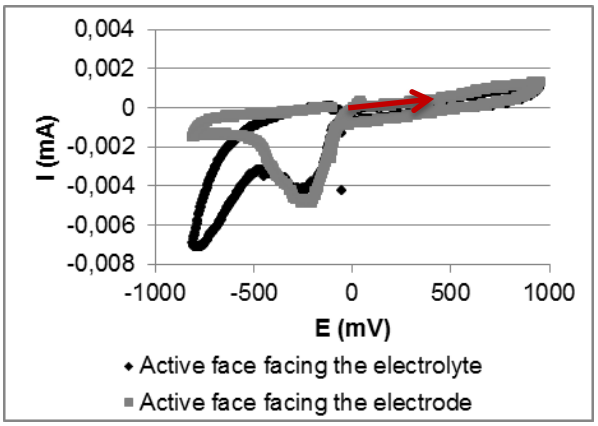

Figure 4-42 – Cyclic voltammograms of UFCA400-30ZAg0,07 membrane, active face facing the electrolyte and the electrode (initial scan towards positive potentials: -100mV → 950mV → -800mV → -100mV, scan rate: 10 mV/s, 1st cycle).

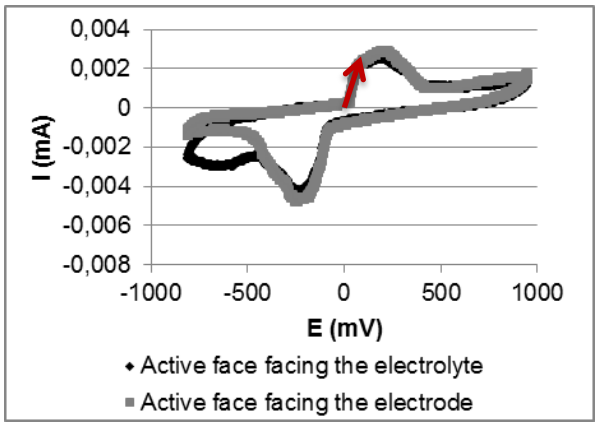

Figure 4-43 – Cyclic voltammograms of UFCA400-30ZAg0,07 membrane, active face facing the electrolyte and the electrode (initial scan towards positive potentials: -100mV → 950mV → -800mV → -100mV, scan rate: 10 mV/s, 2nd cycle).

Comparing the experiments with the active face of the membrane facing the electrolyte and the electrode, it was decided to evaluate the first option for being similar to the experiments with the silver containing zeolite.

The voltammogram of the UFCA400-30ZAg0,07 membrane starting towards positive potentials (Figure 4-42) show no oxidation peak in the first cycle, which indicates the absence of metallic silver.

Starting with reduction scan (Figure 4-40), two reduction peaks appear, at -180 mV and -560 mV. The integration of the electric current over time between -100 mV and -700 mV lead to an electric charge of the reduction peaks of 0,2 mC, which corresponds to a silver mass of 0,0002 mg. The UFCA400-30ZAg0,07 membrane, with 0,07% of silver (chapter 3.2.3), weighted 1,0 mg and, accordingly, contained 0,0007 mg of silver. Taking into account the uncertainties of the two measurements, the results are comparable.

It was not possible to perform more experiments using this method since there was adsorption of silver by the Pt disc electrode, affecting the following results.

4.5 THERMOGRAVIMETRIC ANALYSIS

The thermogravimetric analysis (TGA) was used to indirectly characterize the seven prepared membranes in terms of their composition by measuring the amount of change in the weight of the samples as a function of temperature/time, in a controlled temperature programme and atmosphere, as described in chapter 3.4.3.

In the TGA programme, the weight and heat flow changes as a function of time were obtained for the seven prepared membranes and the comparison is shown in Figure 4-44 and Figure 4-45, respectively. In the first graphic, the descending TG curve indicates a weight loss; in the second graphic, a positive peak indicates an endothermic process while a negative one indicates an exothermic process.

The TGA thermal curves obtained for each membrane are presented in appendix 1A.3, Figure A-1 – Figure A-21 (weight, heat flow and temperature as a function of time, weight and heat flow as a function of time and weight and temperature as a function of time).

As it is shown in both Figure 4-44 and Figure 4-45, there are two distinct steps: the first one corresponds to the water loss and the second to the cellulose acetate combustion. The dehydration of the membrane starts immediately and stops before the second isothermal step (110℃); the cellulose acetate combustion happens in the second heating ramp, between 350℃ and 600℃.

By the analysis of the results shown in Figure 4-44, the final weight of each sample was obtained, considering the CA400-30 membrane as the reference value for weight loss, as well as the evaporated water percentage, and is summarized in Table 4-3 and Figure 4-46. The final weight indicates the presence in the membranes of the incorporated materials (silver, zeolite and silver containing zeolite) and its percentage was compared with the initial percentage of the component added to the casting solution, as presented in chapter 3.2.3, in Table 4-4 (wet and dry base, that is, initial weight before and after the water evaporation, respectively).

The membranes have around 79% of non-structural water. The final weight obtained for each membrane (Table 4-3 and Figure 4-46) follows the tendency of the percentages of the incorporated materials in the casting solutions (Table 3-4 and Table 3-5): the membrane with the lowest final weight was UFCA400-30ZAg0,005 and with the highest was UFCA400-30ZSM5. It is visible an increasing weight with the increasing concentration of silver loaded zeolite.

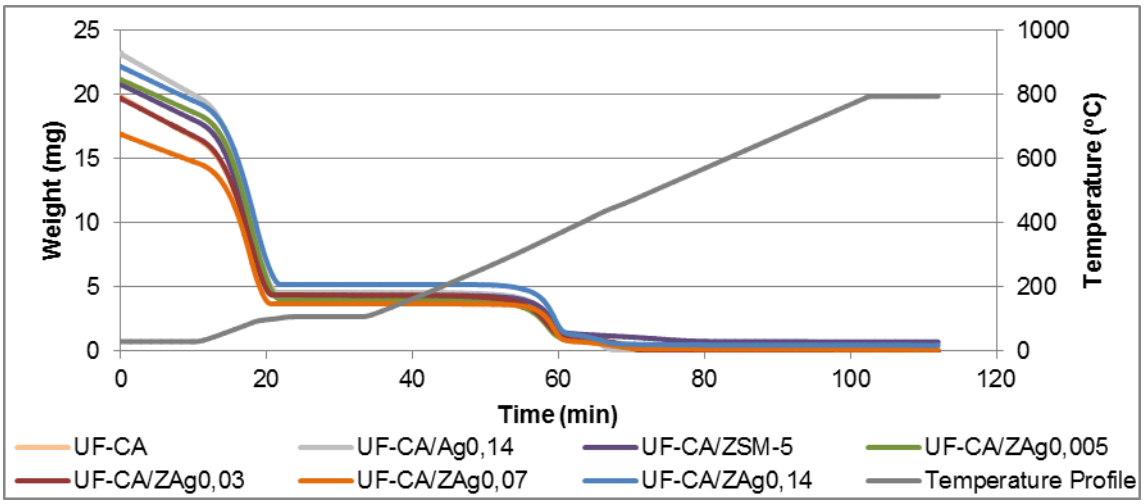

Figure 4-44 – TG curve (weight as a function of time) of the seven prepared membranes.

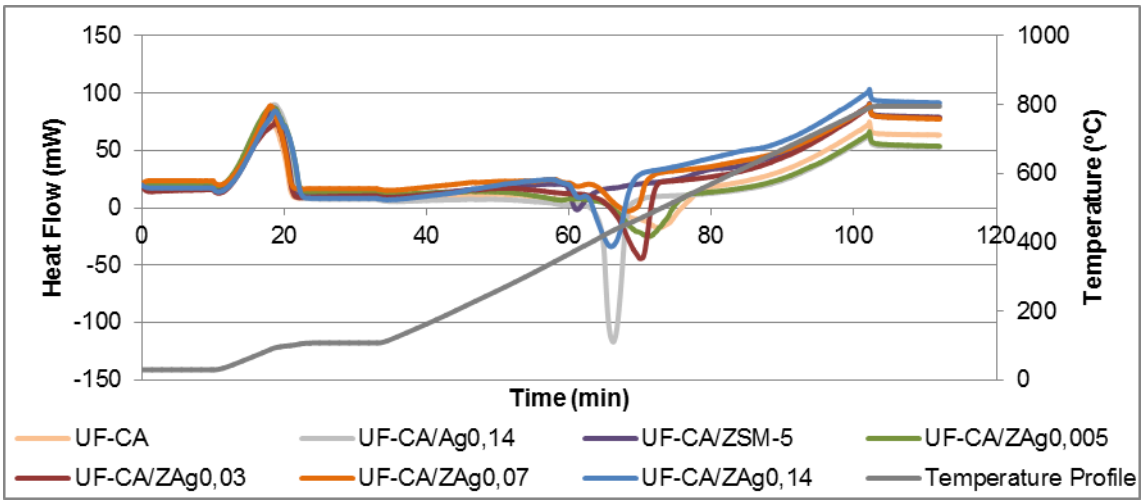

Figure 4-45 – TG curve (heat flow as a function of time) of the seven prepared membranes.

Table 4-3 – Samples weight at the end of the TGA programme and evaporated water percentage.

Membrane	Final weight (mg)	Evaporated water (%)
UFCA400-30	0,0000	78,0
UFCA400-30Ag0,14	0,0462	80,3
UFCA400-30ZSM5	0,8266	79,1
UFCA400-30ZAg0,005	0,0030	80,9
UFCA400-30ZAg0,03	0,1239	78,0
UFCA400-30ZAg0,07	0,2229	78,3
UFCA400-30ZAg0,14	0,5629	76,6

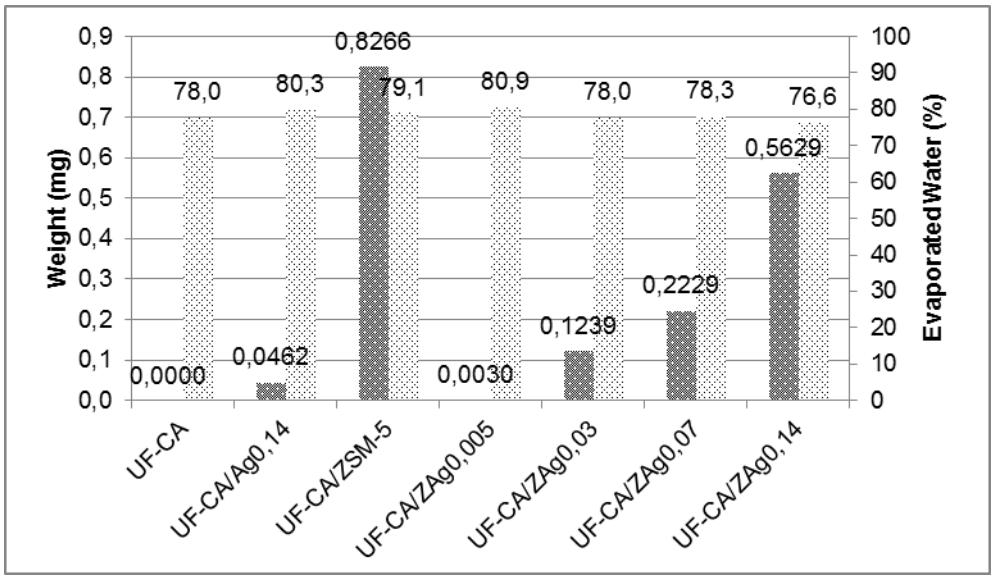

Figure 4-46 – Samples weight at the end of the TGA programme and evaporated water percentage.

Table 4-4 – Comparison of final weight percentage at the end of TGA programme and incorporated components percentage in the casting solution.

Membrane	Wet base		Dry base	
	Weight of AgNP/ZSM-5/ZAg in casting solution (%)	Final weight after TGA (%)	Weight of AgNP/ZSM-5/ZAg in casting solution (%)	Final weight after TGA (%)
UFCA400-30	0,00	0,00	0,00	0,00
UFCA400-30Ag0,14	0,14	0,20	0,85	1,01
UFCA400-30ZSM5	3,91	3,97	19,43	19,03
UFCA400-30ZAg0,005	0,10	0,01	0,58	0,07
UFCA400-30ZAg0,03	0,53	0,63	3,07	2,85
UFCA400-30ZAg0,07	1,46	1,32	8,04	6,06
UFCA400-30ZAg0,14	2,85	2,54	14,73	10,85

As it can be seen in Table 4-4, in wet base and, accordingly, in dry base, the obtained results are in general similar to the expected, except for the membrane UFCA400-30ZAg0,005. A second experiment with this membrane was performed and 0,2517 mg was obtained as the final mass, which correspond to a final weight percentage of 1,22. The incorporated silver loaded zeolite in the membrane UFCA400-30ZAg0,005 may not be homogeneously dispersed.

4.6 DETERMINATION OF THE ZETA POTENTIAL

The zeta potential of the NF membranes were determined with a 0,001 M KCl electrolyte solution in the pH range of 4 to 10, as explained in chapter 3.4.4, and the obtained results are presented in Figure 4-47.

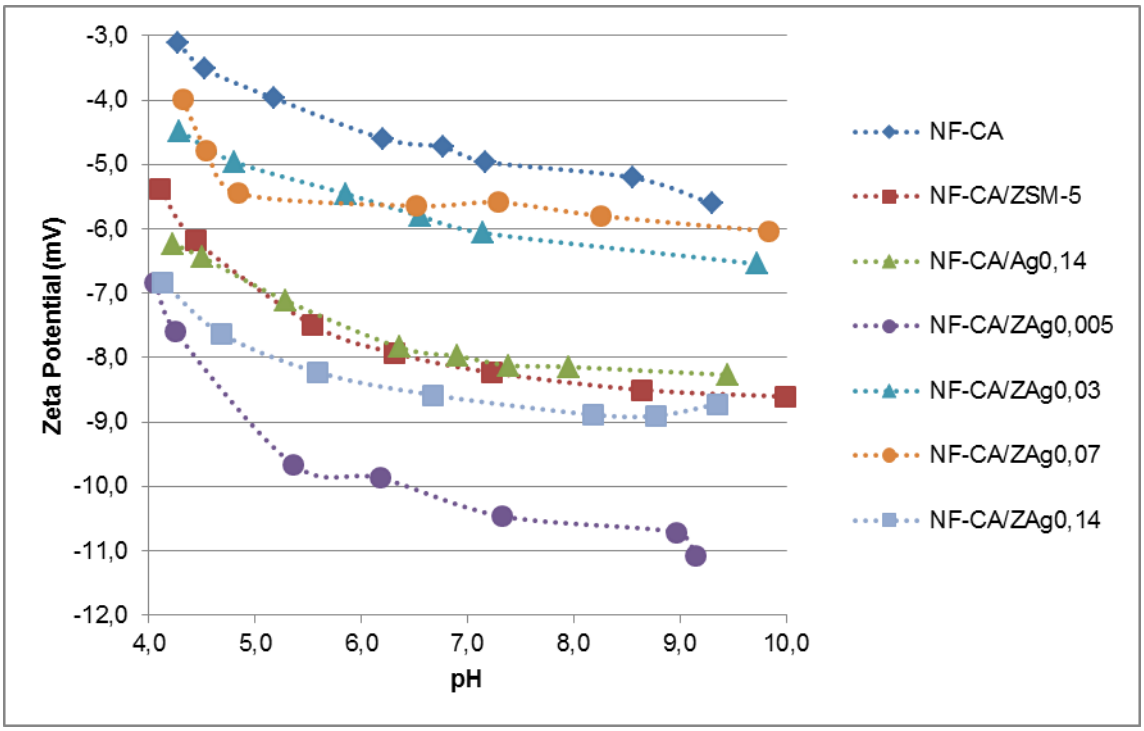

Figure 4-47 – Zeta potentials in the range of pH 4 – 9.

The obtained results show a variation of zeta potential with pH: with increasing pH, zeta potential decreases, becoming more negative, which is typical of NF cellulose acetate membranes, due to the negatively charge surface (Abitoye, Mukherjee, and Jones 2005). The dependence of zeta potential with pH is different for each membrane: NFCA400-30ZAg0,14 membrane is the least influenced by the pH (difference of 1,9 mV). The NFCA400-30Ag0,14, NFCA400-30ZAg0,07, NFCA400-30ZAg0,03, NFCA400-30, NFCA400-30ZSM5 and NFCA400-30ZAg0,005 membranes show an increasing dependency on the pH (difference of 2,0 mV, 2,0 mV, 2,1 mV, 2,5 mV, 3,2 mV and 4,2 mV, respectively). Approximately from pH 6 it is visible a zeta potential stabilization, with a maximum variation of 1,2 mV. From the initial pH to around pH 6, the membrane with highest zeta potential dependency is NFCA400-30ZAg0,005 with a variation of 3,0 mV, contrasting with NFCA400-30ZAg0,03 membrane with 1,3 mV. The remaining membranes (NFCA400-30, NFCA400-30Ag0,14, NFCA400-30ZAg0,07, NFCA400-30ZAg0,14 and NFCA400-30ZSM5) show a zeta potential difference of, respectively, 1,5 mV, 1,6 mV, 1,6 mV, 1,8 mV and 2,6 mV. The zeta potential of the modified membranes decreases relatively to the NF CA membrane. The less modified membrane (NFCA400-30ZAg0,005) has the lowest zeta potential, as reported by J. Abitoye et al. (Abitoye, Mukherjee, and Jones 2005).

4.7 EVALUATION OF THE BACTERICIDAL PROPERTIES

The antibacterial effect of seven different membranes was determined against *P. aeruginosa* and *E. coli*, as explained in chapter 3.5, using the percentage of the initial number of colony forming units (%CFU). The results of the first experiment with *P. aeruginosa* are presented in Figure 4-48 and Figure 4-49 and the results of the second experiment with *E. coli* and *P. aeruginosa* are presented in Figure 4-50 – Figure 4-53. The results are summarized in appendix 1A.4, Table A-3 – Table A-10

(cumulative time, number of colonies and CFU percentage). The membranes used were annealed, as mentioned in chapter 3.2.5.

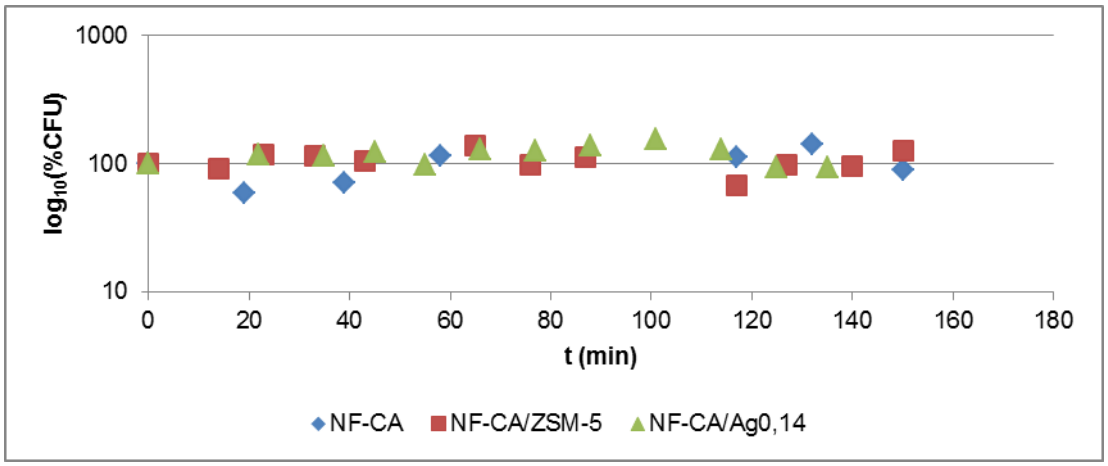

Figure 4-48 – Bactericidal effect of NFCA400-30, NFCA400-30ZSM5 and NFCA400-30Ag0,14 membranes against *P. aeruginosa* (1st).

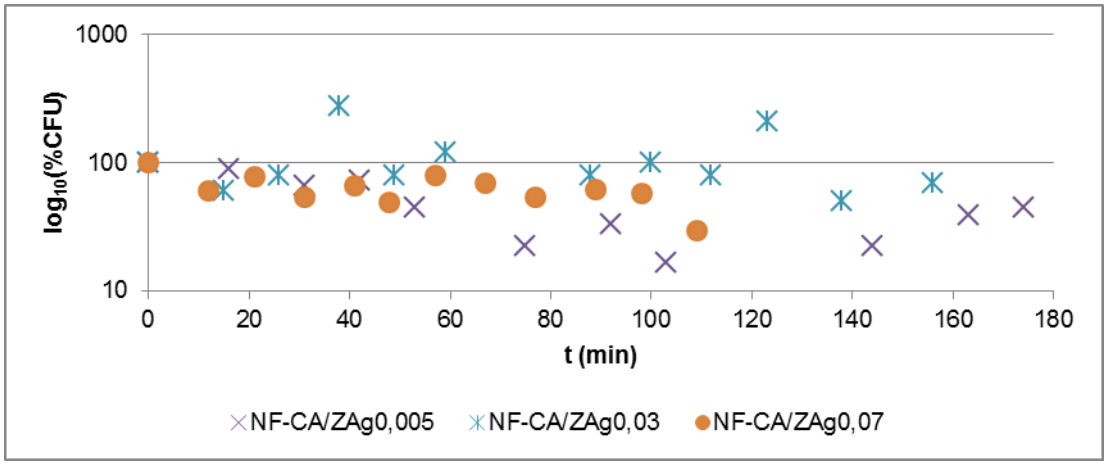

Figure 4-49 – Bactericidal effect of NFCA400-30ZAg0,005, NFCA400-30ZAg0,03 and NFCA400-30ZAg0,07 membranes against *P. aeruginosa* (1st).

In Figure 4-48 are shown the results obtained for NFCA400-30, NFCA400-30ZSM5 and NFCA400-30Ag0,14 membranes against *P. aeruginosa*. These membranes revealed a bacteriostatic effect, with final CFU percentage of 90%, 125% and 93%, respectively. The membranes with zeolite and silver nanoparticles showed a high bacterial growth after 18 hours of incubation. The results obtained for *P. aeruginosa* for NFCA400-30ZAg0,005, NFCA400-30ZAg0,03 and NFCA400-30ZAg0,07 membranes (Figure 4-49) showed bactericidal effect after 100 minutes, with inactivation ranging from 20% for NFCA400-30ZAg0,03 to 83% for NFCA400-30ZAg0,005. The highest bactericidal effect for the NFCA400-30ZAg0,005 membrane can be explained by the inhomogeneity of the membrane, result obtained in thermogravimetric analysis, in which the membrane had a higher percentage of silver loaded zeolite than the expected. After this time, an increase in the bacterial growth was observed in NFCA400-30ZAg0,005 membrane, although still below 100% (44% CFU after 174 minutes). In the end of the experiment with NFCA400-30ZAg0,03 membrane, a decrease of 30% in the bacterial growth was observed. The membranes with silver exchanged zeolite, with 0,005% and 0,03% of silver in the membrane, also showed no antimicrobial effect after 18 hours.

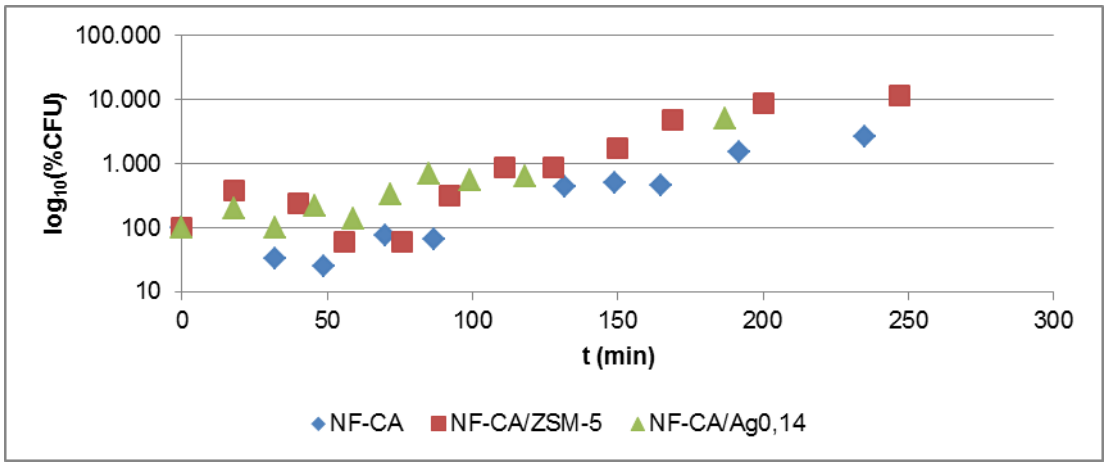

Figure 4-50 – Bactericidal effect of NFCA400-30, NFCA400-30ZSM5 and NFCA400-30Ag0,14 membranes against *E. coli*.

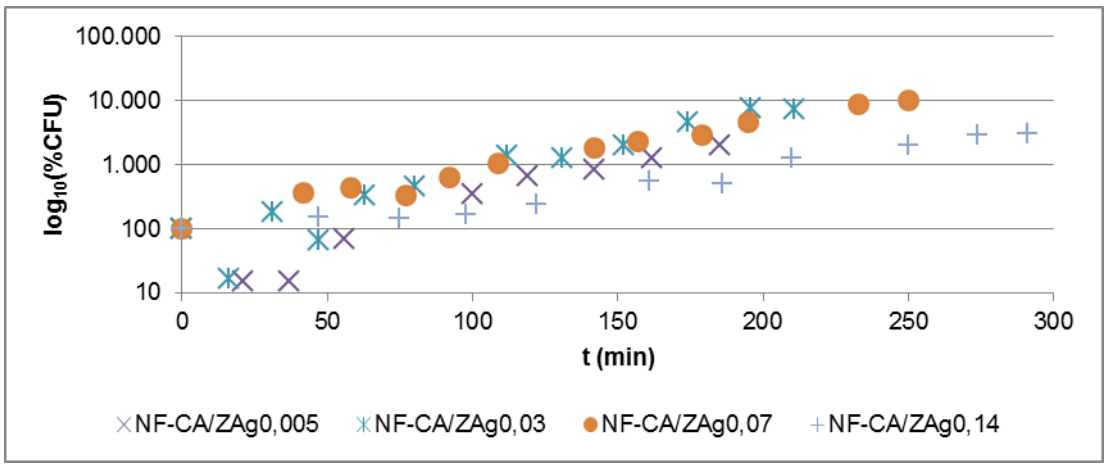

Figure 4-51 – Bactericidal effect of NFCA400-30ZAg0,005, NFCA400-30ZAg0,03, NFCA400-30ZAg0,07 and NFCA400-30ZAg0,14 membranes against *E. coli*.

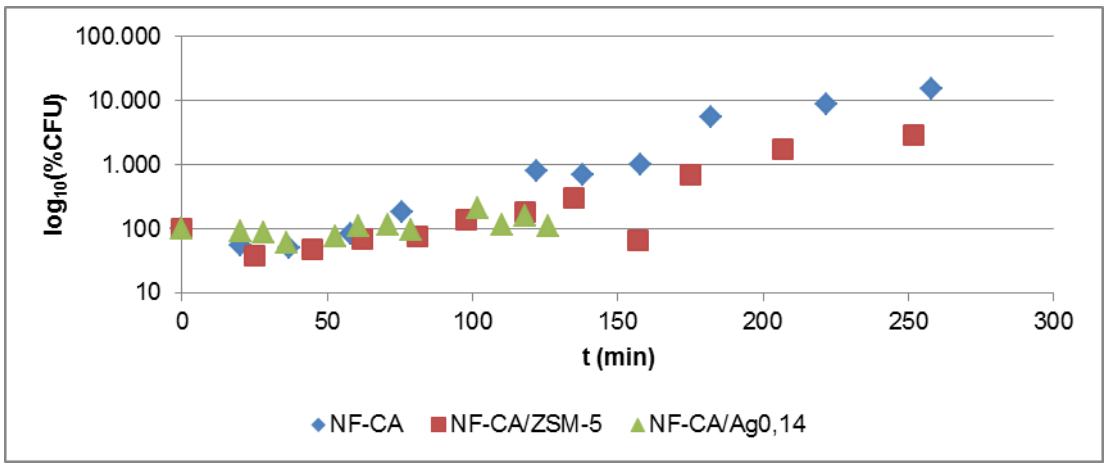

Figure 4-52 – Bactericidal effect of NFCA400-30, NFCA400-30ZSM5 and NFCA400-30Ag0,14 membranes against *P. aeruginosa* (2nd).

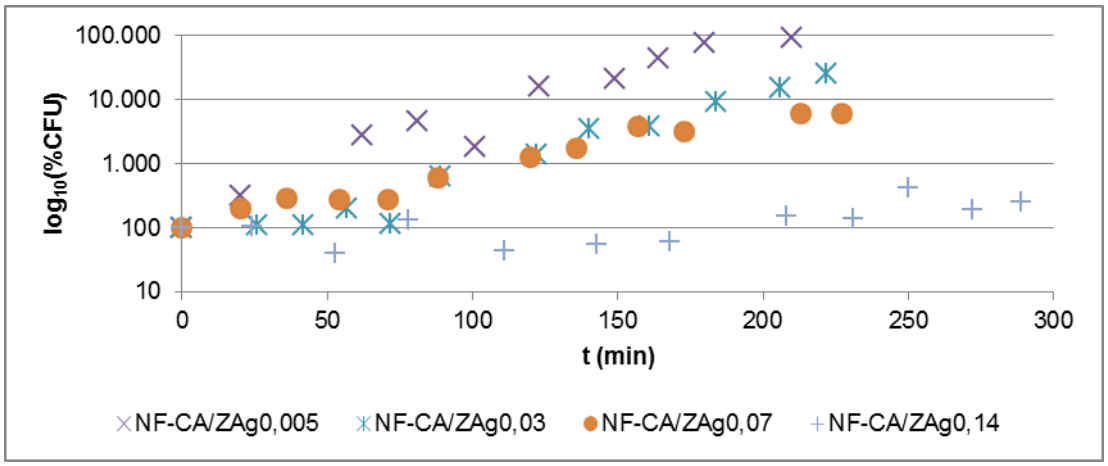

Figure 4-53 – Bactericidal effect of NFCA400-30ZAg0,005, NFCA400-30ZAg0,03, NFCA400-30ZAg0,07 and NFCA400-30ZAg0,14 membranes against *P. aeruginosa* (2nd).

The results obtained for membranes against *E. coli* (Figure 4-50 and Figure 4-51) revealed the absence of antibacterial effect, with a visible growth. The tendency of the membranes with silver loaded zeolite is similar to the obtained in the first experiment with *P. aeruginosa*. Against *P. aeruginosa* there was also no antibacterial effect (Figure 4-52 and Figure 4-53), with all the membranes showing bacterial growth with the exception of NFCA400-30Ag0,14, which presented a bacteriostatic effect. However, the time of the experiment with the silver nanoparticles membrane was around two hours while with the other six membranes it was over four hours. Against *P. aeruginosa* there is an increasing bacterial growth with the decreasing concentration of silver containing zeolite. For both cultures, the NFCA400-30ZAg0,14 membrane showed the lowest bacterial growth after five hours. This result is expected since the membrane has the highest silver content in the membrane (0,14%), which is trapped inside the ZSM-5 zeolite and results in a gradual and more lasting release of silver ions (Matsuura et al. 1997). The result obtained for NFCA400-30Ag0,14 against *E. coli* contrasts with the one obtained by Beisl (Beisl 2015), in which a high bacterial effect was observed: inactivation of 99,8% after 180 minutes. The general absence of bactericidal effect may be related with the annealing process. Although incorporated particles, prepared *ex-situ*, are preferentially located in the skin layer of nanocomposite membranes during phase inversion process, which results in more accessible particles, the more intensive annealing treatment described in chapter 3.2.5 tightened the pores on the surface, which may have made the silver nanoparticles, zeolite and silver zeolite less accessible (Murphy and de Pinho 1995; Sile-Yuksel et al. 2014; Taurozzi et al. 2008). This assumption may be corroborated with the results after 18 hours of incubation, in which a decrease or a more controlled growth of *P. aeruginosa* was observed for NFCA400-30Ag0,14, NFCA400-30ZAg0,07 and NFCA400-30ZAg0,14.

The antibacterial effect of ZSM-5 zeolite and silver containing zeolite powder against *E. coli* and *P. aeruginosa* was also evaluated, as described in chapter 3.5. A change in the silver exchanged zeolite colour was observed after approximately 1,25 hours. Since it only occurred in the silver loaded zeolite, it can be stated that the colour change is due to the silver release from the zeolite to the agar medium, which may be due to the exchange between the silver inside the zeolite and the sodium present in the

agar medium (15 g/L of tryptone, 5 g/L of papaic digest of soybean meal, 5g/L of sodium chloride and 15 g/L bacteriological agar).

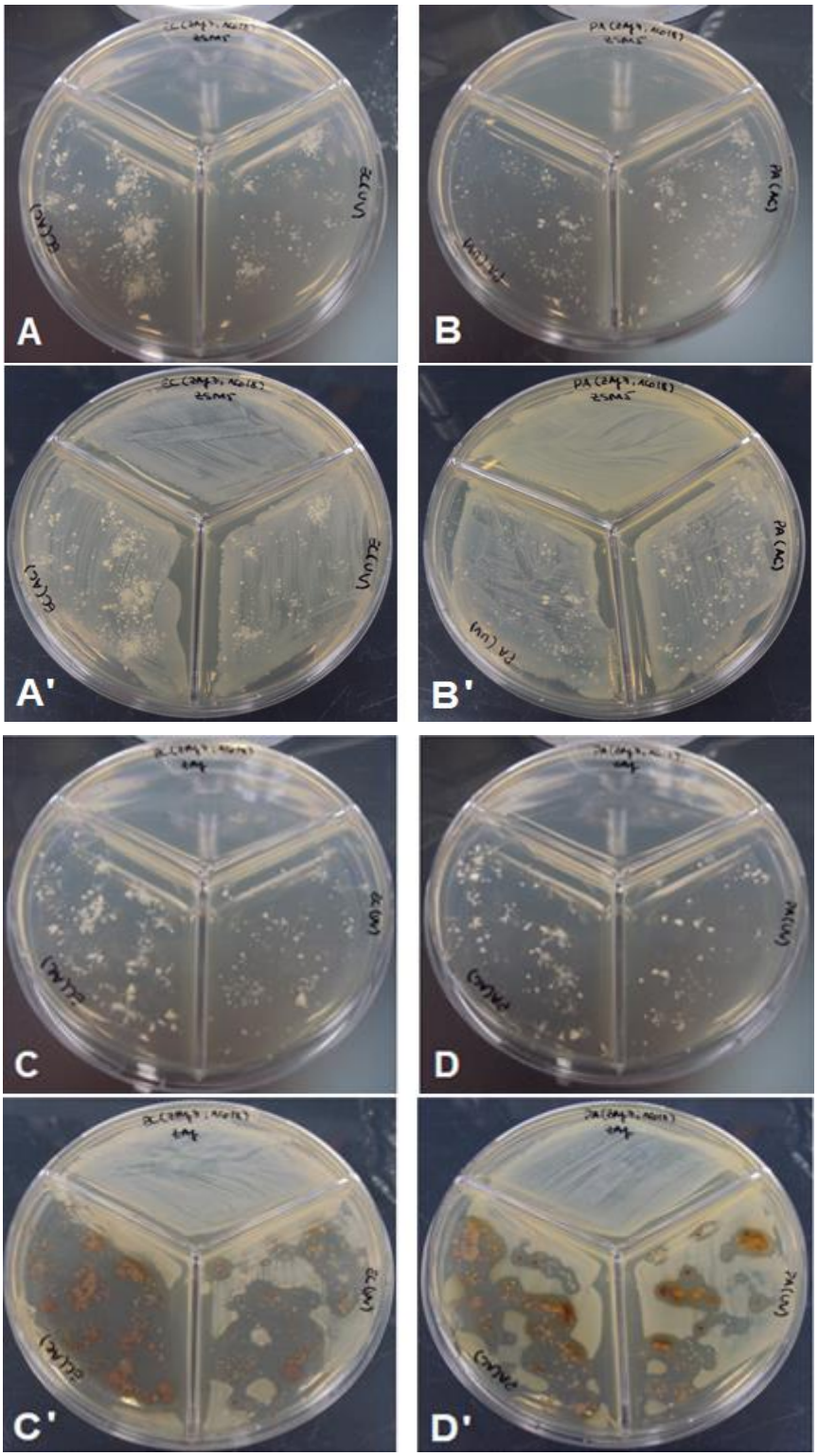

Figure 4-54 – Antimicrobial effect of zeolite and silver zeolite (before and after incubation, respectively): A/A') *E. coli* with ZSM-5 zeolite; B/B') *P. aeruginosa* with ZSM-5 zeolite; C/C') *E. coli* with ZAg; D/D') *P. aeruginosa* with ZAg.

Figure 4-54 shows the difference in bacteria growth in the presence of ZSM-5 zeolite/ZAg, compared with the blank sample. ZSM-5 zeolite shows no antibacterial effect in both cultures, since there was no growth inhibition. The silver containing zeolite revealed a strong bactericidal effect for both cultures, being the effect more pronounced in *E. coli* than in *P. aeruginosa*.

5 CONCLUSIONS

The experiments made with the asymmetric mixed matrix membranes, with silver nanoparticles, ZSM-5 zeolite and silver loaded zeolite incorporated, showed interesting results.

From the UV absorption spectra, it can be stated that the silver suspension prepared to incorporate in the cellulose acetate membrane has well-dispersed spherical silver nanoparticles. However, the red shift of the maximum absorption and the bandwidth increase with time indicates an increase in the particle size and a possible aggregation. The formation of the silver nanoparticles prepared at fixed concentration of reducing agent $NaBH_4$ can be described by a second order kinetics and exhibits absorption peaks around 400 nm with increasing absorbance with time. The addition of formamide leads to the appearance of a broad extinction band, which can indicate the presence of different distributions of particles sizes.

The incorporation of materials influences hydraulic permeability. In ultrafiltration, the incorporation of silver nanoparticles increased the hydraulic permeability of the membrane in 39,6% comparing with the cellulose acetate membrane. In contrast, the incorporation of ZSM-5 zeolite decreases the hydraulic permeability of the membrane in 52,6%. The addition of silver exchanged zeolite also decreases the hydraulic permeability, becoming higher with the increasing concentration (71,5%, 59,2% and 5,3% for the CA400-30ZAg0,005, CA400-30ZAg0,03 and CA400-30ZAg0,07 membranes, respectively). In nanofiltration, the hydraulic permeability increases with the addition of silver nanoparticles and ZSM-5 zeolite comparing with the cellulose acetate membrane (83,1% and 4,5%, respectively). As mentioned for ultrafiltration membranes, hydraulic permeability increases with increasing concentration of silver containing zeolite (difference of -9,7%, -3,2% and 44,8% for CA400-30ZAg0,005, CA400-30ZAg0,03 and CA40030ZAg0,07 membranes). The CA400-30ZAg0,14 membrane does not follow the tendency (hydraulic permeability 35,6% lower than CA400-30), probably indicating the existence of a maximum silver zeolite concentration from which the hydraulic permeability decreases.

The results for rejection coefficients of the ultrafiltration membranes for NaCl, Na_2SO_4, $MgCl_2$, $MgSO_4$ and glucose vary, not showing a tendency with the incorporated materials or rejected species. With the nanofiltration membranes, the rejection coefficients are higher for the Na_2SO_4 salt, except for the CA400-30ZAg0,14 membrane, and lower for the $MgCl_2$ salt, which can be related with the negative charge of the membrane surface and the stronger electrostatic interaction forces with bivalent anions.

The rejection coefficients of CA400-30, CA400-30ZSM5, CA400-30Ag0,14, CA400-30ZAg0,005, CA400-30ZAg0,03, CA400-30ZAg0,07 and CA400-30ZAg0,14 membranes for Na_2SO_4 are, respectively, 95,9%, 93,4%, 84,4%, 94,6%, 95,4%, 90,8% and 85,7%. For $MgCl_2$ are, respectively, 74,6%, 61,5%, 55,6%, 73,1%, 73,7%, 66,4% and 84,8%. The majority of the rejection coefficients results for the membranes with incorporated materials are lower than the ones obtained for the cellulose acetate membrane.

The electrochemical studies performed via cyclic voltammetry revealed that the silver present in the zeolite, in powder form and incorporated in the membrane, is in the cationic form. The silver inside the zeolite seems to diffuse into more stable sites in the zeolite with time.

The thermogravimetric analysis, used to indirectly characterize the membranes composition, revealed that membranes have around 79% of non-structural water. In general the final weight of the membranes was similar to the expected by the casting solutions, except for the least modified membrane, CA400-30ZAg0,005, in which the incorporated components may not be homogeneously dispersed in the membrane.

The negative zeta-potential of the membranes decreased with increasing pH, in the pH range of 4 – 9. The zeta potential of the modified membranes decreased relatively to the cellulose acetate membrane. The CA400-30ZAg0,005 membrane has the lowest zeta potential and the CA400-30ZAg0,14 membrane is the least influenced by the pH. Approximately from pH 6 the zeta potential of the membranes stabilize, with a maximum variation of 1,2 mV.

The antibacterial effect of the asymmetric membranes was determined against *Pseudomonas aeruginosa* and *Escherichia coli*. In the first experiment with *P. aeruginosa*, the CA400-30, CA400-30ZSM5 and CA400-30Ag0,14 membranes revealed a bacteriostatic effect after 150 minutes and the CA400-30ZAg0,005, CA400-30ZAg0,03 and CA400-30ZAg0,07 membranes showed bactericidal effect after 100 minutes. The membranes showed a high bacterial growth after 18 hours. The results obtained against *E. coli* and *P. aeruginosa* (second experiment) revealed the absence of antibacterial effect, with a visible growth. Against *P. aeruginosa* there was an increasing bacterial growth with the decreasing concentration of silver containing zeolite. For both cultures, the CA400-30ZAg0,14 membrane showed the lowest bacterial growth after five hours which is expected due to the higher silver content (0,14%) trapped inside the ZSM-5 zeolite, resulting in a gradual and more lasting release of silver ions. The evaluation of the bacteria growth in the presence of the ZSM-5 zeolite/silver zeolite powder revealed that ZSM-5 zeolite shows no antibacterial effect in both cultures, since there was no growth inhibition. In contrast, the silver containing zeolite revealed strong bactericidal for both cultures, being the effect more pronounced in *E. coli* than in *P.aeruginosa*.

Combining the experiments performed, the most promising membrane is the CA400-30ZAg0,07, since the casting of the membrane is not difficult, it has higher hydraulic permeability than the nanofiltration cellulose acetate membrane, it has rejection coefficients from 67% to $MgCl_2$ and 91% to Na_2SO_4 and one of the highest antibacterial effects.

5.1 PERSPECTIVES FOR FUTURE WORK

As future work, the following suggestions are pointed out:

- Investigate the role of PVP as support of silver reducing agents;
- Investigate the role of the system of solvents (acetone and formamide) in the silver loaded zeolite incorporated in the casting solutions;
- Investigate the silver oxidation state of silver nanoparticles through electrochemical studies;
- Investigate the silver leaching from the membranes to the medium;
- Determine the antibacterial activity of the asymmetric cellulose and mixed matrix membranes, annealed at 95℃, against *E. coli* and *P. aeruginosa*;
- Investigate the antibacterial properties of silver nanoparticles suspension in contact with different bacteria;
- Investigate the antibacterial properties of mixed matrix membranes in long term permeation conditions of a solution containing bacteria;
- Investigate the biofouling formation at membranes surfaces in long term permeation conditions.

BIBLIOGRAPHY

Abitoye, Joshua Olufemi, Parna Mukherjee, and Kimberly Jones. 2005. “Ion Implantation: Effect on Flux and Rejection Properties of NF Membranes.” *Environmental Science and Technology* 39(17): 6487–93.

Afonso, Maria Diná, and Maria Norberta De Pinho. 1990. “Ultrafiltration of Bleach Effluents in Cellulose Production.” *Desalination* 79(2–3): 115–24.

———. 2000. “Transport of MgSO4, MgCl2, and Na2SO4 across an Amphoteric Nanofiltration Membrane.” *Journal of Membrane Science* 179(1–2): 137–54.

Ali, M. A., B. Brisdon, and W. J. Thomas. 2003. “Synthesis, Characterization and Catalytic Activity of ZSM-5 Zeolites Having Variable Silicon-to-Aluminum Ratios.” *Applied Catalysis A: General* 252(1): 149–62.

American Public Health Association, American Water Works Association, Water Environment Federation. 1999. Standard Methods *Standard Methods for the Examination of Water and Wastewater*.

Applegate, Lynn E., Carl W. Erkenbrecher, and Harvey Winters. 1989. “New Chloroamine Process to Control Aftergrowth and Biofouling in permasepR B-10 RO Surface Seawater Plants.” *Desalination* 74(C): 51–67.

Arthanareeswaran, G., and P. Thanikaivelan. 2010. “Fabrication of Cellulose Acetate-Zirconia Hybrid Membranes for Ultrafiltration Applications: Performance, Structure and Fouling Analysis.” *Separation and Purification Technology* 74(2): 230–35.

Asapu, Sunitha, Santosh Pant, Cyndee L. Gruden, and Isabel C. Escobar. 2014. “An Investigation of Low Biofouling Copper-Charged Membranes for Desalination.” *Desalination* 338(1): 17–25.

Baia, Lucian, and Simion Simon. 2007. “UV-VIS and TEM Assessment of Morphological Features of Silver Nanoparticles from Phosphate Glass Matrices.” *Modern Research and Educational Topics in Microscopy*: 576–83.

Beier, S. et al. 2010. “Treatment of Hospital Wastewater Effluent by Nanofiltration and Reverse Osmosis.” *Water Science and Technology* 61(7): 1691–98.

Beisl, Stefan. 2015. “Investigation of the Influence of Silver Nanoparticles on the Permeation and Bactericidal Properties of Nanofiltration Membranes.” Technischen Universität Wien; Instituto Superior Técnico.

Bhattacharjee, Sourav. 2016. “DLS and Zeta Potential - What They Are and What They Are Not?” *Journal of Controlled Release* 235: 337–51.

Boschetto, Daiane Lúcia et al. 2012. “Preparation and Antimicrobial Activity of Polyethylene Composite Films with Silver Exchanged Zeolite-Y.” *Chemical Engineering Journal* 204–205: 210–16.

Boussahel, R., S. Bouland, K.M. Moussaoui, and A. Montiel. 2000. “Removal of Pesticide Residues in Water Using the Nanofiltration Process.” *Desalination* 132(October): 205–9.

Bower, Nathan, and Anne Yu. 2011. 88 Journal of Chemical Education *Exploiting Mass Measurements in Different Environments: Density, Magnetic Susceptibility, and*

Thermogravimetry.

Van Der Bruggen, B., K. Everaert, D. Wilms, and C. Vandecasteele. 2001. “Application of Nanofiltration for Removal of Pesticides, Nitrate and Hardness from Ground Water: Rejection Properties and Economic Evaluation.” *Journal of Membrane Science* 193(2): 239–48.

Van der Bruggen, B., M. Mänttäri, and M. Nyström. 2008. “Drawbacks of Applying Nanofiltration and How to Avoid Them: A Review.” *Separation and Purification Technology* 63(2): 251–63.

Canterbury, University of. 2015. “Determination of Chloride Ion Concentration by Titration (Mohr ’S Method).” : 1–2.

Caro, C. et al. 2010. Nanotechnology and Nanomaterials *Silver Nanoparticles*. ed. David Pozo. InTech.

Caro, Jürgen, Martin Bülow, and Wolfgang Schirmer. 1985. “Microdynamics of Methane, Ethane and Propane in ZSM-5 Type Zeolites.” *Journal of the Chemical Society, Faraday Transactions 1* 81: 2541–50.

Center for Environmental Research Information. 1990. “Environmental Pollution Control Alternatives: Drinking Water Treatment for Small Communities.” : 1–82.

Chou, Wen-Li, Da-Guang Yu, and Ming-Chien Yang. 2005. “The Preparation and Characterization of Silver-Loading Cellulose Acetate Hollow Fiber Membrane for Water Treatment.” *Polymers for Advanced Technologies* 16(8): 600–607.

Corporation, Shimadzu. 2009. *Total Organic Carbon Analyzer TOC-VCPH/CPN*.

Crison. 2001. *Conductimetros GLP 31/32: Manual Del Usuario*. Alella.

Das, Ratan, Sneha Gang, and Siddhartha Sankar Nath. 2011. “Preparation and Antibacterial Activity of Silver Nanoparticles.” *Journal of Biomaterials and Nanobiotechnology* 2(4): 472–75.

Dean, Derrick. 2014. *Thermal Gravimetric Analysis*.

Delgado, A. V. et al. 2005. “Measurement and Interpretation of Electrokinetic Phenomena (IUPAC Technical Report).” *Pure and Applied Chemistry* 77(10): 1753–1805.

Desai, Rucha, Venu Mankad, Sanjeev K. Gupta, and Prafulla K. Jha. 2012. “Size Distribution of Silver Nanoparticles: UV-Visible Spectroscopic Assessment.” *International Journal of Nanoscience* 4: 30–34.

Dong, Lei xi et al. 2015. “Fabrication and Anti-Biofouling Properties of Alumina and Zeolite Nanoparticle Embedded Ultrafiltration Membranes.” *Desalination* 365: 70–78.

Elimelech, Menachem, Xiaohua Zhu, Amy E. Childress, and Seungkwan Hong. 1997. “Role of Membrane Surface Morphology in Colloidal Fouling of Cellulose Acetate and Composite Aromatic Polyamide Reverse Osmosis Membranes.” *Journal of Membrane Science* 127(1): 101–9.

Fairbrother, Fred, and Harold Mastin. 1924. “CCCXII.—Studies in Electro-Endosmosis. Part I.” *J. Chem. Soc., Trans.* 125: 2319–30.

Ferreira, Liliana et al. 2012. “Antimicrobial Activity of Faujasite Zeolites Doped with Silver.” *Microporous and Mesoporous Materials* 160: 126–32.

Figueiredo, Ana Sofia et al. 2015. “Tailoring of Structures and Permeation Properties of Asymmetric Nanocomposite Cellulose Acetate/silver Membranes.” *Journal of Applied Polymer Science*

132(21).

———. 2016. “Asymmetric Nanocomposite Cellulose Acetate/silver Ultrafiltration Membranes – Permeation Performance and Antibacterial Effect.” Instituto Superior Técnico.

GmbH, Anton Paar. 2003. *EKA: Electro Kinetic Analyzer Instruction Manual*. Austria.

Gottenbos, Bart, Henny C. Van Der Mei, and Henk J. Busscher. 1999. “Models for Studying Initial Adhesion and Surface Growth in Biofilm Formation on Surfaces.” *Methods in Enzymology* 310: 523–34.

Guillen, Gregory R., Yinjin Pan, Minghua Li, and Eric M V Hoek. 2011. “Preparation and Characterization of Membranes Formed by Nonsolvent Induced Phase Separation: A Review.” *Industrial and Engineering Chemistry Research* 50(7): 3798–3817.

Gwon, Eun M., Myong J. Yu, Hee Kyong Oh, and Yong H. Ylee. 2003. “Fouling Characteristics of NF and RO Operated for Removal of Dissolved Matter from Groundwater.” *Water Research* 37(12): 2989–97.

Hilal, Nidal et al. 2004. “A Comprehensive Review of Nanofiltration Membranes: Treatment, Pretreatment, Modelling, and Atomic Force Microscopy.” *Desalination* 170(3): 281–308.

Huang, Weijuan et al. 2016. “Fabrication of Flexible Self-Standing All-Cellulose Nanofibrous Composite Membranes for Virus Removal.” *Carbohydrate Polymers* 143: 9–17.

Inc., Perkin Elmer. 2004. *A Beginner’s Guide to Thermogravimetric Analysis*.

Jhaveri, Jainesh H., and Z. V. P. Murthy. 2016. “A Comprehensive Review on Anti-Fouling Nanocomposite Membranes for Pressure Driven Membrane Separation Processes.” *Desalination* 379: 137–54.

Khan, Muhammad Tariq, Pei Ying Hong, Nabil Nada, and Jean Philippe Croue. 2015. “Does Chlorination of Seawater Reverse Osmosis Membranes Control Biofouling?” *Water Research* 78: 84–97.

Khan, Zaheer, Shaeel Ahmed Al-Thabaiti, Abdullah Yousif Obaid, and A. O. Al-Youbi. 2011. “Preparation and Characterization of Silver Nanoparticles by Chemical Reduction Method.” *Colloids and Surfaces B: Biointerfaces* 82(2): 513–17.

Kissinger, P. T., and W. R. Heineman. 1983. “Cyclic Voltammetry.” *Journal of Chemical Education* 60(9): 702–6.

Köhler, Stephan J. et al. 2016. “Upgrading Coagulation with Hollow-Fibre Nanofiltration for Improved Organic Matter Removal during Surface Water Treatment.” *Water Research* 89: 232–40.

Koseoglu-Imer, Derya Y., Borte Kose, Mahmut Altinbas, and Ismail Koyuncu. 2013. “The Production of Polysulfone (PS) Membrane with Silver Nanoparticles (AgNP): Physical Properties, Filtration Performances, and Biofouling Resistances of Membranes.” *Journal of Membrane Science* 428: 620–28.

Lalueza, Patricia, Marta Monzón, Manuel Arruebo, and Jesús Santamaría. 2011. “Bactericidal Effects of Different Silver-Containing Materials.” *Materials Research Bulletin* 46(11): 2070–76.

Lauffer, Max A., and Ross Aiken Gortner. 1939. “Electrokinetics. XXI. Electrokinetic Theory. Streaming Potential and the Electroösmotic Counter Effect.” *The Journal of Physical Chemistry* 43(6): 721–32.

Lemos, M.A.N.D.A. et al. 1999. “Modelling the Voltammetric Behaviour of Cobalt Cations inside Zeolites.” *Studies in Surface Science and Catalysis* 122: 443–46.

Li, Jian Hua et al. 2013. “The Double Effects of Silver Nanoparticles on the PVDF Membrane: Surface Hydrophilicity and Antifouling Performance.” *Applied Surface Science* 265: 663–70.

Li, Yong-Jun, and Chun-Yan Liu. 2001. “Silver-Exchanged Zeolite Y-Modified Electrodes: Size Selectivity for Anions.” *Journal of Electroanalytical Chemistry* 517(1–2): 117–20.

Liang, Can Zeng et al. 2014. “Treatment of Highly Concentrated Wastewater Containing Multiple Synthetic Dyes by a Combined Process of Coagulation/flocculation and Nanofiltration.” *Journal of Membrane Science* 469: 306–15.

Maillard, Mathieu, Suzanne Giorgio, and Marie Paule Pileni. 2003. “Tuning the Size of Silver Nanodisks with Similar Aspect Ratios: Synthesis and Optical Properties.” *Journal of Physical Chemistry B* 107(11): 2466–70.

Marconnet, C. et al. 2011. “Membrane Biofouling Control by UV Irradiation.” *Desalination* 276(1–3): 75–81.

Matsuura, T. et al. 1997. “Prolonged Antimicrobial Effect of Tissue Conditioners Containing Silver-Zeolite.” *Journal of dentistry* 25(5): 373–77.

Melorose, J., R. Perroy, and S. Careas. 2015. 1 United Nations *World Population Prospects*.

Moons, Kathleen, and Bart Van der Bruggen. 2006. “Removal of Micropollutants during Drinking Water Production from Surface Water with Nanofiltration.” *Desalination* 199(1–3): 245–47.

Mumpton, Frederick A. 1999. “La Roca Magica: Uses of Natural Zeolites in Agriculture and Industry.” *Proceedings of the National Academy of Sciences of the United States of America* 96(7): 3463–70.

Murphy, Damien, and Maria Norberta de Pinho. 1995. “An ATR-FTIR Study of Water in Cellulose Acetate Membranes Prepared by Phase Inversion.” *Journal of Membrane Science* 106(3): 245–57.

Myers, John A, Brandon S Curtis, and Wayne R Curtis. 2013. “Improving Accuracy of Cell and Chromophore Concentration Measurements Using Optical Density.” *BMC Biophysics* 6(1): 4.

National Environmental Services Center. 1966. 1 National Dirinking Water Clearinghouse Fact Sheet *Tech Brief - Disinfection*.

Ochando Pulido, Javier Miguel, and Antonio Martínez Férez. 2015. “Impacts of Operating Conditions on Nanofiltration of Secondary-Treated Two-Phase Olive Mill Wastewater.” *Journal of Environmental Management* 161: 219–27.

Ong, Yee Kang et al. 2014. “Nanofiltration Hollow Fiber Membranes for Textile Wastewater Treatment: Lab-Scale and Pilot-Scale Studies.” *Chemical Engineering Science* 114: 51–57.

Le Ouay, Benjamin, and Francesco Stellacci. 2015. “Antibacterial Activity of Silver Nanoparticles: A Surface Science Insight.” *Nano Today* 10(3): 339–54.

Palma, P. et al. 2016. “Membranes Technology Used in Water Treatment: Chemical, Microbiological and Ecotoxicological Analysis.” *Science of the Total Environment* 568: 998–1009.

Park, Minkyu et al. 2016. “Pre-Ozonation for High Recovery of Nanofiltration (NF) Membrane System: Membrane Fouling Reduction and Trace Organic Compound Attenuation.” *Journal of Membrane*

Science 523(September 2016): 255–63.

Pendergast, MaryTheresa M., and Eric M. V. Hoek. 2011. “A Review of Water Treatment Membrane Nanotechnologies.” *Energy & Environmental Science* 4(6): 1946–71.

De Pinho, Maria Norberta. 1988. “Annealing Effect of Cellulose Acetate Membranes on Ethanol and Glucose Reverse Osmosis Separation.” *Desalination* 68(2–3): 211–21.

Pinnau, I., and B. D. Freeman. 1999. “Formation and Modification of Polymeric Membranes: Overview.” *Membrane Formation and Modification* 744: 1.

Prescott, Lansing M, Donald A Klein, and John P Harley. 2002. Microbiology *Microbiology*.

Rai, Mahendra, Alka Yadav, and Aniket Gade. 2009. “Silver Nanoparticles as a New Generation of Antimicrobials.” *Biotechnology Advances* 27(1): 76–83.

Rauwel, Protima, Erwan Rauwel, Stanislav Ferdov, and Mangala P. Singh. 2015. “Silver Nanoparticles : Synthesis, Properties and Applications.” 2015: 2–4.

Rosa, Maria João, and Maria Norberta De Pinho. 1994. “Separation of Organic Solutes by Membrane Pressure-Driven Processes.” *Journal of Membrane Science* 89(3): 235–43.

Sadrzadeh, Mohtada, and Subir Bhattacharjee. 2013. “Rational Design of Phase Inversion Membranes by Tailoring Thermodynamics and Kinetics of Casting Solution Using Polymer Additives.” *Journal of Membrane Science* 441: 31–44.

Schaep, Johan et al. 1998. “Removal of Hardness from Groundwater by Nanofiltration.” *Desalination* 119(1–3): 295–302.

Schweiss, Ruediger, Petra B. Welzel, Carsten Werner, and Wolfgang Knoll. 2001. “Dissociation of Surface Functional Groups and Preferential Adsorption of Ions on Self-Assembled Monolayers Assessed by Streaming Potential and Streaming Current Measurements.” *Langmuir* 17(14): 4304–11.

Scott, K., and R. Hughes. 1997. Journal of Membrane Science *Industrial Membrane Separation Technology*.

Sile-Yuksel, Merve, Bahar Tas, Derya Y. Koseoglu-Imer, and Ismail Koyuncu. 2014. “Effect of Silver Nanoparticle (AgNP) Location in Nanocomposite Membrane Matrix Fabricated with Different Polymer Type on Antibacterial Mechanism.” *Desalination* 347: 120–30.

Sivakumar, Muthusamy, Doraisamy Raju Mohan, and Ramamoorthy Rangarajan. 2006. “Studies on Cellulose Acetate-Polysulfone Ultrafiltration Membranes: II. Effect of Additive Concentration.” *Journal of Membrane Science* 268(2): 208–19.

Structure Commission of the International Zeolite Association (IZA). 2007. “Framework Type MFI.” : 212–13. http://rcsr.fos.su.se/IZA-SC/ftc_fw.php?STC=MFI (October 23, 2016).

Taurozzi, Julian S. et al. 2008. “Effect of Filler Incorporation Route on the Properties of Polysulfone-Silver Nanocomposite Membranes of Different Porosities.” *Journal of Membrane Science* 325(1): 58–68.

Thielbeer, Frank, Ken Donaldson, and Mark Bradley. 2011. “Zeta Potential Mediated Reaction Monitoring on Nano and Microparticles.” *Bioconjugate Chemistry* 22(2): 144–50.

UNEP. 2008. United Nations Environment Programme (UNEP) *Vital Water Graphics: An Overview of the State of the World’s Fresh and Marine Waters*.

US Environmental Protection Agency. 1995. “Environmental Planning for Small Communities A Guide for Local Decision-Makers.” (September): 156.

USGS. 2015. “The USGS Water Science School.” *http://water.usgs.gov/edu/earthgwlandsubside.html*.

Verlicchi, P., A. Galletti, M. Petrovic, and D. BarcelÓ. 2010. “Hospital Effluents as a Source of Emerging Pollutants: An Overview of Micropollutants and Sustainable Treatment Options.” *Journal of Hydrology* 389(3–4): 416–28.

Wang, Hongshui et al. 2005. “Mechanisms of PVP in the Preparation of Silver Nanoparticles.” *Materials Chemistry and Physics* 94(2–3): 449–53.

Wang, Jinwen et al. 2014. “A Critical Review of Transport through Osmotic Membranes.” *Journal of Membrane Science* 454: 516–37.

Wang, Xiao-Lin et al. 2009. “Characterization and Applications of Nanofiltration Membranes: State of the Art.” *Desalination* 236(1–3): 316–26.

Wang, Xiao-Lin, Ai-ling Ying, and Wei-ning Wang. 2002. “Nanofiltration of L-Phenylalanine and L-Aspartic Acid Aqueous Solutions.” *Journal of Membrane Science* 196: 59–67.

Wang, Xiao-Lin, Chenghong Zhang, and Pingkai Ouyang. 2002. “The Possibility of Separating Saccharides from a NaCl Solution by Using Nanofiltration in Diafiltration Mode.” *Journal of Membrane Science* 204(1–2): 271–81.

Weerasekara, Nuwan A., Kwang Ho Choo, and Chung Hak Lee. 2016. “Biofouling Control: Bacterial Quorum Quenching versus Chlorination in Membrane Bioreactors.” *Water Research* 103: 293–301.

Widoniak, J., S. Eiden-Assmann, and G. Maret. 2005. “Silver Particles Tailoring of Shapes and Sizes.” *Colloids and Surfaces A: Physicochemical and Engineering Aspects* 270–271(1–3): 340–44.

Wiesner, M R, and S Chellam. 1999. “The Promise of Membrane Technologies.” *Environmental science & technology* 33(17): 360–66.

X-Flow. “Membrane Technology: For Every Industry and Filtration Application.” http://xflow.pentair.com/en/technologies/membrane-technology-in-general (October 18, 2016).

Xie, He, Tomonori Saito, and Michael A. Hickner. 2011. “Zeta Potential of Ion-Conductive Membranes by Streaming Current Measurements.” *Langmuir* 27(8): 4721–27.

Yang, Qingchun et al. 2016. “Hydrochemical Characterization and Pollution Sources Identification of Groundwater in Salawusu Aquifer System of Ordos Basin, China.” *Environmental Pollution* 216: 340–49.

Zhang, Wenxiang, Jianquan Luo, Luhui Ding, and Michel Y. Jaffrin. 2015. “A Review on Flux Decline Control Strategies in Pressure-Driven Membrane Processes.” *Industrial and Engineering Chemistry Research* 54(11): 2843–61.

Zhou, Dong et al. 2015. “Development of Lower Cost Seawater Desalination Processes Using Nanofiltration Technologies - A Review.” *Desalination* 376(1219): 109–16.

Zielińska, Anna et al. 2009. “Preparation of Silver Nanoparticles with Controlled Particle Size.” *Procedia Chemistry* 1(2): 1560–66.

Zulaikha, S., W. J. Lau, A. F. Ismail, and J. Jaafar. 2014. “Treatment of Restaurant Wastewater Using Ultrafiltration and Nanofiltration Membranes.” *Journal of Water Process Engineering* 2: 58–62.

A. APPENDIX

A.1 MANUFACTURING OF THE MEMBRANES

PREPARATION OF SILVER NANOPARTICLES

The concentration of the chemicals used in the preparation of the silver nanoparticles suspension is presented in Table A-1.

Table A-1 – Concentrations used to prepare the nanoparticle suspension.

Chemical	$m_{weighted}$ (g)	C (g/mL)	C (mol/L)
PVP	0,0812	0,010	-
$AgNO_3$	0,5038	0,126	0,741
$NaBH_4$	0,0302	0,008	0,200

A.2 DETERMINATION OF THE ZETA-POTENTIAL

The zeta potential as a function of pH for each membrane is presented in Table A-2.

Table A-2 – Zeta potential as a function of pH for each prepared membrane.

NFCA400-30		NFCA400-30ZSM5		NFCA400-30Ag0,14	
pH	ZP (mV)	pH	ZP (mV)	pH	ZP (mV)
4,274	-3,117	4,108	-5,378	4,223	-6,229
4,534	-3,518	4,441	-6,178	4,504	-6,439
5,179	-3,970	5,540	-7,488	5,284	-7,108
6,210	-4,599	6,316	-7,928	6,356	-7,836
6,774	-4,728	7,229	-8,229	6,908	-7,975
7,165	-4,957	8,637	-8,499	7,391	-8,120
8,563	-5,206	9,997	-8,603	7,953	-8,143
9,307	-5,607			9,446	-8,266

NFCA400-30ZAg0,005		NFCA400-30ZAg0,03		NFCA400-30ZAg0,07		NFCA400-30ZAg0,14	
pH	ZP (mV)	pH	ZP (mV)	pH	ZP (mV)	pH	ZP (mV)
4,063	-6,835	4,292	-4,479	4,319	-3,995	4,134	-6,827
4,255	-7,600	4,801	-4,955	4,545	-4,791	4,680	-7,624
5,362	-9,657	5,858	-5,456	4,846	-5,450	5,589	-8,225
6,185	-9,871	6,550	-5,798	6,516	-5,641	6,674	-8,578
7,323	-10,460	7,146	-6,062	7,285	-5,587	8,180	-8,884
8,968	-10,710	9,733	-6,546	8,253	-5,796	8,778	-8,901
9,143	-11,070			9,837	-6,036	9,353	-8,718

A.3 THERMOGRAVIMETRIC ANALYSIS

The TGA thermal curves for each prepared membrane are presented in Figure A-1 – Figure A-21.

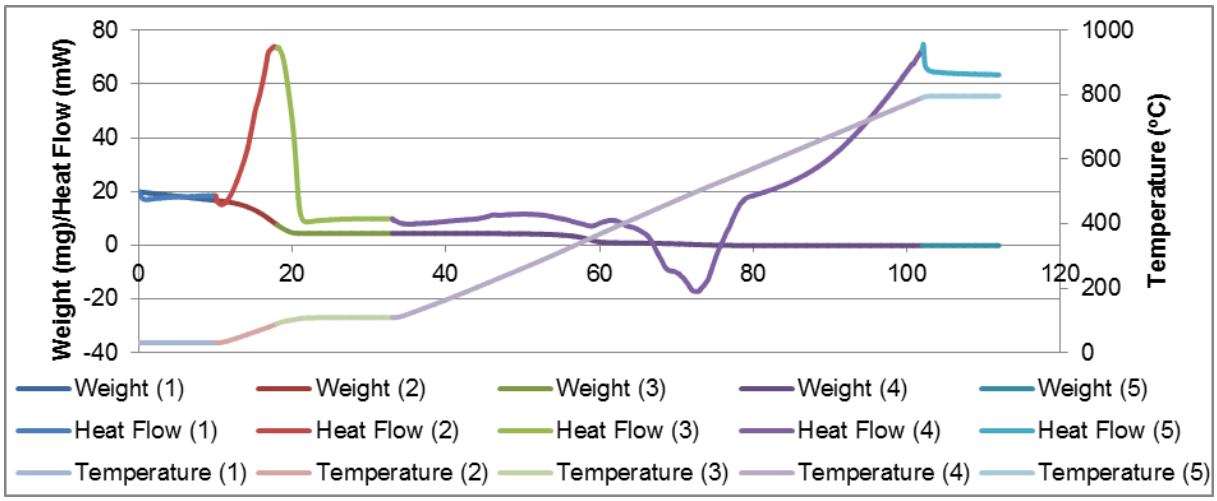

Figure A-1 – TG analysis of the UFCA400-30 membrane (weight, heat flow and temperature as a function of time).

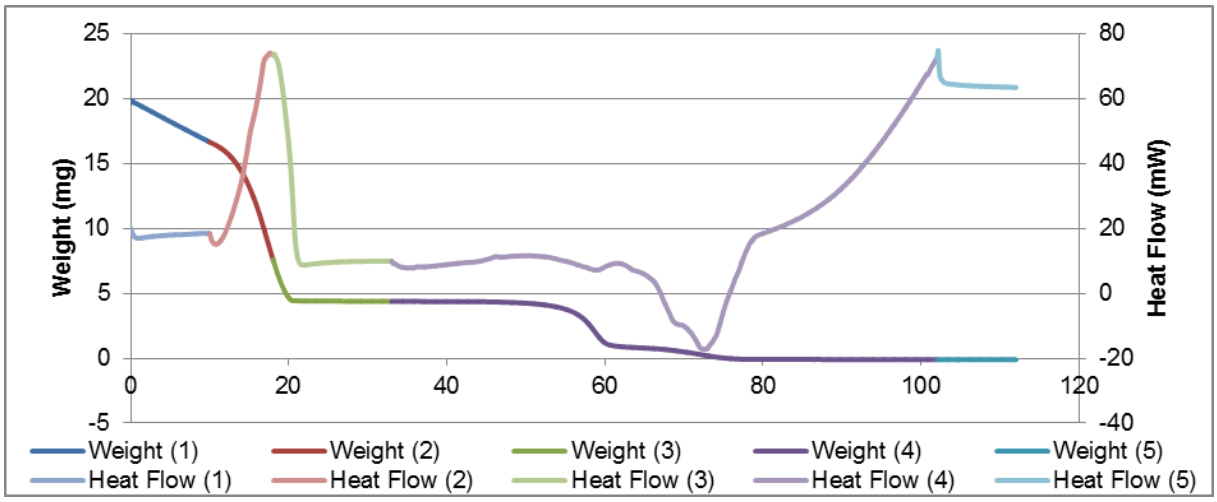

Figure A-2 – TG analysis of the UFCA400-30 membrane (weight and heat flow as a function of time).

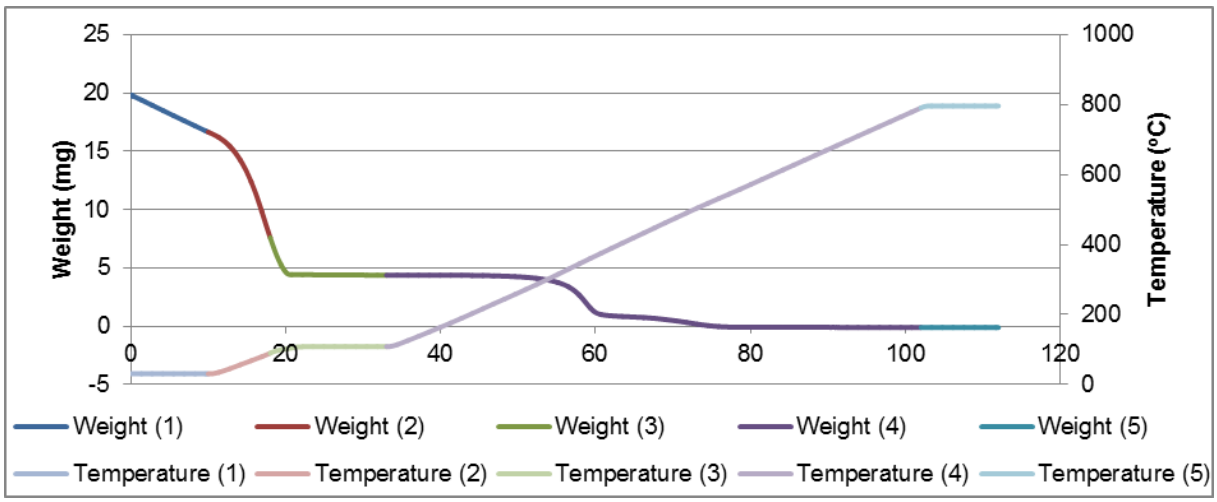

Figure A-3 – TG analysis of the UFCA400-30 membrane (weight and temperature as a function of time).

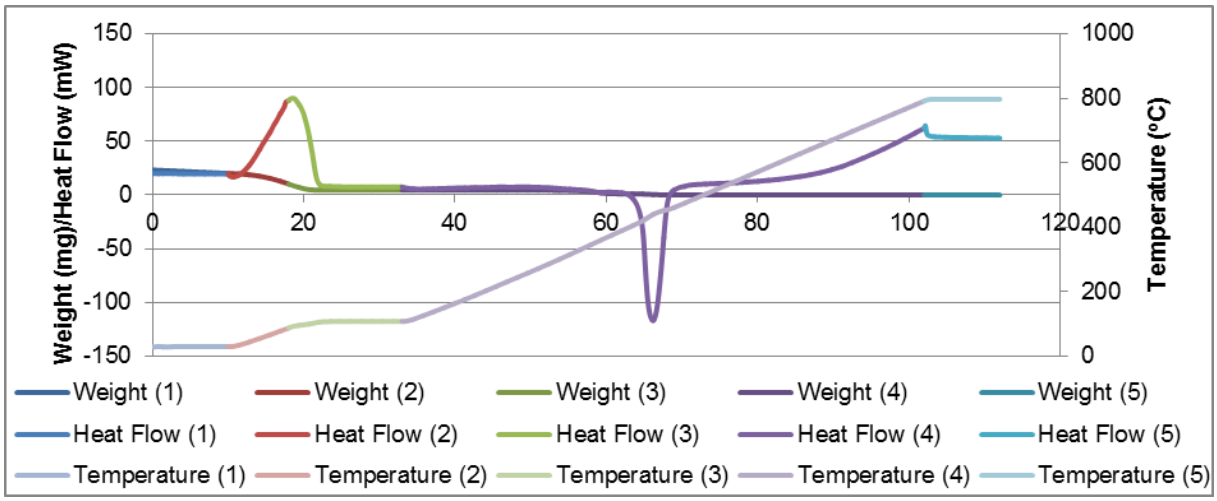

Figure A-4 – TG analysis of the UFCA400-30Ag0,14 membrane (weight, heat flow and temperature as a function of time).

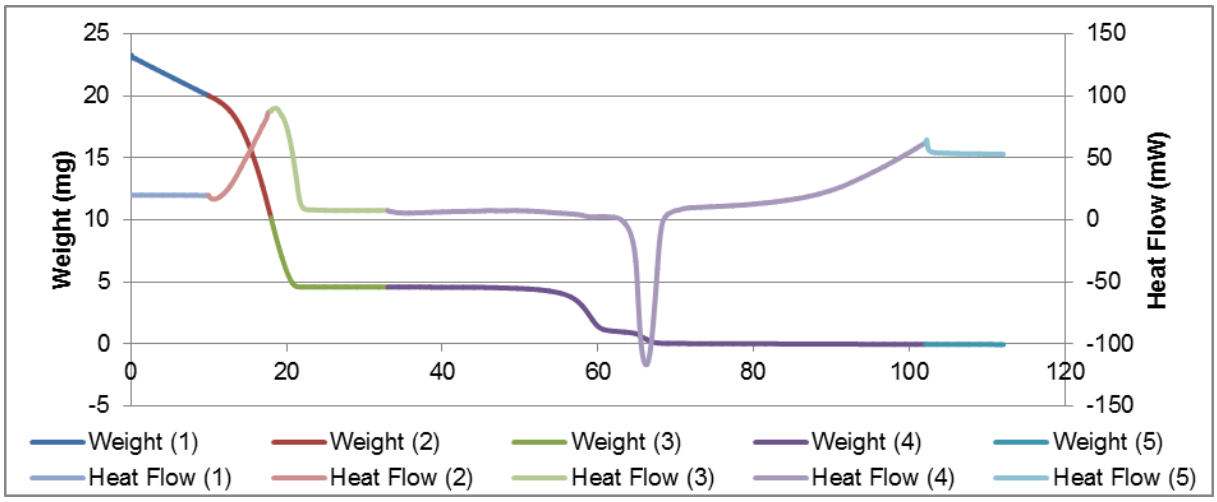

Figure A-5 – TG analysis of the UFCA400-30Ag0,14 membrane (weight and heat flow as a function of time).

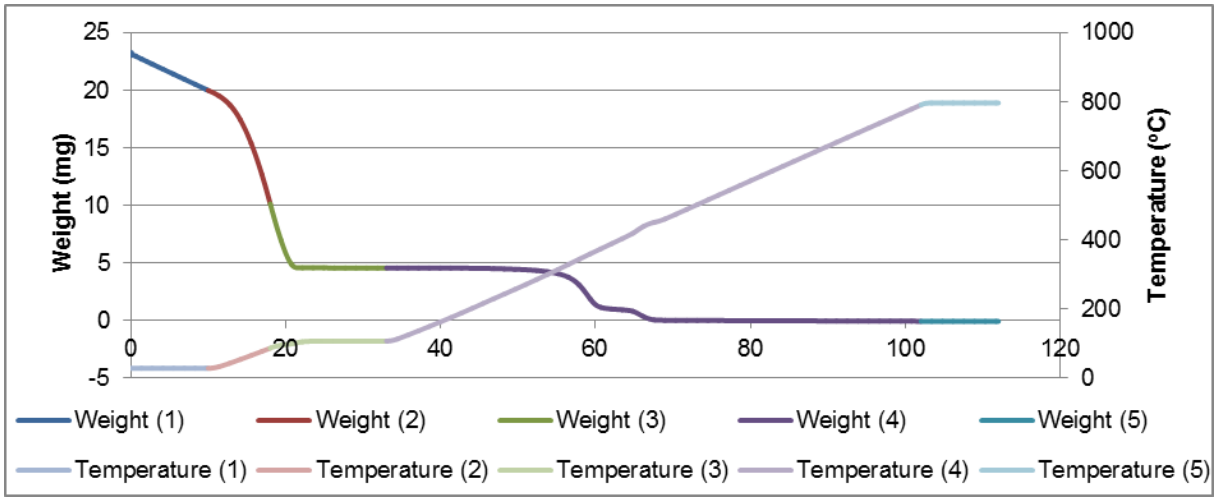

Figure A-6 – TG analysis of the UFCA400-30Ag0,14 membrane (weight and temperature as a function of time).

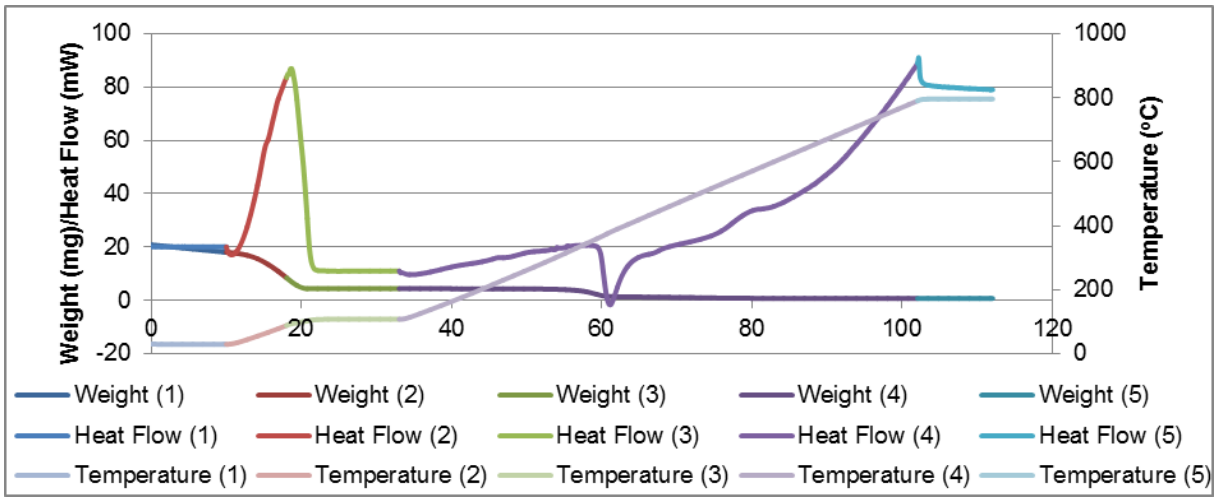

Figure A-7 – TG analysis of the UFCA400-30ZSM5 membrane (weight, heat flow and temperature as a function of time).

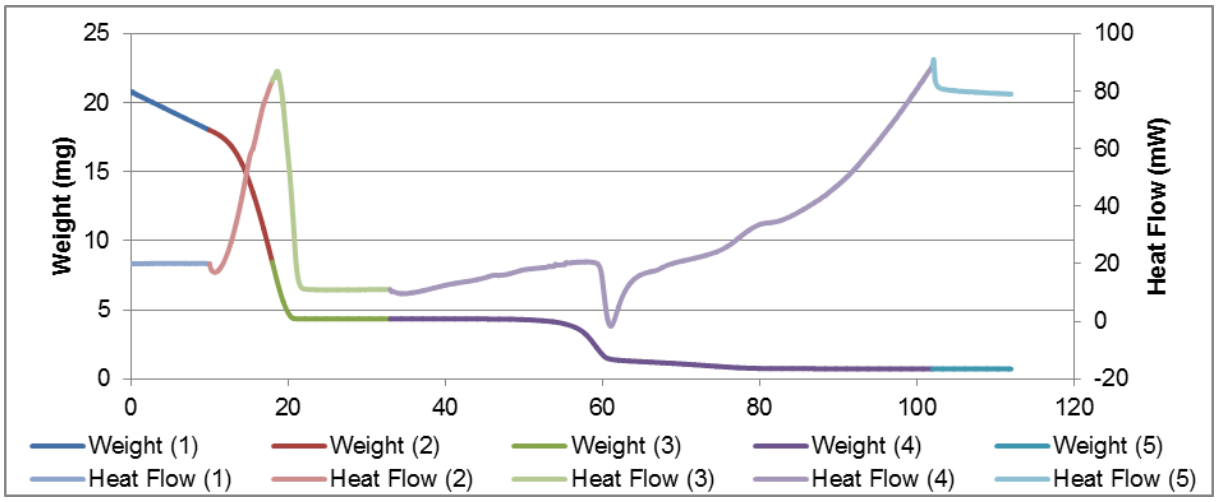

Figure A-8 – TG analysis of the UFCA400-30ZSM5 membrane (weight and heat flow as a function of time).

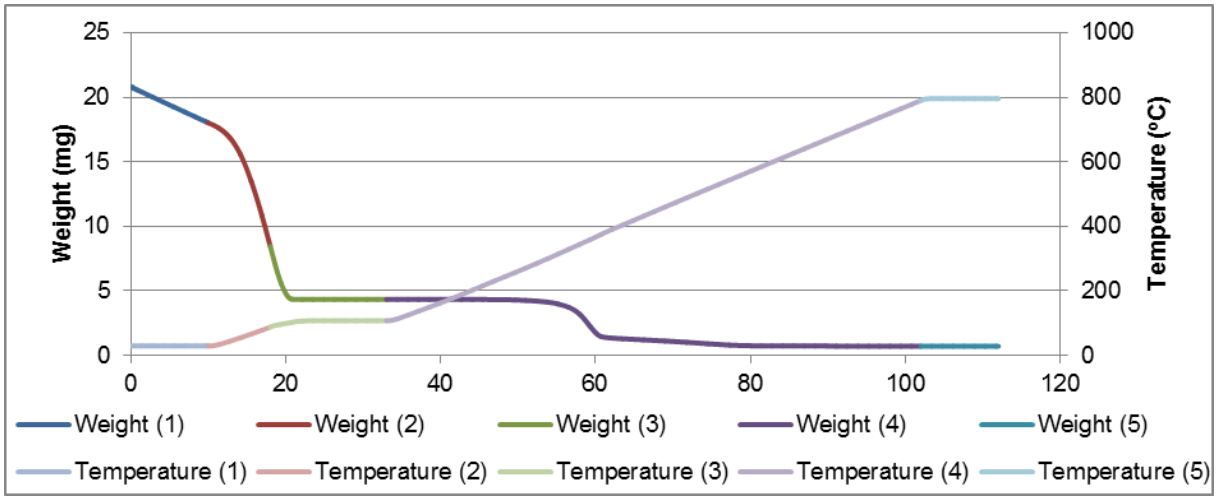

Figure A-9 - TG analysis of the UFCA400-30ZSM5 membrane (weight and temperature as a function of time).

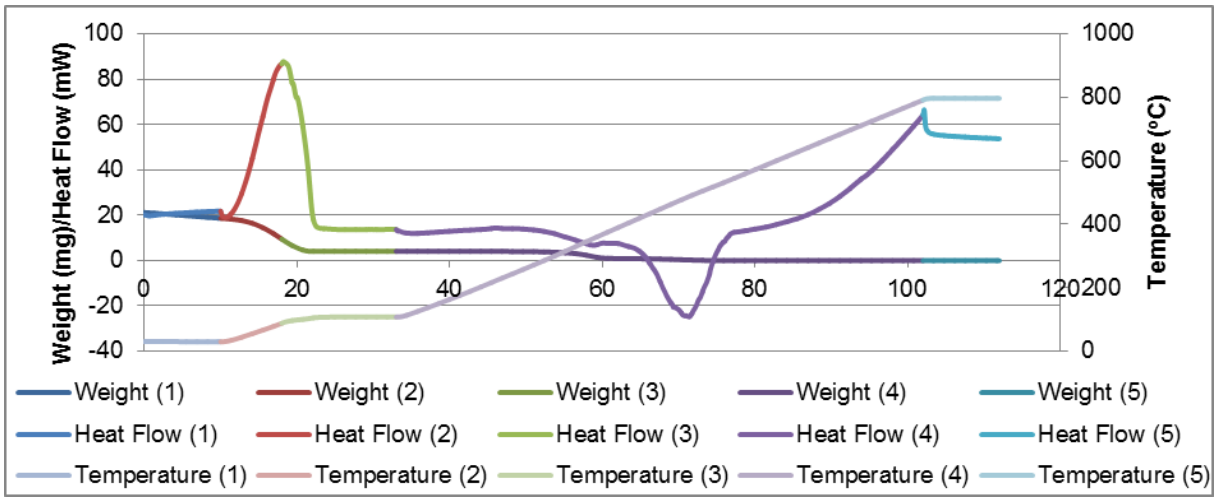

Figure A-10 – TG analysis of the UFCA400-30ZAg0,005 membrane (weight, heat flow and temperature as a function of time).

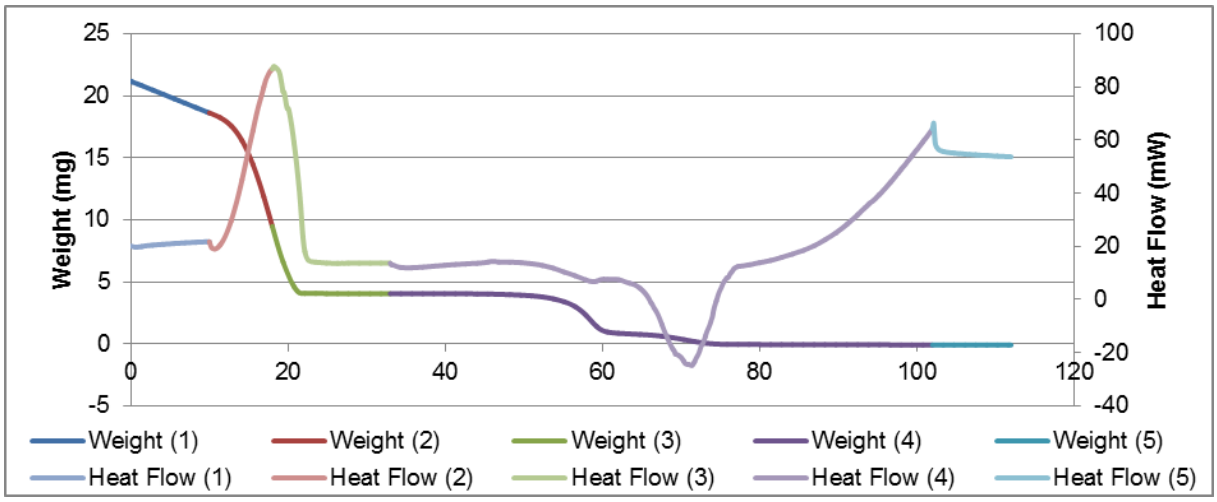

Figure A-11 – TG analysis of the UFCA400-30ZAg0,005 membrane (weight and heat flow as a function of time).

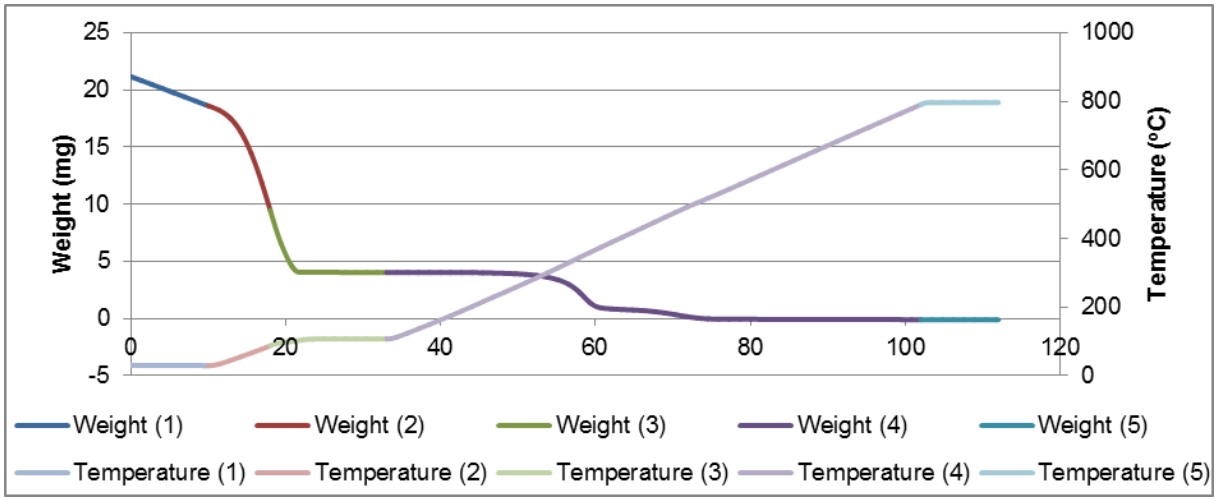

Figure A-12 – TG analysis of the UFCA400-30ZAg0,005 membrane (weight and temperature as a function of time).

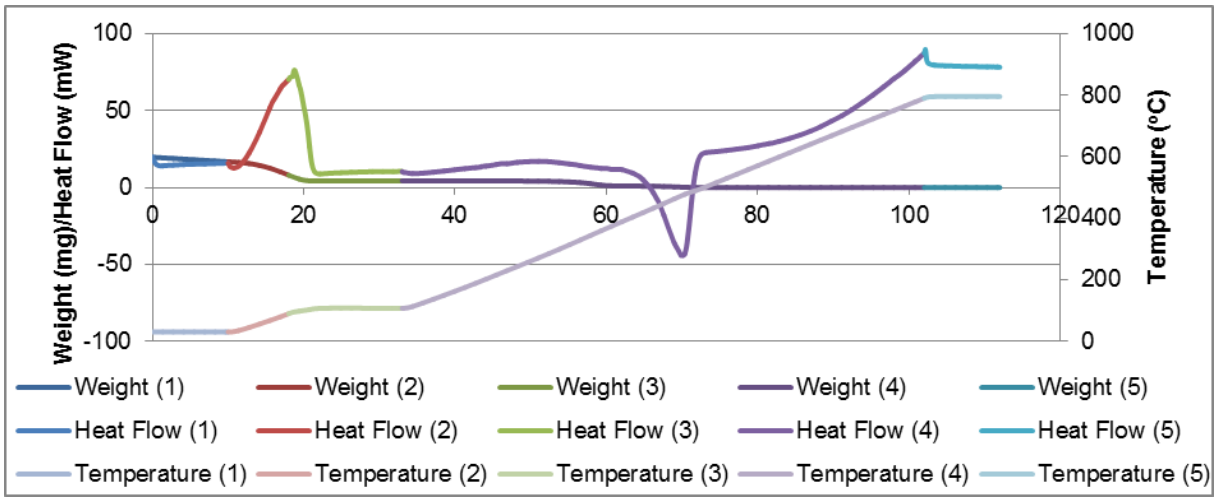

Figure A-13 – TG analysis of the UFCA400-30ZAg0,03 membrane (weight, heat flow and temperature as a function of time).

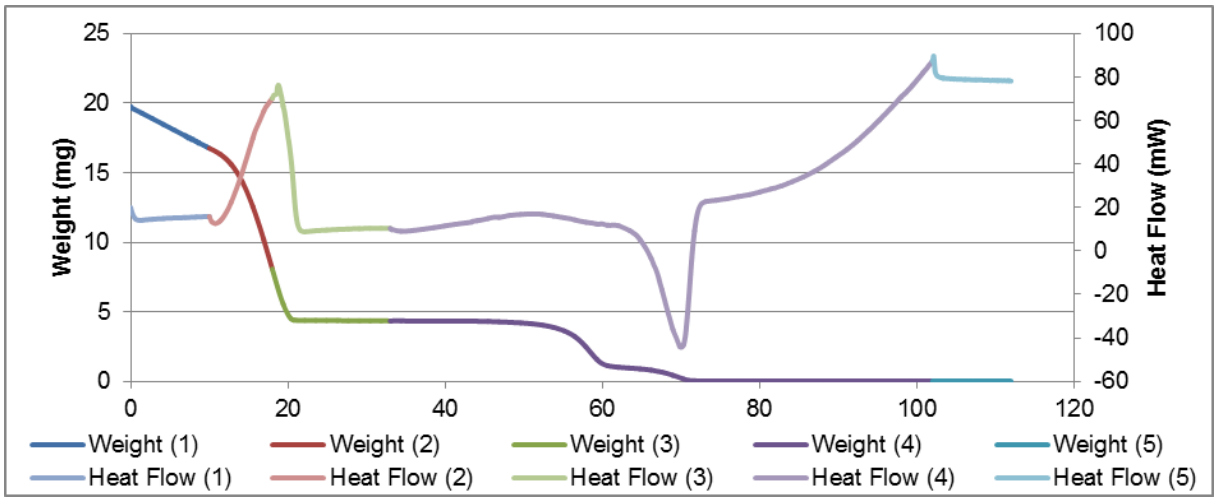

Figure A-14 – TG analysis of the UFCA400-30ZAg0,03 membrane (weight and heat flow as a function of time).

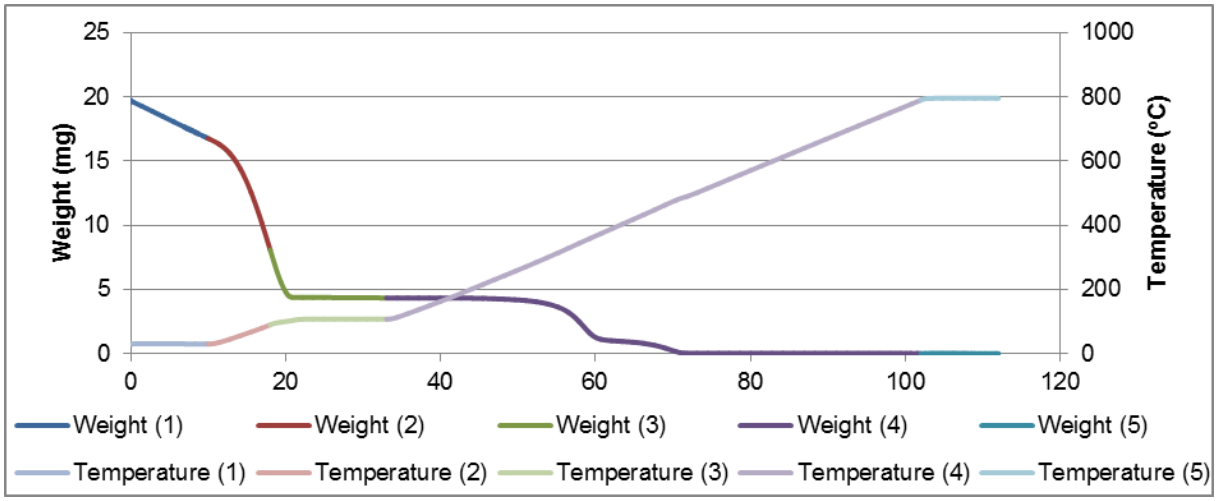

Figure A-15 – TG analysis of the UFCA400-30ZAg0,03 membrane (weight and temperature as a function of time).

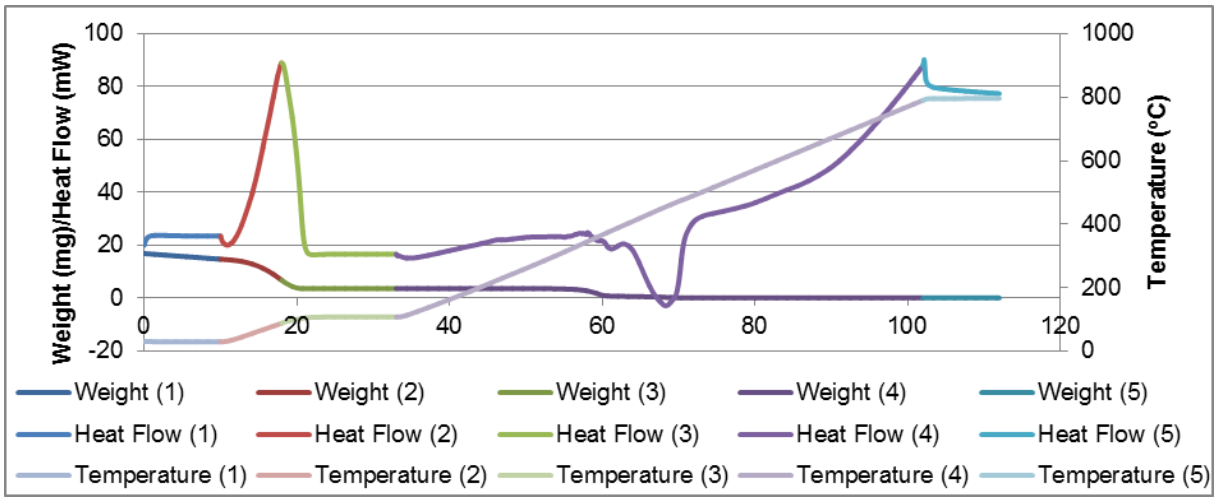

Figure A-16 – TG analysis of the UFCA400-30ZAg0,07 membrane (weight, heat flow and temperature as a function of time).

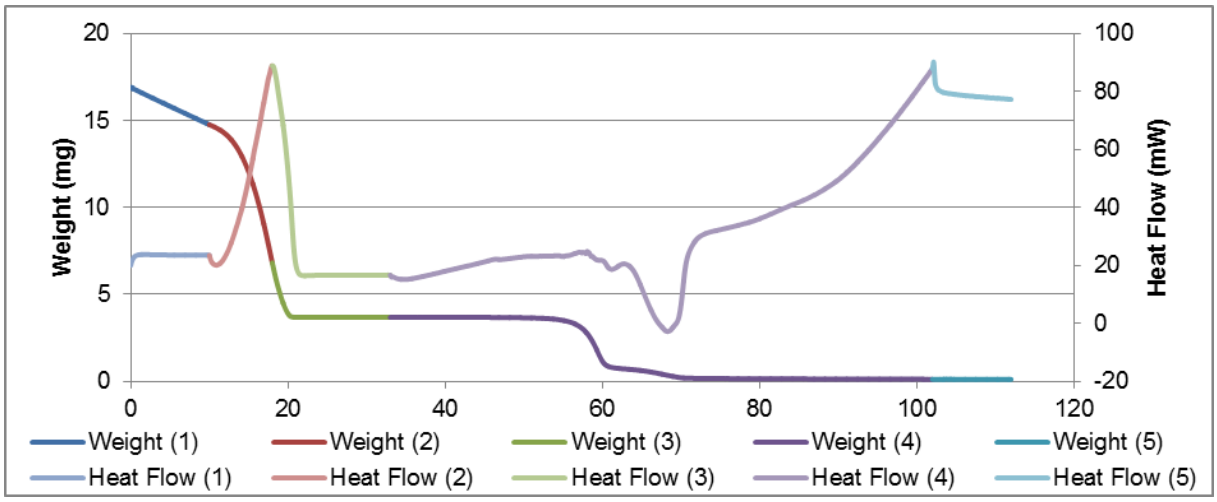

Figure A-17 – TG analysis of the UFCA400-30ZAg0,07 membrane (weight and heat flow as a function of time).

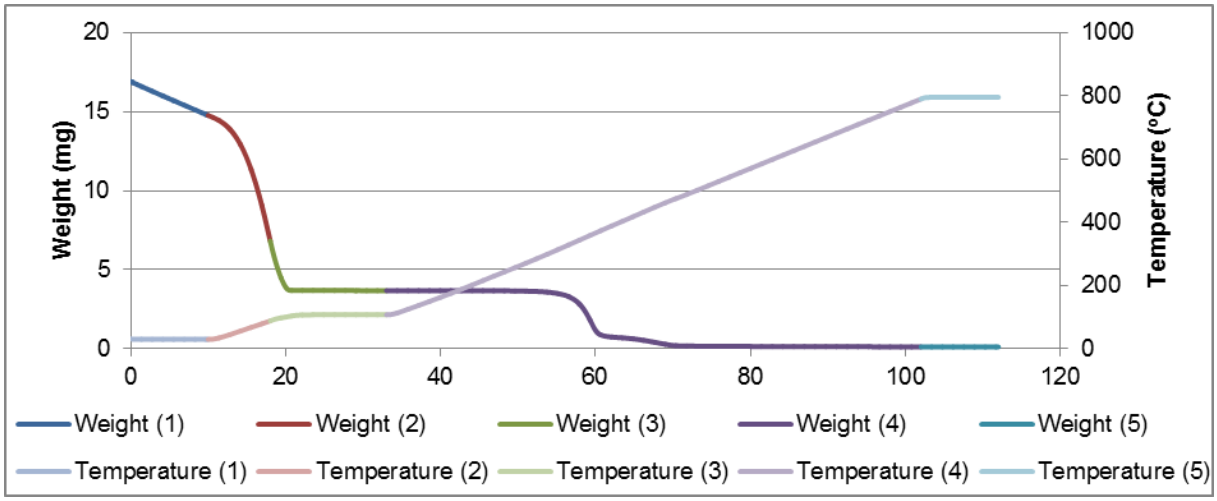

Figure A-18 – TG analysis of the UFCA400-30ZAg0,07 membrane (weight and temperature as a function of time).

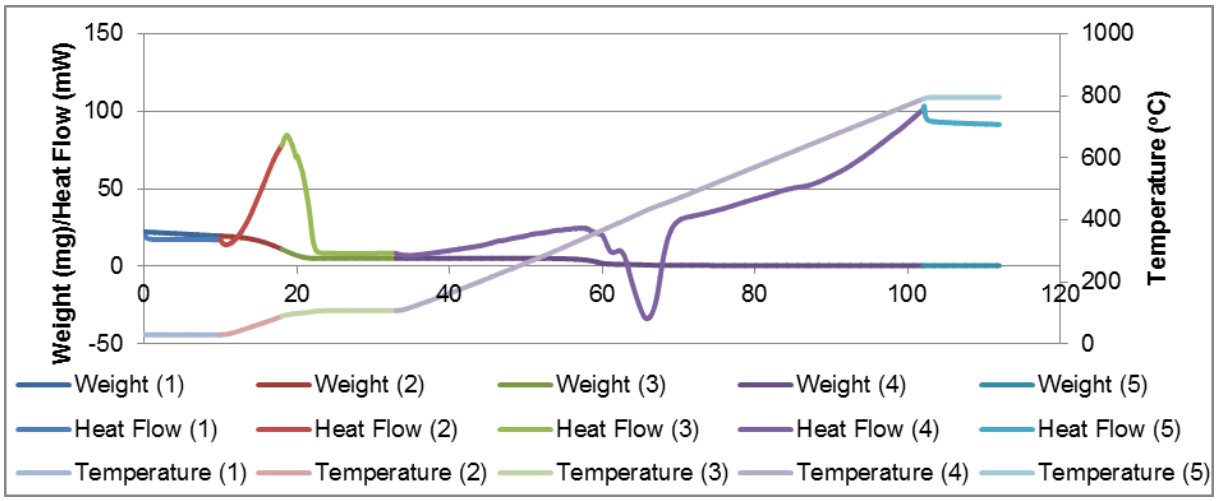

Figure A-19 – TG analysis of the UFCA400-30ZAg0,14 membrane (weight, heat flow and temperature as a function of time).

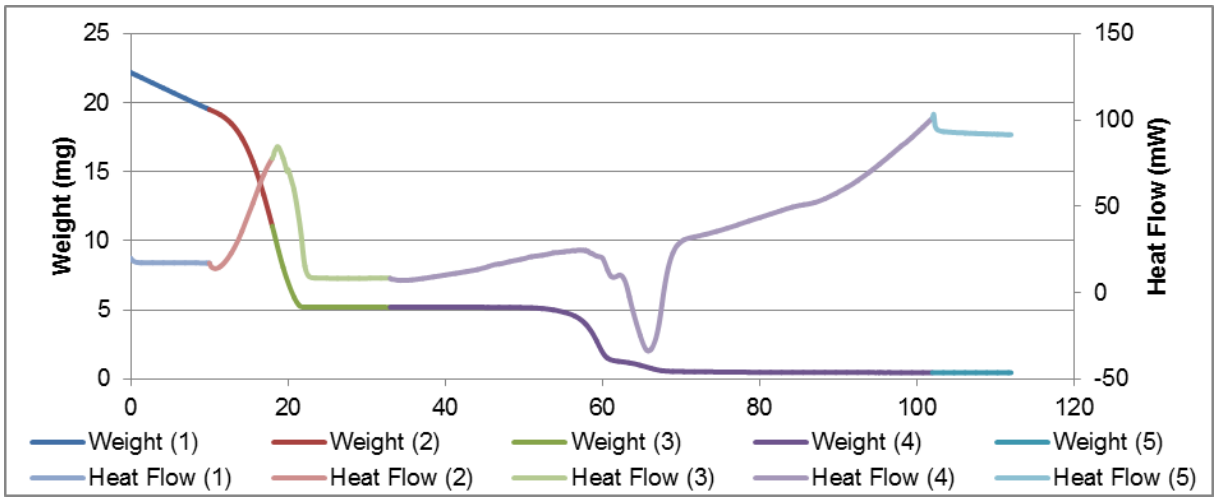

Figure A-20 – TG analysis of the UFCA400-30ZAg0,14 membrane (weight and heat flow as a function of time).

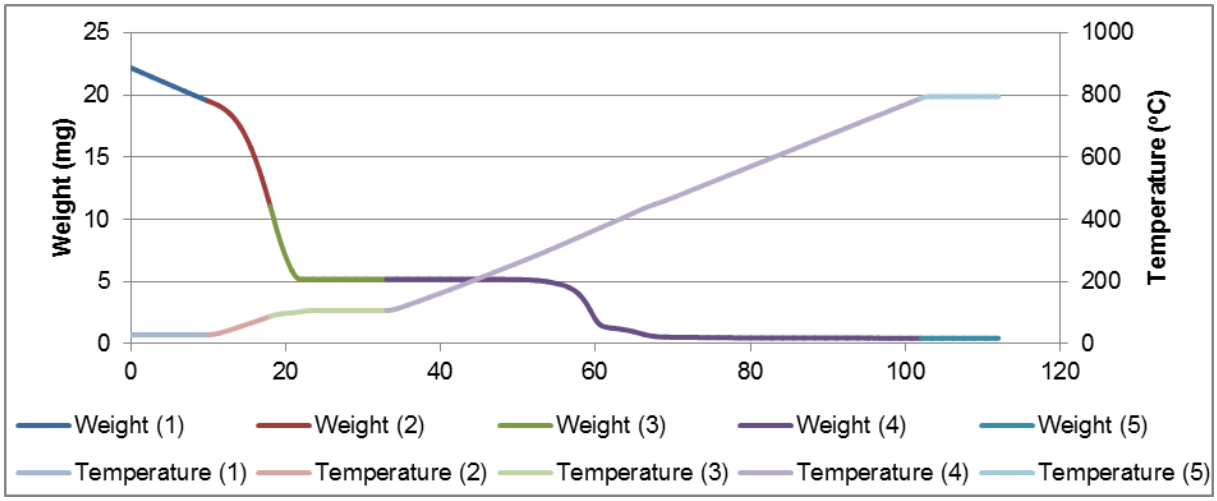

Figure A-21 – TG analysis of the UFCA400-30ZAg0,14 membrane (weight and temperature as a function of time).

A.4 EVALUATION OF THE BACTERICIDAL PROPERTIES

The results obtained in the antibacterial effect of the membranes are presented in Table A-3 – Table A-10.

Table A-3 – Bactericidal effect of NFCA400-30, NFCA400-30ZSM5 and NFCA400-30Ag0,14 membranes against P. aeruginosa (1st).

NFCA400-30			NFCA400-30ZSM5			NFCA400-30Ag0,14		
t (min)	#Colonies	%CFU	t (min)	#Colonies	%CFU	t (min)	#Colonies	%CFU
0	940.000	100	0	1.100.000	100	0	1.295.000	100
19	550.000	59	14	1.010.000	92	22	1.545.000	119
39	670.000	71	23	1.300.000	118	35	1.510.000	117
58	1.090.000	116	33	1.270.000	115	45	1.600.000	124
117	1.070.000	114	43	1.160.000	105	55	1.260.000	97
132	1.340.000	143	65	1.530.000	139	66	1.695.000	131
150	850.000	90	76	1.080.000	98	77	1.650.000	127
			87	1.230.000	112	88	1.790.000	138
			117	740.000	67	101	1.995.000	154
			127	1.090.000	99	114	1.685.000	130
			140	1.060.000	96	125	1.225.000	95
			150	1.380.000	125	135	1.210.000	93

Table A-4 – Bactericidal effect of NFCA400-30ZAg0,005, NFCA400-30ZAg0,03 and NFCA400-30ZAg0,07 membranes against *P. aeruginosa* (1st).

NFCA400-30ZAg0,005			NFCA400-30ZAg0,03			NFCA400-30ZAg0,07		
t (min)	#Colonies	%CFU	t (min)	#Colonies	%CFU	t (min)	#Colonies	%CFU
0	1.800.000	100	0	1.000.000	100	0	2.490.000	100
16	1.600.000	89	15	600.000	60	12	1.490.000	60
31	1.200.000	67	26	800.000	80	21	1.930.000	78
42	1.300.000	72	49	800.000	80	31	1.350.000	54
53	800.000	44	59	1.200.000	120	41	1.640.000	66
75	400.000	22	88	800.000	80	48	1.220.000	49
92	600.000	33	100	1.000.000	100	57	1.990.000	80
103	300.000	17	112	800.000	80	67	1.730.000	69
144	400.000	22	138	500.000	50	77	1.330.000	53
163	700.000	39	156	700.000	70	89	1.540.000	62
174	800.000	44				98	1.450.000	58
						109	730.000	29

Table A-5 – Bactericidal effect of NFCA400-30, NFCA400-30ZSM5 and NFCA400-30Ag0,14 membranes against *E. coli*.

NFCA400-30			NFCA400-30ZSM5			NFCA400-30Ag0,14		
t (min)	#Colonies	%CFU	t (min)	#Colonies	%CFU	t (min)	#Colonies	%CFU
0	1.200.000	100	0	500.000	100	0	500.000	100
32	400.000	33	18	1.900.000	380	18	1.000.000	200
49	300.000	25	40	1.200.000	240	32	500.000	100
70	900.000	75	56	300.000	60	46	1.100.000	220
87	800.000	67	76	300.000	60	59	700.000	140
132	5.200.000	433	92	1.600.000	320	72	1.700.000	340
149	6.000.000	500	111	4.400.000	880	85	3.500.000	700
165	5.600.000	467	128	4.400.000	880	99	2.800.000	560
192	18.500.000	1.542	150	8.600.000	1.720	118	3.200.000	640
235	31.400.000	2.617	169	23.800.000	4.760	187	24.900.000	4.980
			200	44.600.000	8.920			
			247	58.800.000	11.760			

Table A-6 – Bactericidal effect of NFCA400-30ZAg0,005 and NFCA400-30ZAg0,03 membranes against *E. coli*.

NFCA400-30ZAg0,005			NFCA400-30ZAg0,03		
t (min)	#Colonies	%CFU	t (min)	#Colonies	%CFU
0	1.300.000	100	0	600.000	100
21	200.000	15	16	100.000	17
37	200.000	15	31	1.100.000	183
56	900.000	69	47	400.000	67
100	4.600.000	354	63	2.000.000	333
119	8.700.000	669	80	2.800.000	467
142	10.800.000	831	112	8.200.000	1.367
162	16.400.000	1.262	131	7.500.000	1.250
185	26.800.000	2.062	152	12.300.000	2.050
			174	28.000.000	4.667
			196	46.200.000	7.700
			211	44.500.000	7.417

Table A-7 – Bactericidal effect of NFCA400-30ZAg0,07 and NFCA400-30ZAg0,14 membranes against *E. coli*.

NFCA400-30ZAg0,07			NFCA400-30ZAg0,14		
t (min)	#Colonies	%CFU	t (min)	#Colonies	%CFU
0	300.000	100	0	1.300.000	100
42	1.100.000	367	47	2.000.000	154
58	1.300.000	433	75	1.900.000	146
77	1.000.000	333	98	2.200.000	169
92	1.900.000	633	122	3.200.000	246
109	3.100.000	1.033	161	7.300.000	562
142	5.600.000	1.867	186	6.700.000	515
157	6.900.000	2.300	210	16.800.000	1.292
179	8.700.000	2.900	250	26.800.000	2.062
195	13.800.000	4.600	274	38.500.000	2.962
233	26.800.000	8.933	291	39.200.000	3.015
250	30.700.000	10.233			

Table A-8 – Bactericidal effect of NFCA400-30, NFCA400-30ZSM5 and NFCA400-30Ag0,14 membranes against *P. aeruginosa* (2nd).

NFCA400-30			NFCA400-30ZSM5			NFCA400-30Ag0,14		
t (min)	#Colonies	%CFU	t (min)	#Colonies	%CFU	t (min)	#Colonies	%CFU
0	490.000	100	0	1.450.000	100	0	1.070.000	100
20	275.000	56	25	555.000	38	20	960.000	90
37	245.000	50	45	705.000	49	28	925.000	86
58	400.000	82	62	985.000	68	36	650.000	61
76	910.000	186	81	1.090.000	75	53	805.000	75
122	3.885.000	793	98	2.000.000	138	61	1.170.000	109
138	3.485.000	711	118	2.595.000	179	71	1.235.000	115
158	4.855.000	991	135	4.350.000	300	79	1.045.000	98
182	27.500.000	5.612	157	950.000	66	102	2.255.000	211
222	44.100.000	9.000	175	10.300.000	710	110	1.225.000	114
258	75.350.000	15.378	207	25.200.000	1.738	118	1.695.000	158
273	95.000.000	19.388	252	42.300.000	2.917	126	1.155.000	108

Table A-9 – Bactericidal effect of NFCA400-30ZAg0,005 and NFCA400-30ZAg0,03 membranes against *P. aeruginosa* (2nd).

NFCA400-30ZAg0,005			NFCA400-30ZAg0,03		
t (min)	**#Colonies**	**%CFU**	**t (min)**	**#Colonies**	**%CFU**
0	100.000	100	0	315.000	100
20	320.000	320	26	345.000	110
62	2.780.000	2.780	42	350.000	111
81	4.565.000	4.565	57	630.000	200
101	1.800.000	1.800	72	365.000	116
123	16.250.000	16.250	89	2.035.000	646
149	21.250.000	21.250	122	4.325.000	1.373
164	44.400.000	44.400	140	11.000.000	3.492
180	76.000.000	76.000	161	12.100.000	3.841
210	95.000.000	95.000	184	28.550.000	9.063
			206	47.700.000	15.143
			222	79.000.000	25.079

Table A-10 – Bactericidal effect of NFCA400-30ZAg0,07 and NFCA400-30ZAg0,14 membranes against *P. aeruginosa* (2nd).

NFCA400-30ZAg0,07			NFCA400-30ZAg0,14		
t (min)	**#Colonies**	**%CFU**	**t (min)**	**#Colonies**	**%CFU**
0	720.000	100	0	595.000	100
20	1.475.000	205	24	630.000	106
36	2.080.000	289	53	240.000	40
54	1.965.000	273	78	780.000	131
71	2.035.000	283	111	260.000	44
88	4.300.000	597	143	335.000	56
120	9.200.000	1.278	168	360.000	61
136	12.800.000	1.778	208	910.000	153
157	27.200.000	3.778	231	830.000	139
173	22.900.000	3.181	250	2.500.000	420
213	43.050.000	5.979	272	1.135.000	191
227	44.300.000	6.153	289	1.515.000	255